The Paleocene – Eocene Thermal Maximum in the Gulf of Mexico

a low latitude paleoenvironmental reconstruction

Master thesis, 2009

Linda van Roij

Supervision by

Dr. Appy Sluijs
Prof. Dr. Henk Brinkhuis

Palaeoecology, Institute of Environmental Biology,
Laboratory of Palynology and Palaeobotany,
Department of Biology, Faculty of Sciences, Utrecht University

and

Dr. Gert-Jan Reichart

Geochemistry,
Department of Earth Sciences, Faculty of Geosciences, Utrecht University

Outline

1. Introduction

The Early Paleogene is characterized by globally high temperatures and high atmospheric carbon dioxide concentrations or so called 'greenhouse' conditions (Dickens et al. 1997, Zachos et al. 2001). A short period of extreme warming occurred at boundary between the Paleocene and the Eocene, approximately 55.5 My ago (Röhl et al. 2007). This global event was named the Paleocene – Eocene Thermal Maximum (PETM) (Zachos et al. 2003).

Deep marine sediments corresponding to the PETM show distinct carbonate dissolution. The microfossil content of the remaining clay-rich sediments show an extinction of benthic foraminifera (Thomas and Shackleton 1996). Planktonic species of foraminifera and dinoflagellates migrated towards the poles or changed their morphology in order to adapt to the changing environment of the PETM (Kelly et al. 1996, Crouch et al. 2001). Also mammals migrated to higher latitudes and some species show radiation and dwarfing during this warming phase (Bowen et al. 2002, Bowen et al. 2006, Smith et al. 2006).

The stable oxygen isotope ratio, expressed in $\delta^{18}O$ values, of biogenic carbonates drops abruptly by ~1.5‰ (Kennett and Stott 1991, Zachos et al. 2001, Zachos et al. 2003). This indicates that the oceans must have warmed rapidly in this ice-free world. Furthermore, stable carbon isotope ($\delta^{13}C$) records based on either organic matter, biogenic carbonate or bulk sediment all show a significant negative carbon isotope excursion (CIE) which marks the onset of the PETM (Kennett and Stott 1991). The CIE is associated with destabilization of methane hydrates, which potentially have a $\delta^{13}C$ value of ~-60‰ (Dickens et al. 1995, Dickens et al. 1997). The released methane caused, due to a reaction with oxygen, a rapid injection of carbon dioxide in the atmosphere that would have had a large impact on global air temperature (Weijers et al. 2007a) and sea water temperature (Sluijs et al. 2006, Zachos et al. 2006, Sluijs et al. 2007b) as well as on ocean acidification (Zachos et al. 2005).

Perturbations in the global carbon cycle associated with the PETM are reflected in the CIE. However, other proxies suggest that the earliest changes in temperature (Thomas et al. 2002, Tripati and Elderfield 2005, Sluijs et al. 2007b) and in biotical assemblages (Sluijs et al. 2007b) preceded the CIE. Sluijs et al. (2007b) generated high resolution PETM records of two sites located on the New Jersey shelf, Wilson Lake and Bass River in Pennsylvania, USA. Both sites show that the CIE is preceded by an increase in TEX_{86} based sea surface temperature by approximately 3 ka and by an abundant occurrence (acme) of dinoflagellate cyst *Apectodinium* by 4-5 ka (Figure 1). Apparently, this early onset of the initial warming suggests it was not an effect of the CIE and may have in fact caused methane hydrate dissociation (Thomas et al. 2002, Tripati and Elderfield 2005). Furthermore, *Apectodinium* responded to a changing variable other than temperature or the effects of the CIE. However, no clear difference in initiation of the CIE, temperature increase and *Apectodinium* acme could be determined for an Arctic site (Sluijs et al. 2006). Moreover, high resolution studies on the succession of the CIE and temperature increase only apply to high and mid latitude sites, whereas the preceding onset of both *Apectodinium* and temperature is reported for solely mid latitude locations: the New Jersey sites, a site in the North Sea and possibly a site in the Southwest Pacific (Sluijs et al., 2007 and Supplementary Information). A high resolution record of low latitude site is required in order to study the potentially global nature of the succession.

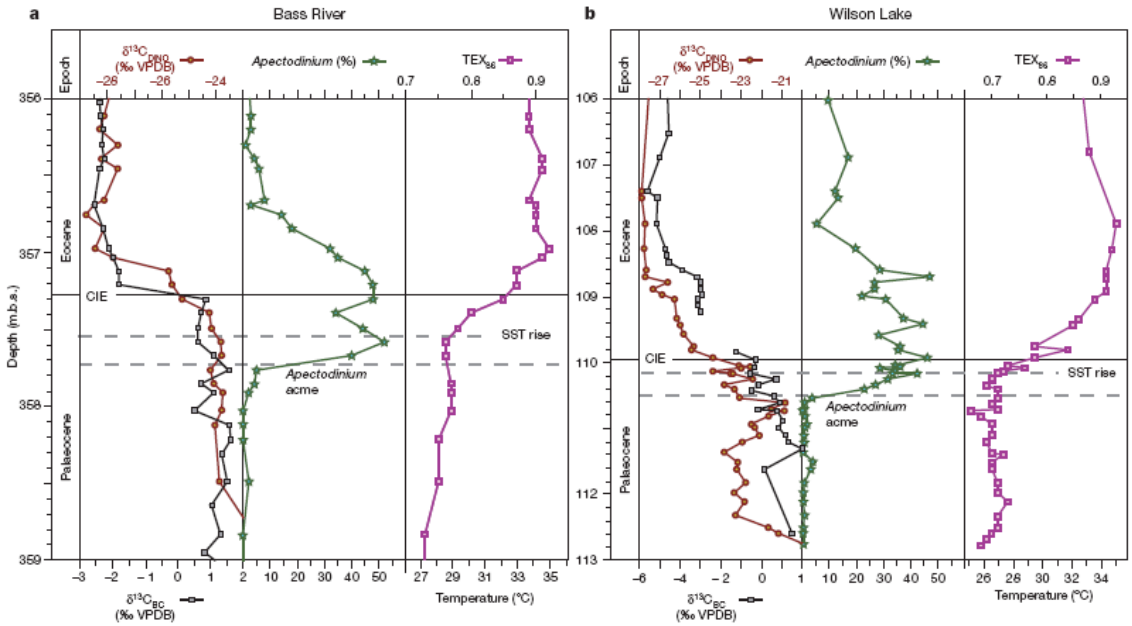

Figure 1. High-resolution records across the onset of the PETM at the New Jersey Shelf sites. Bass River (a): Bulk carbonate $\delta^{13}C$ data are from Zachos et al. (2007). Wilson Lake (b): Part of the TEX86 data are from Zachos et al. (2006). Solid horizontal lines at 357.3 mbs and 110.0 mbs for Bass River and Wilson Lake, respectively, represent the onset of the CIE; dashed lines represent the onsets of the *Apectodinium* acme and surface warming. BC, bulk carbonate; DINO, dinocysts; VPDB, Vienna Pee Dee Belemnite; mbs, meters below surface. Scale at TEX86 temperatures represents the calibration from Schouten et al. (2003). From Sluijs et al. (2007b), full records and details in their Supplementary Information.

The Late Paleocene and Early Eocene are characterized by high sea surface temperatures (Sluijs et al. 2006, Zachos et al. 2006, Sluijs et al. 2007b). During the PETM, sea surface temperatures increased by ~5 to 8 ºC in the tropics as well as at mid and high latitude (Kennett and Stott 1991, Zachos et al. 2003, Sluijs et al. 2006, Zachos et al. 2006). Thus, latitudinal temperature gradients remained low with temperatures at the equator being only ~15 ºC higher than in the Arctic (Sluijs et al. 2006, Pearson et al. 2007, Weijers et al. 2007a). Climate models, however, fail to reproduce this small temperature gradient suggesting that either temperature proxies generate values that are too low for low latitudes or climate models lack processes affecting polar temperature amplification or equatorial cooling (Shellito et al. 2003). Study of PETM temperatures has been done for high latitudes (Sluijs et al. 2006, Weijers et al. 2007a) and mid-latitudes (Zachos et al. 2006, Sluijs et al. 2007b) using stable oxygen isotopes, Mg/Ca ratios, MBT and TEX_{86} analysis. Accurate determination of low latitude temperatures is necessary to study the equator to pole temperature gradient.

In this study, Late Paleocene and Early Eocene marginal sediments of the Harrell core and St. Stephens core are used to determine the succession of the *Apectodinium* acme, warming and the CIE as well as the temperature increase at low latitude. Furthermore, these two extended records from the North American margin along the Gulf of Mexico contain dinocyst assemblages that are used for the reconstruction of the paleoenvironment in the subtropics during the PETM. The sediments are studied for their magnetic susceptibility, carbonate content, stable carbon isotopes, palynomorphs and biomarkers.

2. Background information

2.1. Shape of the carbon isotope excursion

The shape of the CIE and its recovery is different for every site and measured substrate. A general picture has been sketched, however, so various records can be compared (Bowen et al. 2006, Sluijs et al. 2007a) (Figure 2). The onset of the CIE is characterized by a sharp drop in $\delta^{13}C$ that established in only a few thousands of years. In between the onset and the recovery, low $\delta^{13}C$ values maintain during a phase termed the CIE-body. This phase may represent a fundamentally different climate state (Bowen et al. 2004) and may be an indication for a long term lag between the input of ^{13}C depleted carbon in the ocean and atmosphere reservoirs and its removal out of this system (Bowen et al. 2006). Subsequently, the $\delta^{13}C$ gradually return towards higher values comparable to the latest Paleocene during the recovery phase.

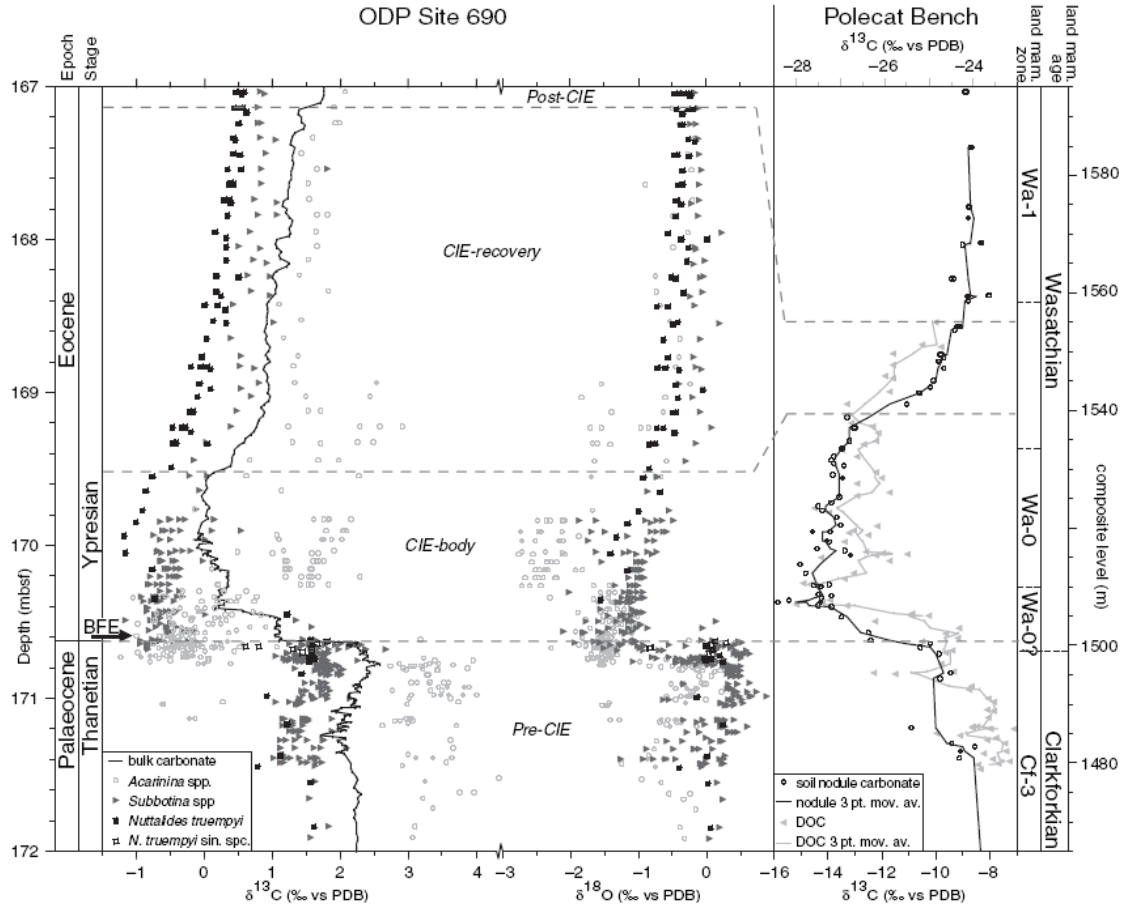

Figure 2. Compilation of $\delta^{13}C$ and $\delta^{18}O$ records. Values derived from planktonic foraminifera (surface-dweller *Acarinina* and thermocline-dweller *Subbotina* spp.; mostly single specimen), benthic foraminifera (*Nuttallides truempyi*) and bulk carbonate from ODP Site 690 in the Weddell Sea (data from (Kennett & Stott 1991; Bains et al. 1999; Thomas et al. 2002; Kelly et al. 2005), soil carbonate nodule (Bowen et al. 2001) and dispersed organic carbon (DOC) (Magioncalda et al. 2004) d13C records from the Polecat Bench section in the Bighorn Basin, Wyoming, USA. BFE refers to the main phase of benthic foraminifer extinction according to Thomas (2003). Mbsf, meters below sea-floor. From Sluijs et al., 2007a.

2.2. Carbon cycling

The CIE indicating the onset of the PETM has an estimated magnitude of -3‰ in marine carbonates and even up to -6.5‰ in plant organic matter and soil carbonates (Koch et al. 1992, Pagani et al. 2006a). The CIE is too large to be explained by fluxes in biomass and soils alone (Dickens et al. 1995). Possibly, destabilization of methane hydrates resulted in the release of carbon that is strongly depleted in ^{13}C, with a $\delta^{13}C$ value of ~-60‰ (Dickens et al. 1995, Dickens et al. 1997). Destabilization may have been triggered by long term warming by (Dickens et al. 1997) and short term warming by changes in ocean circulation (Dickens et al. 1995), but also by slope failure (Katz et al. 1999). Uncertainties remain about the size and isotopic composition of the ^{13}C depleted carbon source as well as carbon fluxes between different reservoirs, and the sensitivity of Earths climate to changes in the carbon cycle (Pagani et al. 2006a). Recovery to pre-PETM $\delta^{13}C$ values lasted for ~170 ka (Röhl et al. 2007, Abdul Aziz et al. 2008).

In theory, the large scale carbon injection led to dissolution of carbon dioxide in the oceans as well as to an increase of air and ocean water temperatures. Ocean acidification resulted in a shoaling of the calcite compensation depth (CCD) explaining the carbonate dissolution (Zachos et al. 2008). High temperatures caused enhancement of the global hydrological cycle (Robert and Kennett 1994, Bowen et al. 2004, Pagani et al. 2006b), thereby changing precipitation patterns and river runoff. Changes in temperature and hydrology (Pagani et al. 2006b) affected salinity (Schmitz et al. 1997, Pagani et al. 2006b), sea level (Schmitz and Pujalte 2003, Sluijs et al. 2008a) and continental weathering (Kelly et al. 2005).

During the Early Eocene, the PETM was followed by another two events of rapid global warming. The onset of the PETM as well as the Eocene Thermal Maximum 2 (ETM2) (53 Ma) (Lourens et al. 2005) and ETM3 (52 Ma) (Röhl et al. 2005) may have been triggered by insolation changes as they coincide with ~100 ka eccentricity maxima (Lourens et al. 2005, Westerhold et al. 2007).

2.3. Dinoflagellates

Dinoflagellates are single celled eukaryotes that live in typically neritic settings of the oceans world wide during their motile life stage (Fensome et al. 1996a). As many dinoflagellates are amongst the main marine primary producers, they are part of the global carbon cycle (Brasier 1985). However, other species may also be assigned to the trophic levels of herbivores, predators or parasites (Loeblich 1984, Gaines and Elbrachter 1987, Taylor 1987, Schnepf and Elbrachter 1992, Fensome et al. 1996c, Hansen and Calado 1999, Jeong 1999). Heterotrophic dinoflagellates may feed on other dinoflagellates, diatoms, bacteria, ciliates and organic debris (Gaines and Taylor 1984, Lessard and Swift 1985, Jacobson and Anderson 1986, Jacobson and Anderson 1996). Moreover, species that combine autotrophic and heterotrophic feeding strategies are widespread (Bockstahler and Coats 1993a, Bockstahler and Coats 1993b, Jacobson and Anderson 1996, Stoecker 1999). These mixotrophs are increasingly more found (Jeong et al. 2005) and their abundance may be related to nutrient supply (Burkholder et al. 2008). Extremely high abundances of dinoflagellates may result into harmful algal blooms (Smayda 1997). As resting stage within their life cycle, some species of dinoflagellates form organic-walled cysts (dinocysts), while others may form calcareous or siliceous cysts. Cyst formation is associated with sexual reproduction and induced by certain environmental variables that usually include seasonal nutrient depletion (Taylor 1987).

The fossil record contains only the more resistant cysts rather than the motile stage of dinoflagellates. Similar to foraminifera, coccolithophores, diatoms and radiolaria, dinocysts can be used as indicators for the marine paleoenvironment. Whereas the dinoflagellate lineage is thought to have originated in the Precambrian

or Early Cambrian (Fensome et al. 1996b, Moldowan and Talyzina 1998), the oldest cysts are found in Mid Triassic sediments succeeded by an increase in diversity until the Mid Cretaceous (MacRae et al. 1996). Although diversity steadily dropped since the Eocene, Quaternary assemblages contain the highest number of extant taxa and therefore are most useful for reconstructing the paleoenvironment. By means of an actuo-paleontological approach, dinocyst assemblages are proven to show high sensitivity for changing water properties throughout the Quaternary (Matthiessen et al. 2005). In addition to the knowledge derived from actuo- en Quaternary studies, an increase in Paleogene dinocyst data used in multidisciplinary studies has made pre-Quaternary reconstructions more reliable (Brinkhuis et al. 2003, Sluijs et al. 2003, Huber et al. 2004, Röhl et al. 2004a, Röhl et al. 2004b, Schellenberg et al. 2004, Stickley et al. 2004, Williams et al. 2004, van Simaeys et al. 2005, Sluijs et al. 2006, Sluijs et al. 2007b, Sluijs et al. 2008b).

2.4. TEX_{86}, MBT and BIT

The core membrane lipids of mesophilic Crenarchaeota are glycerol dialkyl glycerol tetraethers (GDGTs). They are characterized by their isoprenoid carbon chain and ether bonds which form a structure that is membrane spanning, whereas core membrane lipids of bacteria typically contain n-alkyl chains and ester bonds (Kates 1977). The GDGTs contain up to eight cyclopentane rings strongly depending on the temperature in which they were synthesized (Gliozzi et al. 1983, De Rosa and Gambacorta 1988, Uda et al. 2001). As a result, the distribution of the various GDGT structures is assumed to reflect the growth temperature of the surface-dwelling archaea and GDGTs that have been preserved in sediments can be used as paleothermometer for mean annual sea surface temperature (MASST) (Schouten et al. 2002). However, besides the archaeal isoprenoid GDGTs also branched GDGTs are found (Schouten et al. 2000). Based on their stereoconfiguration and branched carbon chain structure, they are considered to be derived from anaerobic soil bacteria rather than from archaea (Weijers et al. 2006a).

When aiming to calculate the MASST, the distribution of GDGTs that are derived from marine settings should be used. The TEX_{86} index reflects a ratio of several types of marine GDGTs and shows a significant correlation with MASST (Schouten et al. 2002). This index has proven to be useful as a paleothermometer proxy for the PETM at mid and high latitude (Sluijs et al. 2006, Zachos et al. 2006).

The distribution of the branched GDGTs can be used to calculate methylization and cyclization indices (MBT and CBT ratio, respectively; (Weijers et al. 2007b). As branched GDGTs are considered to be terrestrially derived (Weijers et al. 2006b), temperature reconstructions based on the MBT and CBT ratios represent MAAT (Weijers et al. 2007b). MAAT reconstructions using branched GDGTs have successfully been applied for the Arctic PETM (Weijers et al. 2007a).

Since the occurrence of terrestrially derived GDGTs in the ocean would bias MASST reconstructions, the branched and isoprenoid tetraether (BIT) index should be taken into account. The BIT index is the ratio of branched GDGTs versus the marine GDGT crenarchaeol and reflects the amount of soil input (Hopmans et al. 2004). For BIT values greater than 0.3, the TEX_{86} index is considered to be less reliable due to a possible contamination of GDGTs produced by soil archaea (Weijers et al. 2006b). Vice versa, MAAT is considered to be less reliable when BIT values are too low due to potential *in situ* production of branched GDGTs in marine settings (Peterse et al. 2009).

The first MASST calibration for TEX_{86} was made by Schouten et al. (2002). They used 44 core top data and found a linear correlation of TEX_{86} with MASST. Kim et al.

(2008) used 287 core tops from widely dispersed settings and found that the correlation was in fact non-linear due to low sensitivity of TEX_{86} for temperatures below 5 °C. After excluding data from the polar oceans and the substantially deviating data from the Red Sea, a new linear correlation was obtained that is considered to be reliable for MASSTs between 5 and 30 °C. The authors do, however, recognize possible biasing by seasonality and the growth depth of Crenarchaeota. A non-linear calibration is proposed by Liu et al. (2009) based on the complete dataset of Kim et al. (2008). This calibration leads to MASSTs very similar to the calibration of Kim et al. (2008) for moderate ocean temperatures. However, calculations of MASSTs for TEX_{86} values below 0.4 will be much cooler as well as less accurate. When TEX_{86} exceeds 0.65, MASST will be increasingly lower compared to the calibration of Kim et al. (2008). The latter is especially important as temperature is expected to be high in the Early Paleogene and particularly during the PETM. Temperature reconstructions considering the PETM are generally based on the calibration of Kim et al. (2008). Therefore, this calibration will be further used for discussion and comparisons.

Weijers et al. (2007b) found a strong correlation (R^2=0.77) between MBT, CBT and MAAT following: MBT = 0.122 + 0.187*CBT + 0.020*MAAT. So far, no corrections have been made for this calibration.

3. Material and methods

3.1. Material

Lower Paleogene sediments are found along the margins of the Gulf of Mexico in Mississippi and Alabama, USA, currently at 32 ºN (Gibson and Bybell 1994, Harrington 2001, Harrington 2003) (Figure 3). The Tuscahoma Formation and the Bashi-Hatchetigbee Formation are assigned to the latest Paleocene and earliest Eocene and may therefore contain the PETM (Figure 4). Units are relatively thicker towards the west, where deltas entered the basin and sedimentation rates were highest.

The Tuscahoma Formation is composed of fine sand, silt and clay laminations with carbonaceous debris, cross-bedded sand and lignite beds (Gibson and Bybell 1994). Up to 4 beds of shelly glauconitic sands or marls are found within this marine formation throughout the basin. The Tuscahoma Formation is dated using sparse nannoplankton (Gibson et al. 1982) and placed in Zone NP9. The uppermost part of the formation does not contain calcareous microfossils. Pollen records indicate brackish water and swamp deposits of Late Paleocene age for the lower and middle part of the Tuscahoma Formation (Harrington et al. 2004) succeeded by pollen of Early Eocene in the uppermost Tuscahoma Formation. Conclusively, the Paleocene – Eocene boundary, and therefore possibly also the PETM, lies within the uppermost Tuscahoma Formation.

The Bashi-Hatchetigbee Formation lies on top of a sequence boundary and consists of the Bashi Marl Member and an unnamed member (Toulmin 1977). The Bashi Marl Member is a fossiliferous, glauconitic, silty, fine-grained sand unit and is assigned to zone NP10 (Gibson and Bybell 1994). The unnamed member is composed of very fine to fine graded sand with laminations of very fine sand, silt and clay beds and does not contain significant amounts of glauconite or carbonate (Gibson 1983, Gibson and Bybell 1994). The Bashi Marl Member is dated for the Early Eocene using planktonic foraminifera (Berggren 1965, Gibson 1980, Mancini 1981) and nannoplankton (Gibson et al. 1982).

The first locality used in this study is Meridian, Lauderdale County, Mississippi (Figure 3). The Harrell core obtained here corresponds to the western end of the basin. It contains the upper Tuscahoma Formation and the Bashi-Hatchetigbee Formation (Figure 4) and is stored at the Geological Survey of Mississippi in Jackson, USA. The Harrell core stretches from 115.39 to 128.57 meters below surface (mbs). From this interval, 144 samples have been obtained. The boundary between the Tuscahoma Formation and the Bashi-Hatchetigbee Formation is at 118.7 mbs.

The second core is the St. Stephens core from western Alabama (Figure 3). It is located east of the Harrell core locality and thereby more towards the center of the basin. The studied interval is of latest Paleocene and earliest Eocene age. The interval between 186.84 and 249.63 mbs was sampled for 27 samples with spacing of 1.10 to 5.49 m. The boundary between the Tuscahoma Formation and the Bashi-Hatchetigbee Formation is at 212 mbs.

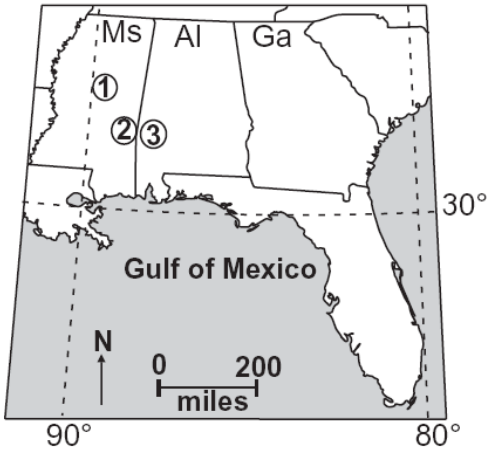

Figure 3. Study area. Location of the Harrell core is indicated by number 2. The locality of the St. Stephens core is not specifically indicated, but should be close to Walahak #2 core corresponding to number 3. From Harrington et al. (2004).

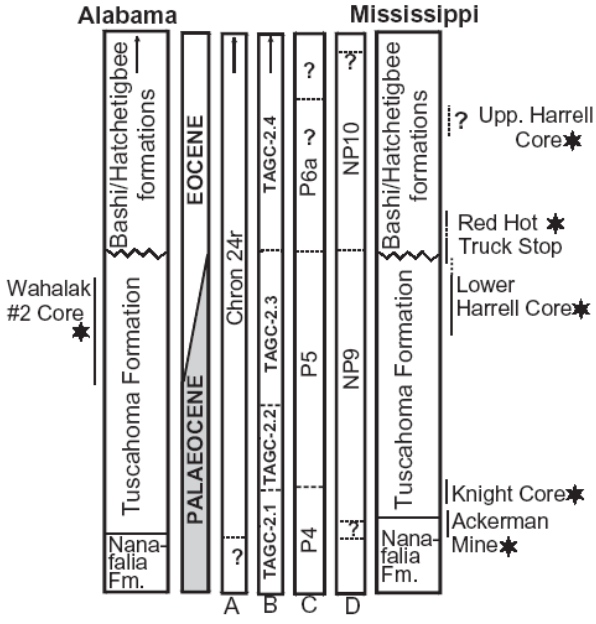

Figure 4. Stratigraphy of the eastern US Gulf Coast. Parts of the Harrell core are indicated. The PE boundary lies in the upper Tuscahoma Formation in Zone NP9. From Harrington et al. (2004).

3.2. Methods

A pilot study on the dinocyst content of the St. Stephens and the Harrell core shows the abundant presence of *Apectodinium* suggesting the PETM is likely to occur in the studied intervals. The first aim is to find the PETM using stable carbon isotope analysis on total organic carbon (TOC). Then, temperature reconstructions are made with the organic sea surface temperature proxy TEX_{86} and with mean annual air temperature calibrations based on terrestrial MBT and CBT ratios. Finally, detailed analysis of the dinocyst assemblages of pre-, during and post-PETM sediments will be done for a paleo-environmental reconstruction of the subtropical shelf sea.

All samples are freeze dried and subsequently measured for magnetic susceptibility using an AGICO KLY-3 at Fort Hoofddijk, Utrecht University. Magnetic susceptibility (MS) is expressed in SI units per gram of sediment.

For analyzing the carbon content and $\delta^{13}C$, approximately 1 gram sediment of the samples is crushed. The carbonate is removed from the sediment by acidification

with 1M HCl. Weight loss reflects a rough estimate of the amount of dissolved carbonate. The remaining sediments are analyzed for $\delta^{13}C$ using a Fison NA 1500 CNS analyzer that is connected to a Finnigan Delta Plus mass spectrometer. Sample preparation and analysis is done in the Geolab at Utrecht University.

For organic geochemistry, sediment is crushed and extracted with a Dionex accelerated solvent extractor (ASE) in the Geolab at Utrecht University. The total lipid extract obtained from the ASE is dissolved in a mixture with dichloromethane/methanol (9:1, v/v) and is further condensed by rotary evaporation under decreasing air pressure. The extract is then separated into an apolar and polar fraction using a column with activated Al_2O_3 powder using dichloromethane and dichloromethane/methanol (1:1, v/v), respectively. The polar fraction is dried under a nitrogen flow, redissolved in hexane/isopropanol (99:1, v/v) and filtered through a 0.4 µm PTFE filter. The GDGTs are detected by an Agilent 1100 MSD high performance liquid chromatography / mass spectrometry (HPLC/MS) at the Royal Netherlands Institute of Sea Research (NIOZ), Texel, the Netherlands. Quantification is done by integration of the peak areas of the corresponding GDGTs. TEX_{86} is calculated following Schouten et al. (2002) and corresponding MASST follows from calibrations by Kim et al. (2008) and Liu et al. (2009).

For palynological analysis, 3 to 3.5 gram sediment is crushed and a known number of the exote *Lycopodium* is added. Carbonates and siliciclastic material is dissolved using 30% HF and 30% HCl at the Laboratory of Palaeobotany and Palynology at Utrecht University. The organic residue is sieved with a 125 µm and subsequently a 15 µm sieve. The organic matter of the 15-125 µm fraction is diluted in glycerin water and put onto a microscope slide. The content of each slide is studied using a light microscope. Dinocysts are determined the genus or species level. Taxonomy follows Fensome and Williams (2004). Absolute quantitative numbers are calculated using the relative number of *Lycopodium*.

Several modern dinoflagellate species produce cysts that are morphologically dependent on prevailing environmental variables such as ocean water chemistry and physics as well as various biological and ecological aspects (Ellegaard 2000, Mertens et al. 2009). Therefore, and due to the absence of preserved genetic structures, the taxonomy of dinocysts used to reconstruct the paleoenvironment is based on morphotypes. The cysts can be grouped in single species, groups of species, genera or complexes (groups of genera) if all morphotypes within one group are considered to represent consistent environmental parameters. In this study, ecological grouping is done following (Sluijs and Brinkhuis 2009). Recently, the affinity of several dinocysts groups for various environmental variables has been statistically analyzed using CCA and PCA plots (Sluijs and Brinkhuis 2009).

4. Results

4.1. Carbonate content

A rough estimate of the carbonate content shows fluctuations between 6 and 19% between the base of the Harrell core and 118.6 mbs. Around 121.5 mbs a decreasing trend initiates with a minimum of 1.8% carbonate at 117.8 mbs. Much larger fluctuations of 5 to 25% occur throughout the top of the record (Figure 5a).

The carbonate content of the St. Stephens core generally fluctuates with irregular depth intervals between 6 and 18% (Figure 5b). Two peaks of approximately 22% are indicated at 208 and 204 mbs, preceded by an outstanding peak of 53% at 212 mbs.

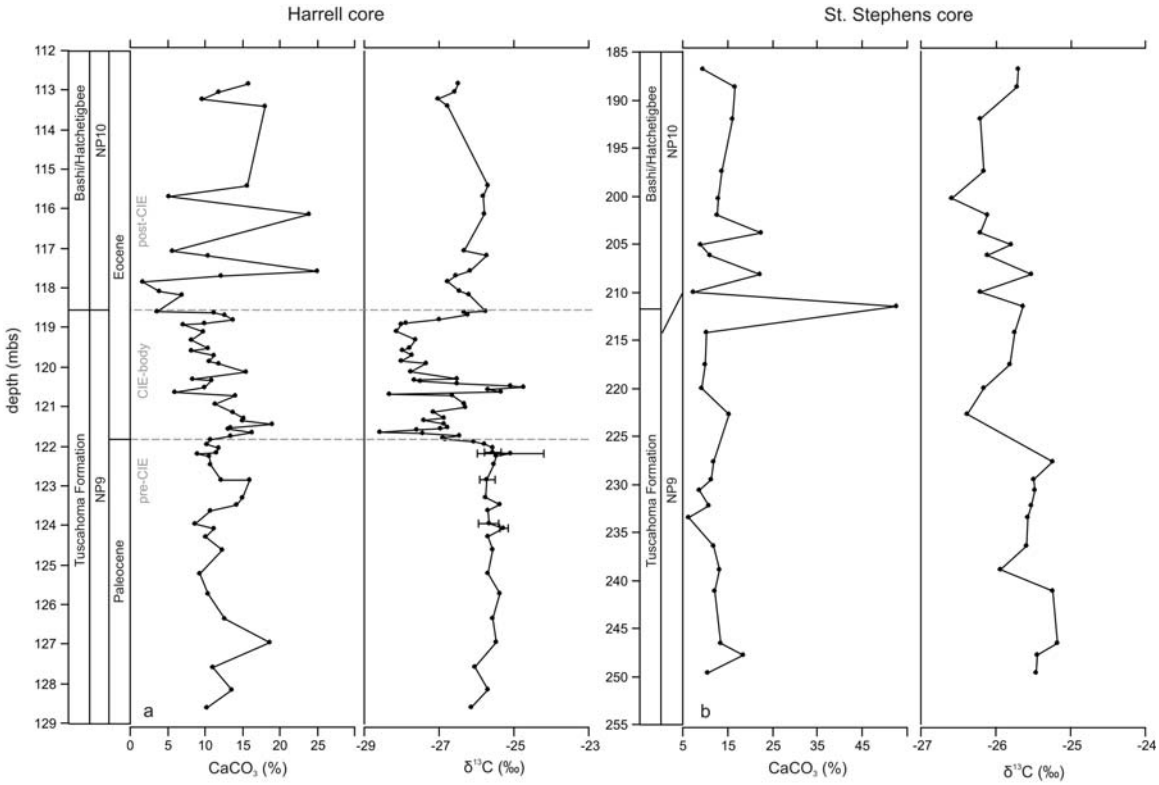

Figure 5. Carbonate content and stable carbon isotopes of the Harrell core and the St. Stephens core. Harrell core (a) and St. Stephens core (b). Carbonate content as weight percentage of total sediment and $\delta^{13}C$ is in ‰ VPDB). Dashed lines indicate sequence boundaries coinciding with the onset and termination of the CIE-body.

4.2. Stable carbon isotopes

The stable carbon isotope data of the Harrell core is obtained in five different runs which are corrected for a possible drift, sample size effect and compared to an international standard (Appendix I). This results in a record based on 75 samples representing the interval between 128.6 and 112.8 mbs (Figure 5a). The $\delta^{13}C$ compilation record fluctuates between -26.2 to -25.1‰ between 129 and 122 mbs. Between 122.0 and 121.8 mbs, $\delta^{13}C$ rapidly drops from -25.6 to -26.9‰. A small peak at 121.7 mbs is followed by further decrease to -28.6‰ at 121.6 mbs. The two phases of $\delta^{13}C$ decrease are considered to be a two-step CIE. Between 121.9 and 118.9 mbs, $\delta^{13}C$ values remain low. This trend is interrupted by 1.5-2.0‰ shifts: a sharp negative peak at 120.7 mbs and a positive peak between 120.6 and 120.5 mbs. Between 118.9 and 118.7 mbs, $\delta^{13}C$ returns to pre-CIE values. Subsequently, post-CIE fluctuations of ~1‰ last up to 115.4 mbs. Samples between 113.4 and 112.8 mbs vary between -27.0 and -26.6‰.

The St. Stephens core shows a gradual trend from -25.5‰ to -26.5‰ $\delta^{13}C$ in the interval from 250 to 190 mbs (Figure 5b). Fluctuations are usually smaller than 0.5‰.

4.3. Magnetic susceptibility

The upper Tuscahoma Formation of the Harrell core shows magnetic susceptibility (MS) that generally fluctuates between 7.3 and 11.3 SI g^{-1} (Figure 6). An exception is a sharp increase between 121.9 and 121.7 mbs with a maximum of 20.9 SI g^{-1} at 121.8 mbs. The Bashi-Hatchetigbee Formation shows an average MS that is 6 SI g^{-1} lower than for the Tuscahoma Formation.

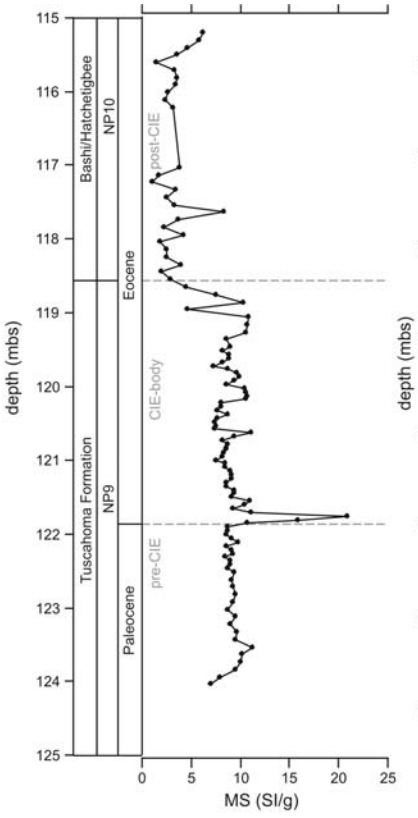

Figure 6. Magnetic susceptibility of the Harrell core. Magnetic susceptibility is expressed in SI g^{-1}. Dashed lines indicate sequence boundaries coinciding with the onset and termination of the CIE-body.

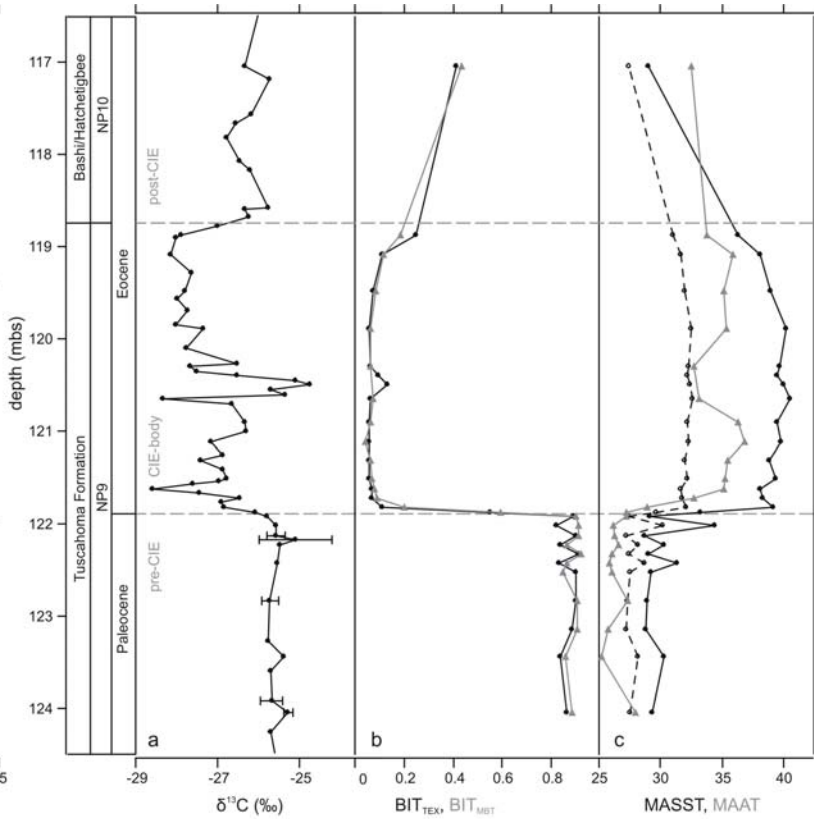

Figure 7. $\delta^{13}C$, BIT, MASST and MAT of the Harrell core. $\delta^{13}C$ (a); BIT_{TEX} (black) and BIT_{MBT} (grey) (b); $MASST_{Kim}$ (black, closed line), $MASST_{Liu}$ (black, dashed line) and MAAT (grey) (c). Dashed lines indicate sequence boundaries coinciding with the onset and termination of the CIE-body.

4.4. TEX_{86}, MBT and BIT

Analysis of the isoprenoid GDGTs from the Harrell core leads to a record of the BIT_{TEX} index as shown in Figure 7b. Values are extremely high (0.82 to 0.91) from the base of the record up to the CIE. Between 122.5 and 121.9 mbs, 3 regularly spaced drops in BIT occur. A sharp shift at the CIE mbs precedes an interval of values as low as 0.06 to 0.11 for the uppermost Tuscahoma Formation. A slight increase within this phase to a maximum of 0.13 occurs at 120.5 to 120.4 mbs. In the Bashi-Hatchetigbee Formation, two data points suggest an increasing trend to 0.41 during the post-CIE. The BIT index that follows from the branched tetraethers (BIT_{MBT}) shows a very similar pattern with slightly higher (up to 0.11) values in the CIE-body (Figure 7b). Another difference is that no data could be obtained for samples at 120.5 and 120.4 mbs where BIT_{TEX} shows a slight increase.

Original TEX_{86} data are shown in Appendix II. MASST calculations following Kim et al. (2008) and Liu et al. (2009) ($MASST_{Kim}$ and $MASST_{Liu}$, respectively) are plotted together with MAAT calculations following Weijers et al. (2007b) in Figure 7c.

$MASST_{Kim}$ fluctuates around ~30 °C below the CIE, whereas $MASST_{Liu}$ is approximately 28 °C. The fluctuations in the pre-CIE of both records are strongly correlated to BIT_{TEX}. Above the CIE and up to the formation boundary, $MASST_{Kim}$ varies between 38 to 40 °C. $MASST_{Liu}$ shows a smaller 5 °C increase up to ~32.5 °C and also fluctuations are smaller within the interval. Both $MASST_{Kim+}$ and $MASST_{Liu}$ return to a pre-CIE value in the Bashi-Hatchetigbee Formation.

MAAT fluctuates between 25.3 and 27.9 °C throughout the pre-CIE interval. Subsequently, MAAT increases at the CIE and continues to 35.2 °C at 121.62 mbs. Temperatures remain high within the CIE-body, although they are ~2.5 °C lower at 120.65 and 120.29 mbs. In the Bashi-Hatchetigbee Formation, MAAT drops by ~1 °C.

4.5. Palynology

Terrestrial palynomorphs are extremely abundant in pre-CIE samples of the Harrell core, whereas dinocysts are almost absent (Figures 8 and 9). At the CIE, percentages drop from an average of 96% to 70% and further down to almost 10% at 120.09 mbs. At 119.48 and 117.55 mbs the terrestrial input slowly goes back up to a maximum of 59%. This trend is interrupted by a peak of 68% corresponding to the sample at 120.50 mbs containing very few palynomorphs (Figure 9). Other marine palynomorphs such as acritarchs and foraminiferal linings are more abundant during the pre-CIE compared to the CIE-body and post-CIE.

The occurrence of *Muratodinium fimbriatum* is restricted to the latest Paleocene and earliest Eocene (Powell et al. 1996) indicating that the presence of this species in the Harrell core confirms this time interval. The same is suggested by the presence of *Florentinia reichartii* which was until now only been observed for latest Paleocene and earliest Eocene sediments from the New Jersey shelf (Sluijs and Brinkhuis 2009). *Diphyes colligerum* also originated in the Late Paleocene, but occurred until the latest Eocene (Bujak and Mudge 1994, Powell et al. 1996).

Dinocyst assemblages of the Harrell core contain significant relative abundances (>5%) of specimens assigned to the *Areoligera* complex, *Cordosphaeridium* complex, *Senegalinium* complex and *Spiniferites* complex. Other common or abundant taxa are *Apectodinium*, *Diphyes colligerum*, *Florentinia reichartii* and *Operculodinium*. *Apectodinium* is studied as a total genus containing the traditional species *A. homomorphum*, *A. quinquelatum*, *A. parvum* and *A. hyperacanthum*. In addition to the subdivision on the species level, the species are subdivided in two groups. The first group contains all traditional morphotypes with distally closed and rounded processes. The second group is comprised of the same actual species, but the processes are characterized by distal furcations similar to the processes of *Wetzeliella astra* (Costa et al. 1978). Hence, their sub-genera will be further unofficially referred to as *Apectodinium* 'non-astra' and *Apectodinium* 'astra' Percentual abundances of the taxa and complexes described above are plotted together in Figure 8, whereas the absolute abundance per gram sediment is plotted in Figure 9. Pictures of important species are shown on Plate 1-3.

The pre-CIE interval contains less than 500 dinocysts per gram sediment which results in less than 200 cyst counts for one or two analyzed slides. Average percentages per taxon of all assemblages within the pre-CIE interval will be further used to estimate the Late Paleocene dinocyst composition. Also samples at 120.50 and 118.57 mbs contain insufficient dinocyst for quantative interpretations.

The pre-CIE interval contains almost 45% peridinioid cysts, mainly represented by the *Apectodinium* 'non-astra' group and the *Senegalinium* complex (Figure 8). The *Cordosphaeridium* complex, *Operculodinium* and the *Spiniferites* complex are also well represented. The *Areoligera* complex does not appear below 122.43 mbs. From there, abundances are approximately 10%. *Diphyes colligerum* and *Florentinia reichartii* are absent in most of the pre-CIE, but are observed in one or two samples.

At the CIE, all taxa show an abrupt increase in absolute abundance with the exception of the *Senegalinium* complex and *Cordosphaeridium* complex which show a depletion followed by a sharp increase (Figure 9). Subsequently, all taxa show a decline up to the almost barren sample at 120.50 mbs. The total relative abundance of total peridinioids, mainly represented by *Apectodinium*, also follows this trend of strong increase and subsequent decrease (Figure 8). *Apectodinium* 'astra' has a first occurrence in this record of 60% at the CIE and increases more before it decreases down to 0% in the almost barren sample. *Apectodinium* 'non-astra' shows the opposite pattern with a decrease at the CIE and a subsequent increase. At the CIE, *Diphyes colligerum* increases and continues to increase, whereas the *Areoligera* complex remains relatively stable. The *Senegalinium* complex, the *Spiniferites* complex, the *Cordosphaeridium* complex, the *Senegalinium* complex, *Florentinia reichartii* and *Operculodinium* decrease in abundances at the CIE and subsequently remain stable.

The interval between the almost barren samples at 120.50 and 118.57 mbs shows a total amount of dinocysts as well as the relative abundances of most taxa which is comparable to the sample just below the lower barren sample (Figure 8 and 9). The peridinioid assemblage decreases only slightly in relative abundance as a result of a decrease in *Apectodinium* 'astra' versus an increase in *Apectodinium* 'non-astra' and the *Senegalinium* complex (Figure 8).

The post-CIE sample at 117.55 mbs shows a decrease in absolute abundance relative to the youngest quantified CIE-body sample for all taxa with exception of *Cordosphaeridium* complex and *Operculodinium.* This same sample contains a similar relative abundance of peridinioids compared to the youngest CIE-body sample, since the increase in *Apectodinium* 'astra' equals the decrease in *Apectodinium* 'non-astra' and the *Senegalinium* complex. The *Cordosphaeridium* complex and the *Areoligera* complex increase, whereas *Diphyes colligerum* and *Spiniferites* complex decrease. *Operculodinium* reappears in the Bashi Marl Member.

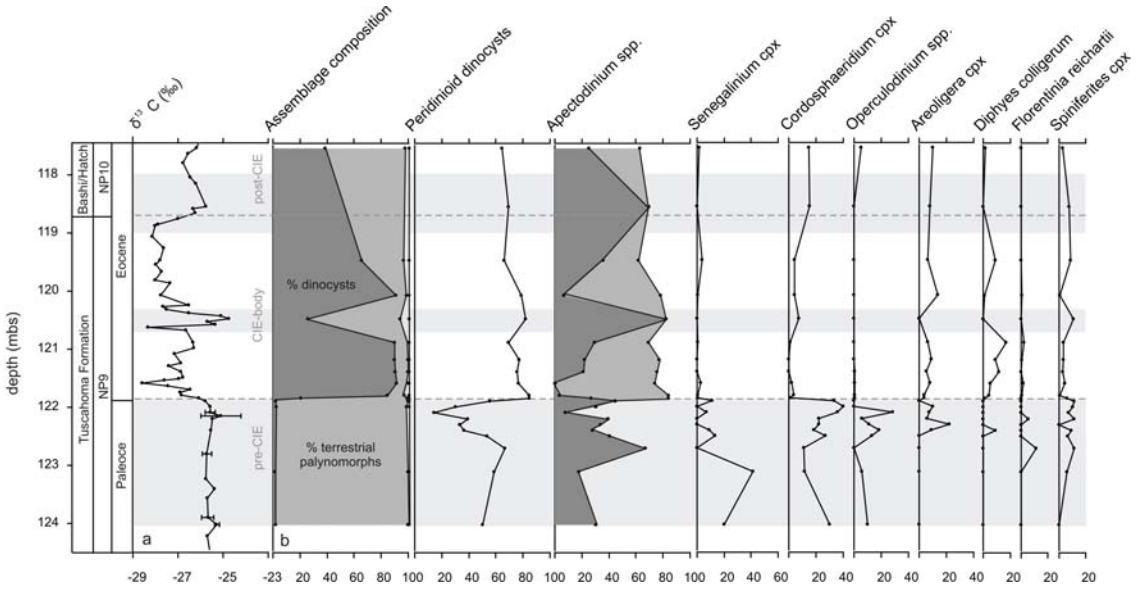

Figure 8. Relative abundance of dinocysts and terrestrial palynomorphs in the Harrell core. Stable carbon isotope record (a) and relative abundance of palynomorphs (b). Assemblage composition represents the percentage of total dinocysts (dark grey), terrestrial palynomorphs (middle grey) and marine palynomorphs other than dinocysts (light grey) relative to total amount of terrestrial and marine palynomorphs. Abundance of total Peridinioids, *Apectodinium* (comprised of *Apectodinium* 'non-astra' (dark grey) and *Apectodinium* 'astra' (middle grey)), *Senegalinium* complex, *Cordosphaeridium* complex, *Operculodinium*, *Areoligera* complex, *Diphyes colligerum*, *Florentinia reichartii* and *Spiniferites* complex as percentage of total dinocyst assemblage. Dashed lines indicate sequence boundaries coinciding with the onset and termination of the CIE-body. Shaded areas are intervals corresponding to the samples with low dinocyst content.

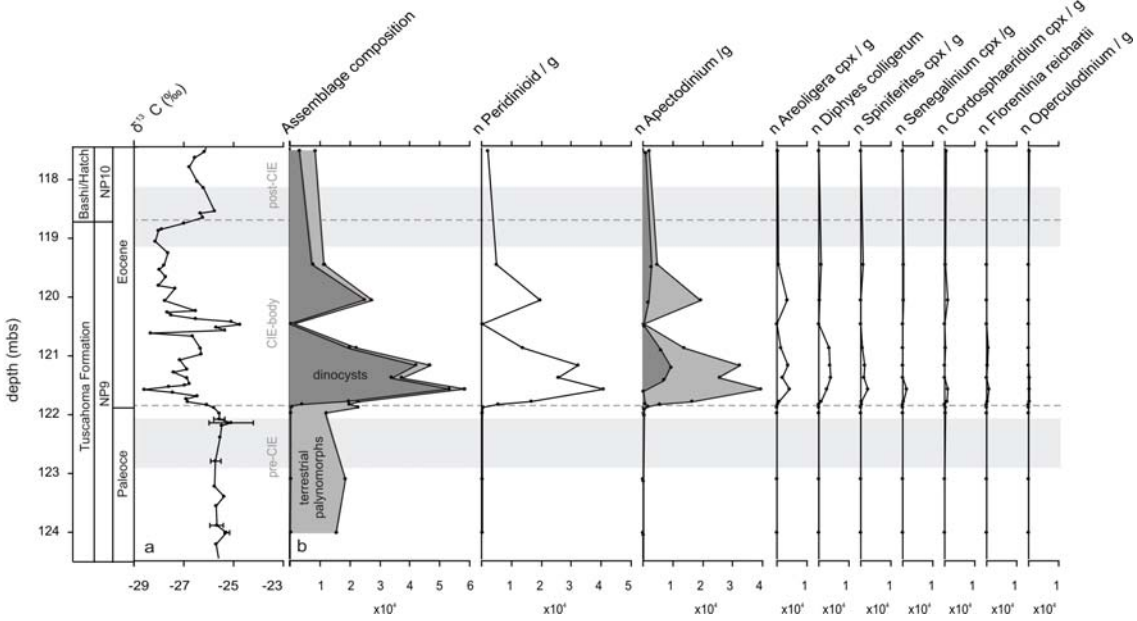

Figure 9. Absolute abundance of dinocysts and terrestrial palynomorphs in the Harrell core. Stable carbon isotope record (a) and absolute abundance of palynomorphs (b). Assemblage composition represents the percentage of total dinocysts (dark grey), terrestrial palynomorphs (middle grey) and marine palynomorphs other than dinocysts (light grey) per gram of sediment. Abundance of total Peridinioids, *Apectodinium* (comprised of *Apectodinium* 'non-astra' (dark grey) and *Apectodinium* 'astra' (middle grey)), *Areoligera* complex, *Diphyes colligerum*, *Spiniferites* complex, *Senegalinium* complex, *Cordosphaeridium* complex, *Florentinia reichartii* and *Operculodinium* per gram of sediment. Dashed lines indicate sequence boundaries coinciding with the onset and termination of the CIE-body. Shaded areas correspond to the samples of which the dinocyst content was only determined qualitatively.

5. Revised stratigraphy

The stable carbon isotope record of the Harrell core shows a distinct negative excursion followed by an interval of more ^{13}C-depleted values (Figure 5a). Although *Apectodinium* was already abundant prior to this CIE, its abundance increases substantially at the CIE assuming this is the *Apectodinium* acme (Figure 8). Therefore, the PETM is considered to be present in this core.

A strong peak in MS coincides with the CIE and is considered to reflect a sequence boundary (Figure 6). Since also sharp changes in BIT, MASST, MAAT and dinocysts assemblages coincide with the CIE and peak in MS (Figures 7 and 8), it is expected that the onset of the PETM is lost due to at least a small hiatus between the latest Paleocene and earliest Eocene. This hiatus is also suggested by the absence of certain pollen species in the top of the Tuscahoma Formation that are present in the latest Paleocene strata in Virginia (Frederiksen 1982). The CIE, the peak in MS and thus the PETM initiate at 121.9 mbs based on a significant deviation of $\delta^{13}C$ and MS from the mean pre-CIE value using a 95% confidence level.

The interval of more depleted $\delta^{13}C$ values corresponding to the *Apectodinium* acme also shows increased sea surface and air temperature and is considered to represent the CIE-body (Figures 5a, 7 and 8). A distinct layer interrupts the CIE-body between 120.60 and 120.45 mbs. Although the BIT index and MASST appear unaffected and thereby exclude the possibility of reworking (Figure 7), the $\delta^{13}C$ record shows a large positive excursion (Figure 5a). This mica-rich layer is highly depleted in both terrestrial and marine palynomorphs and contains slightly less carbonate than the adjacent intervals (Figure 5a and 9).

A negative shift in MS corresponds to the formation boundary which is associated with a sequence boundary (Figure 6). Therefore, another hiatus appears to terminate the CIE-body. Possibly, the tail of the recovery phase is represented in the Bashi Marl Member as $\delta^{13}C$ is still increasing towards pre-CIE values and *Apectodinium* is abundant (Figures 7 and 8). Unfortunately, temperature reconstructions are absent for the lowermost Bashi Marl Member. No accurate estimate of the duration of the hiatus can be made, although Early Eocene dinocysts such as *Florentinia reichartii* and *Muratodinium fimbriatum* are still present and the dinocyst composition does not significantly change (Figure 8).

Another peak in MS occurs at 117.65 mbs within the Bashi Marl Member (Figure 6), but does not coincide with remarkable trends in other proxies. Non-quantitative analysis of samples obtained from above the bed of boulders in the Bashi Marl Member, however, shows that the relative abundance of *Apectodinium* has significantly declined. Furthermore, a clear change in dinocyst assemblage can be seen by the increased diversity of the *Cordosphaeridium* complex and increased abundance of some of its members such as *Muratodinium fimbriatum*. Also, *Impagidinium elegans* and *Wetzeliella articulata* appear at 112.8 mbs suggesting an age further up in the Eocene (Costa and Downie 1976). Therefore, a larger hiatus is expected at the base of the boulders. The entire studied interval of the Bashi Marl Member may still correspond to zone NP10 as it has been assigned to by Gibson and Bybell (1994).

The stable carbon isotope record of the St. Stephens core does not show a distinctive negative excursion. Since the pilot study on the dinocyst content shows that *Apectodinium* is abundant in the lowermost part of the record up to 229.5 mbs, the onset could be situated below the sampled interval. On the other hand, sedimentation rates are expected to be lower compared to the Harrell core since this site is located further towards the basin center. The sampling resolution, however, is much coarser than for the Harrell core so that the PETM could in fact be overlooked.

6. Discussion

6.1. Temperature

MBT and TEX_{86} derived temperatures increase at the onset of the PETM indicating warming of the atmosphere as well as the sea surface (Figure 7). MAAT was ~26.4 °C prior to the PETM and increased by 7.5 °C to an average of 33.9 °C during the PETM. MASST calibrated following Kim et al. (2008) increased by 8.7 °C at the CIE from approximately 30.0 °C to 38.7 °C. Due to high BIT values prior to the PETM, MBT based MAAT is considered to be more reliable since TEX_{86} based MASST could be biased by terrestrial lipids (Weijers et al. 2006b). Low BIT values during the PETM suggest that MAAT may be less reliable for this interval due to potential *in situ* production of branched GDGTs in marine settings (Peterse et al. 2009). Therefore, MAAT is used for pre-PETM temperature estimates, whereas MASST is used to estimate PETM temperatures.

Increase in temperature is considered to have facilitated the expansion of *Apectodinium* to mid and high latitudes (Sluijs et al. 2006). However, temperature alone shows only a weak correlation with the presence of *Apectodinium* (Sluijs and Brinkhuis 2009). At the Gulf Coast, *Apectodinium* was already abundant prior to the PETM indicating that a SST of ~30.0 °C was sufficiently warm to enable the growth of *Apectodinium* (Figure 8). During the PETM, *Apectodinium* increased in abundance suggesting that further warming was in favor of the growth of *Apectodinium* relatively to the growth of other taxa.

A continental temperature reconstruction based on pollen of the Gulf Coast region shows values very similar to the MAAT of the Harrell core suggesting that the MBT proxy works effectively (Figure 7)(Wolfe and Dilcher 2000). TEX_{86} based MASSTs of the Harrell core are almost equal to those obtained for the more northerly situated Bass River and Wilson Lake sites on the New Jersey shelf (Sluijs et al. 2007b). This applies to both the pre-PETM and PETM interval suggesting that pre-CIE MASSTs of the Harrell core may not be significantly biased.

The absolute temperature increase at the CIE is difficult to quantify for the Harrell core. The extent of increase based on either MBT or TEX_{86} would be biased as these proxies generate unreliable values for the PETM or pre-PETM interval, respectively. Instead, pre-PETM MAAT could be compared to PETM MASST resulting in a temperature increase of almost 12 °C. However, MAAT is lower than MASST prior to and during the PETM suggesting that the difference in temperature of the ocean and atmosphere would add up to the actual temperature increase of either realm. Furthermore, the temperature increase based on MBT and TEX_{86} independently is within the range of the temperature increase observed at other mid and high latitude sites (Figure 10)(Sluijs et al. 2006, Zachos et al. 2006, Sluijs et al. 2007b, Weijers et al. 2007a).

Climate models imply larger temperature gradients during the Early Paleogene than observed in several mid and high latitude temperature records based on TEX_{86} and MBT (Shellito et al. 2003, Sluijs et al. 2006, Zachos et al. 2006, Sluijs et al. 2007b, Weijers et al. 2007a). Huber (2008) suggests that traditional temperature proxies such as foraminiferal $\delta^{18}O$ and Mg/Ca are generating inaccurate estimates and that tropical temperatures may in fact have been over 40 °C. This would explain extinction of tropical flora as a result of thermal stress and the extent of changes in the carbon cycle. Moreover, this hypothesis implies a latitudinal temperature gradient larger than observed in proxy data during the Early Paleogene. However, absolute MASSTs of the Harrell core across the PETM are comparable to New Jersey, thereby implying hardly any gradient. This is consistent with the suggestion of a lower latitudinal temperature gradient than implied by climate models (Figure 10)(Shellito et al. 2003, Bijl et al. 2009). Furthermore, although tropical temperatures of

approximately 40 °C would somewhat increase the temperature gradient, it would still be much smaller than implied by climate models (Shellito et al. 2003). Moreover, floral extinction as observed by Harrington and Jaramillo (2007) could have been caused by episodes of warming above 40 °C, whereas the average PETM temperature is below the critical limit of thermal stress. Finally, the temperature increase at the CIE of the Harrell core is of similar extent compared to mid and high latitudinal sites (Sluijs et al. 2006, Zachos et al. 2006, Sluijs et al. 2007b, Weijers et al. 2007a) suggesting that the latitudinal temperature gradient of the latest Paleocene and during the PETM should not deviate much.

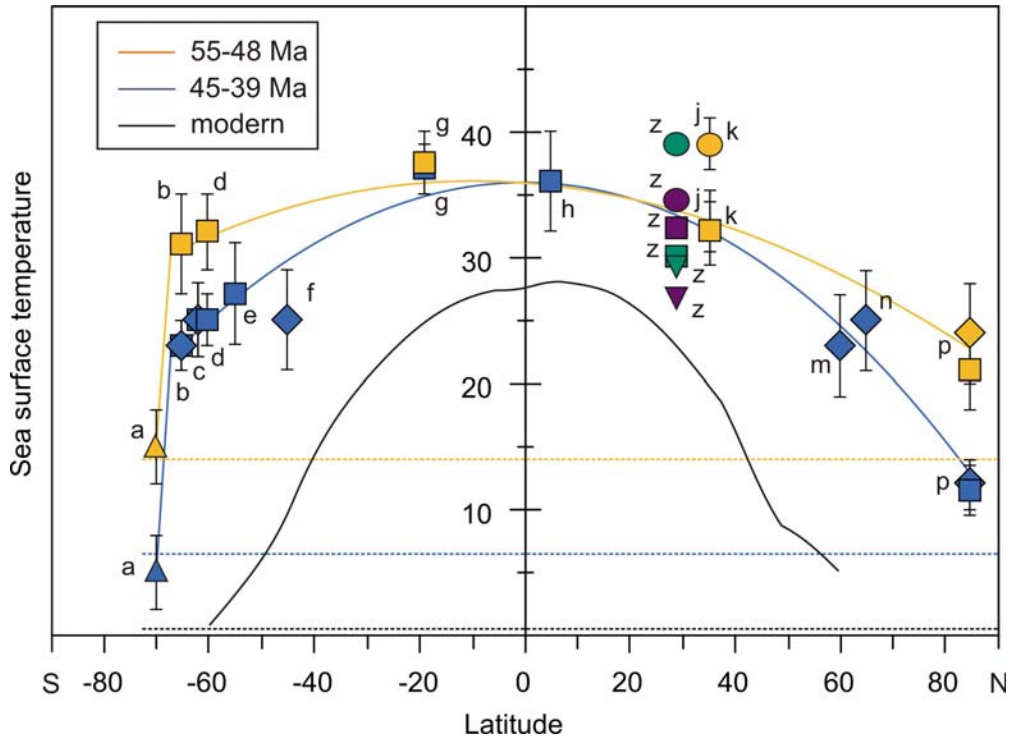

Figure 10. Early and Middle Eocene latitudinal SST gradients. Bivalve-shell $\delta^{18}O$ (up triangles), TEX_{86} (squares) and $U^{k'}_{37}$ (diamonds) SST reconstructions for the Early (orange) and mid-Middle (blue) Eocene. Data are from Seymour Island (a), the East Tasman Plateau (b), Deep Sea Drilling Project (DSDP) Site 277 (c), New Zealand (d), DSDP Site 511 (e), ODP Site 1090 (f), Tanzania (g), ODP Site 925 (h), New Jersey (j, k; circle represents peak PETM SSTs), ODP Site 336 (m), ODP Site 913 (n) and the Arctic Ocean (p). For references see Bijl et al. (2009). Harrell core (z) TEX_{86} SSTs (green) and MBT MAT (purple) of the latest Paleocene (down triangles), PETM (circles) and earliest Eocene (squares). Error bars indicate the range of variation. Gradients represent second-order polynomials, excluding bivalve-shell data. Black and dashed lines represent the present-day zonally averaged latitudinal temperature gradient and age-specific deep-sea temperatures, respectively. Figure after Bijl et al. (2009).

6.2. Sea level

The BIT index shows that branched GDGTs strongly dominate crenarchaeol in the pre-CIE interval suggesting that soil input into the marine basin was extremely high (Figure 7). This is more likely to occur when sea level is low and the studied site is situated near river mouths (Hopmans et al. 2004). Also the palynomorph assemblage implies a very shallow marine setting as the few dinocysts are dominated by high abundances of pollen and spores (Figure 8). However, typical lagoonal dinocysts such as *Eocladopyxis*, *Heteraulacacysta* and *Polysphaeridium* are not significantly abundant. Representatives of the *Areoligera* are considered to have occurred dominantly in inner neritic shelf settings, whereas members of the *Spiniferites*

complex represent more outer neritic as well as inshore conditions (Wall et al. 1977, Brinkhuis 1994, Pross and Brinkhuis 2005, Sluijs et al. 2008a). Also the *Cordosphaeridium* complex predominantly occurs in inner neritic settings (Pross and Brinkhuis 2005, Sluijs and Brinkhuis 2009). The presence of the *Areoligera* complex and peak abundance of the *Cordosphaeridium* complex in the youngest half of the pre-CIE interval corresponds to an inner neritic high energy setting. The sequence boundary at onset of the CIE either represents a phase in which no sedimentation occurred or a phase of relative sea level fall and subsequent erosion. The sediments on top of this unconformity suggest a more outer neritic shelf setting by the increased abundance and diversity of dinocysts (Figure 8). Conclusively, the relative sea level is significantly higher during the PETM compared to the pre-CIE interval. This is consistent with other records indicating sea level rise during the PETM (Sluijs et al. 2008a).

6.3. Other environmental variables

Extant peridinioids of the *Senegalinium* complex have shown to be heterotrophs and are considered to be related to peridinioids such as *Apectodinium* (Bujak and Brinkhuis 1998). Their preference for high nutrient and high food supply settings has also been suggested by Dale and Fjellså (1994) and Sluijs et al. (2005) implying that most of the record reflects a continuous high productivity environment (Figure 8). The drop in relative abundance of peridinioids shortly before the CIE may indicate a less nutrient and food enriched setting. However, the pre-CIE trends in relative abundance of peridinioids may not be reflecting true productivity trends since *Apectodinium* and *Senegalinium* show opposite patterns and dinocyst counts are extremely low in this interval (Figure 8 and 9). High terrestrial input as indicated by high BIT values (Figure 7) is likely to be supplied by river inflow which would then also supply nutrients to the basin. Productivity was highest during the CIE-body and in particular shortly after the CIE where the absolute abundance of the peridinioids peaks (Figure 9).

Living cells producing cysts of the *Senegalinium* complex have shown to be fresh water tolerant (Röhl et al. 2004b, Brinkhuis et al. 2006, Sluijs et al. 2006, Sluijs et al. 2007b, Sluijs et al. 2008b). The presence of the *Senegalinium* complex together with the input of terrestrial palynomorphs and a high BIT index in the pre-CIE interval of the Harrell core imply that river inflow was significant (Figure 7 and 8). High morphological variability of members of the *Cordosphaeridium* complex are possibly related to variable salinity (Sluijs et al. 2005).

Polysphaeridium zoharyi is a typical indicator taxon for hyperstratified sea surface waters (Reichart et al. 2004). Its absence in the Harrell core suggests that the sea surface was most likely not hyperstratified prior to and during the PETM.

Apectodinium 'astra' is yet unknown to respond to any environmental variable. Remarkably, it does not occur before the CIE (Figure 8). Possibly, the formation of this morphotype was initiated during the PETM after the environment changed substantially and may have required high temperature or increased sea level. *Apectodinium* 'astra' is absent in the samples with low dinocyst counts, but remains abundant after the PETM. This implies that sea level is more likely to play a role in the presence of *Apectodinium* 'astra' than temperature, although accompanying changes during the PETM are also not excluded. Salinity is studied for its effects on process development of *Lingulodinium machaerophorum* cysts (Mertens et al. 2009). Possibly, salinity also affected the process development of *Apectodinium*. Another explanation for the appearance of *Apectodinium* 'astra' at the CIE is that this morphotype evolved at this time. Also *Wetzeliella astra* originated from related Wetzeliellans in nannoplankton zone NP10 in the Early Eocene (Powell 1988).

6.4. Leads and lags

Due to the hiatus at the CIE, no interpretations can be made about the succession of the CIE, sea surface warming and the *Apectodinium* acme. *Apectodinium* was already abundant prior to the CIE, but the actual acme is considered to originate at the CIE (Figure 8). MASST appears to show some increase in temperature in the uppermost pre-CIE interval (Figure 7). However, these fluctuations are directly related to the BIT index and therefore unreliable. MAAT in the same interval does not show this temperature suggesting that sea surface temperature most likely did not increase either. As a result, data obtained from the Harrell core are not suitable for supporting the succession of the *Apectodinium* acme, sea surface warming and the CIE in that particular order as observed at Bass River and Wilson Lake at the New Jersey shelf and at a locality in the North Sea (Figure 1.)(Sluijs et al. 2007b).

7. Conclusions

The PETM was detected in the Harrell core from Meridian, Mississippi. The pre-CIE interval is characterized by extremely high terrestrial input into a shallow marine basin. The onset PETM is at least partially lost due to a hiatus. Therefore, the initiation of the CIE, temperature rise and *Apectodinium* acme can not be compared to study the succession of events as observed for three mid latitude sites (Sluijs et al. 2007b). At the CIE, MAAT and MASST increased substantially, though suggesting that the latitudinal temperature gradient was much lower than implied by climate models (Shellito et al. 2003). The range in absolute temperatures as well as the extent of warming are consistent with data obtained from various sites in earlier studies (Wolfe and Dilcher 2000, Sluijs et al. 2006, Zachos et al. 2006, Sluijs et al. 2007b, Weijers et al. 2007a). Dinocysts become much more abundant and diverse after the CIE and the terrestrial input decreases abruptly, both indicative of an increased sea level consistent with observations at other sites (Sluijs et al. 2008a). Within the CIE-body, both temperatures as well as the dinocyst assemblage do not show much change. Only a 15 cm layer of mica-rich sediment shows extreme deviations in stable carbon isotopes and palynomorph composition, whereas BIT and temperature proxies appear unaffected. The PETM is terminated by a sequence boundary. The post-CIE interval suggests that temperatures and the stable isotope record recovered. Sediments on top of the sequence boundary indicate a deeper marine setting compared to the pre-CIE interval as the BIT index is not as high and the dinocyst abundance and diversity is comparable to the latest PETM.

Acknowledgements

Over the past year I've been making progress toward accomplishing this thesis little by little. Every step involved several people who I owe my sincere gratitude. Henk was my key to the world of palaeo-ecology. First, by teaching few of the most interesting courses that combined my beloved field of biology with earth sciences which has always been appealing to me as well. Then, by offering me a project that eventually turned out into this thesis. Appy introduced me to the wonderful world of the PETM and helped me getting grip on the overkill on information, obscurities and contradictions. His inexhaustible enthusiasm has been a great drive for me. I acknowledge the opportunity for me to work in the labs of Gert-Jan and Stefan Schouten. David Dockery of the Geological Survey of Mississippi and Lewis Dean of the Geological Survey of Alabama are thanked for access to the sediment cores and their assistance with sampling. Jocelyn Sessa and Guy Harrington are thanked for sharing information on the Harrell core and for their interest in the project. They were both involved in obtaining and interpreting some of the most interesting data. Jan van Tongeren, Arnold van Dijk, Jort Ossebaar, Micha Ruhl, Peter Bijl and Sander Houben are thanked for assistance in the various labs and with microscopy. Finally, moral support and support in any possible way was supplied by the staff of Palaeo-ecology, Marjolein Mullen, Leonard Bik, Natasja Welters, the palaeo-PhD's, fellow students, friends and family, the notorious SpongeBob tosti-maker and radio 3FM. Last and also definitively least, possible typos or the presence of complete nonsense within this thesis are indisputably due to a certain singing deer.

References

Abdul Aziz, H., F. J. Hilgen, G. M. van Luijk, A. Sluijs, M. J. Kraus, J. M. Pares, and P. D. Gingerich. 2008. Astronomical climate control on paleosol stacking patterns in the upper Paleocene - lower Eocene Willwood Formation, Bighorn Basin, Wyoming. Geology **36**:531-534; doi: 510.1130/G24734A.

Berggren, W. A. 1965. Some problems of Paleocene-lower Eocene planktonic foraminiferal correlations. Micropaleontology **11**:276-300.

Bijl, P. K., S. Schouten, A. Sluijs, G. J. Reichart, C. Zachos James, and H. Brinkhuis. 2009. Early Palaeogene temperature evolution of the southwest Pacific Ocean. Nature **461**:776-779.

Bockstahler, K. R., and D. W. Coats. 1993a. Grazing of the mixotrophic dinoflagellate Gymnodinium sanguineum on ciliate populations of Chesapeake Bay. Marine Biology **116**:477-487.

Bockstahler, K. R., and W. D. Coats. 1993b. Spatial and temporal aspects of mixotrophy in Chesapeake Bay dinoflagellates. Journal of Protozoology **40**:49-60.

Bowen, G. J., D. J. Beerling, P. L. Koch, J. C. Zachos, and T. Quattlebaum. 2004. A humid climate state during the Palaeocene/Eocene thermal maximum. Nature **432**:495-499.

Bowen, G. J., T. J. Bralower, M. L. Delaney, G. R. Dickens, D. C. Kelly, P. L. Koch, L. R. Kump, J. Meng, L. C. Sloan, E. Thomas, S. L. Wing, and J. C. Zachos. 2006. Eocene Hyperthermal Event Offers Insight Into Greenhouse Warming. EOS, Transactions, American Geophysical Union **87**:165, 169.

Bowen, G. J., W. C. Clyde, P. L. Koch, S. Y. Ting, J. Alroy, T. Tsubamoto, Y. Q. Wang, and Y. Wang. 2002. Mammalian dispersal at the Paleocene/Eocene boundary. Science **295**:2062-2065.

Brasier, M. D. 1985. Fossil indicators of nutrient levels. 1: Eutrophication and climate change. Pages 113-132 *in* D. W. J. Bosence and P. A. Allison, editors. Marine

Palaeoenvironmental Analysis from Fossils, Geological Society Special Publication 83.
Brinkhuis, H. 1994. Late Eocene to Early Oligocene dinoflagellate cysts from the Priabonian type-area (Northeast Italy); biostratigraphy and palaeoenvironmental interpretation. Palaeogeography, Palaeoclimatology, Palaeoecology **107**:121-163.
Brinkhuis, H., S. Schouten, M. E. Collinson, A. Sluijs, J. S. Sinninghe Damsté, G. R. Dickens, M. Huber, T. M. Cronin, J. Onodera, K. Takahashi, J. P. Bujak, R. Stein, J. van der Burgh, J. S. Eldrett, I. C. Harding, A. F. Lotter, F. Sangiorgi, H. van Konijnenburg-van Cittert, J. W. de Leeuw, J. Matthiessen, J. Backman, K. Moran, and T. Expedition 302 Scientists. 2006. Episodic fresh surface waters in the Eocene Arctic Ocean. Nature **441**:606-609.
Brinkhuis, H., S. Sengers, A. Sluijs, J. Warnaar, and G. L. Williams. 2003. Latest Cretaceous to earliest Oligocene, and Quaternary dinoflagellate cysts from ODP Site 1172, East Tasman Plateau. Pages 1-48 *in* N. F. Exon, J. P. Kennett, and M. Malone, editors. Proceedings Ocean Drilling Program, Scientific Results.
Bujak, J. P., and H. Brinkhuis. 1998. Global warming and dinocyst changes across the Paleocene/Eocene Epoch boundary. Pages 277-295 *in* M.-P. Aubry, S. G. Lucas, and W. A. Berggren, editors. Late Paleocene - early Eocene climatic and biotic events in the marine and terrestrial records. Columbia University Press, New York.
Bujak, J. P., and D. C. Mudge. 1994. A high-resolution North Sea Eocene dinocyst zonation. Journal of the Geological Society, London **151**:449-462.
Burkholder, J. M., P. M. Glibert, and H. M. Skelton. 2008. Mixotrophy, a major mode of nutrition for harmful algal species in eutrophic waters. Harmful Algae **8**:77-93.
Costa, L. I., C. Denison, and C. Downie. 1978. The Paleocene/Eocene boundary in the Anglo-Paris Basin. Journal of the Geological Society **135**:261-264.
Costa, L. I., and C. Downie. 1976. The Distribution of the Dinoflagellate *Wetzeliella* in the Palaeogene of north-western Europe. Palaeontology **19**:591-614.
Crouch, E. M., C. Heilmann-Clausen, H. Brinkhuis, H. E. G. Morgans, K. M. Rogers, H. Egger, and B. Schmitz. 2001. Global dinoflagellate event associated with the late Paleocene thermal maximum. Geology **29**:315-318.
Dale, B., and A. Fjellså. 1994. Dinoflagellate cysts as paleoproductivity indicators: State of the art, potential and limits. Pages 521-537 *in* R. Zahn, T. F. Pedersen, M. A. Kaminski, and L. Labeyrie, editors. Carbon Cycling in the Glacial Ocean: Constraints on the Ocean's Role in Global Change. Springer, Berlin.
De Rosa, M., and A. Gambacorta. 1988. The lipids of archaebacteria. Progress in Lipid Research **27**:153-175.
Dickens, G. R., M. M. Castillo, and J. C. G. Walker. 1997. A blast of gas in the latest Paleocene: Simulating first-order effects of massive dissociation of oceanic methane hydrate. Geology **25**:259-262.
Dickens, G. R., J. R. O'Neil, D. K. Rea, and R. M. Owen. 1995. Dissociation of oceanic methane hydrate as a cause of the carbon isotope excursion at the end of the Paleocene. Paleoceanography **10**:965-971.
Ellegaard, M. 2000. Variations in dinoflagellate cyst morphology under conditions of changing salinity during the last 2000 years. Review of Palaeobotany and Palynology **109**:65-81.
Fensome, R. A., H. Gocht, and G. L. Williams. 1996a. The Eisenack Catalog of Fossil Dinoflagellates. New Series. Volume **4**. E. Schweizerbart'sche Verlagsbuchhandlung, Stuttgart, Germany.
Fensome, R. A., R. A. MacRae, J. M. Moldowan, F. J. R. Taylor, and G. L. Williams. 1996b. The early Mesozoic radiation of dinoflagellates. Paleobiology **22**:329-338.
Fensome, R. A., J. B. Riding, and F. J. R. Taylor. 1996c. Dinoflagellates. AASP Foundation, Salt Lake City, UT.

Fensome, R. A., and G. L. Williams. 2004. The Lentin and Williams Index of Fossil Dinoflagellates 2004 Edition. American Association of Stratigraphic Palynologists (AASP) Foundation.
Frederiksen, N. O. 1982. Paleocene-Eocene boundary in the eastern Gulf Coast. Transactions of the Gulf Coast Association of Geological Societies **32**:289-294.
Gaines, G., and M. Elbrachter. 1987. Heterotrophic nutrition. Backwell.
Gaines, G., and F. I. R. Taylor. 1984. Extracellular digestion in marine dinoflagellates. Journal of plankton research **6**:1057-1061.
Gibson, T. G. 1980. Molluscan and foraminiferal biostratigraphy of lower Paleogene strata. Geol. Soc. Amer. Ann. Mtg., Atlanta field trip guide books.
Gibson, T. G. 1983. Revision of the Hatchetigbee and Bashi Formations (lower Eocene) in the eastern Gulf Coastal Plain. U. S. Geological Survey Bulletin **1529-H**:H33-H41.
Gibson, T. G., and L. M. Bybell. 1994. Sedimentary Patterns across the Paleocene-Eocene boundary in the Atlantic and Gulf coastal plains of the United States. Bulletin de la Société Belge de Géologie **103**:237-265.
Gibson, T. G., E. A. Mancini, and L. M. Bybell. 1982. Paleocene to middle Eocene stratigraphy of Alabama. Transactions of the Gulf Coast Association of Geological Societies **32**:289-294.
Gliozzi, A., R. Rolandi, M. De Rosa, and A. Gambacorta. 1983. Monolayer black membranes from bipolar lipids of archaebacteria and their temperature-induced structural changes. Journal of Membrane Biology **75**:45-56.
Hansen, P. J., and A. Calado. 1999. Phagotrophic Mechanisms and Prey Selection in Free-living Dinoflagellates1. Journal of Eurkaryotic Microbiology **46**:382-389.
Harrington, G. J. 2001. Impact of Paleocene/Eocene Greenhouse Warming on North American Paratropical Forests. Palaios **16**:266-278.
Harrington, G. J. 2003. Geographic patterns in the floral response to Paleocene-Eocene warming. Pages 381-393 *in* S. L. Wing, P. D. Gingerich, B. Schmitz, and E. Thomas, editors. Causes and Consequences of Globally Warm Climates in the Early Paleogene. Geological Society of America Special Paper 369, Boulder, Colorado.
Harrington, G. J., and C. A. Jaramillo. 2007. Paratropical floral extinction in the Late Palaeocene-Early Eocene. Journal of the Geological Society **164**:323-332.
Harrington, G. J., S. J. Kemp, and P. L. Koch. 2004. Palaeocene-Eocene paratropical floral change in North America: Responses to climate change and plant immigration. Journal of the Geological Society **161**:173-184.
Hopmans, E. C., J. W. H. Weijers, E. Schefuß, L. Herfort, J. S. Sinninghe Damsté, and S. Schouten. 2004. A novel proxy for terrestrial organic matter in sediments based on branched and isoprenoid tetraether lipids. Earth and Planetary Science Letters **224**:107-116.
Huber, M. 2008. A Hotter Greenhouse? Science **321**:353-354.
Huber, M., H. Brinkhuis, C. E. Stickley, K. Döös, A. Sluijs, J. Warnaar, S. A. Schellenberg, and G. L. Williams. 2004. Eocene circulation of the Southern Ocean: Was Antarctica kept warm by subtropical waters? Paleoceanography **19**:doi:10.1029/2004PA001014.
Jacobson, D. M., and D. M. Anderson. 1986. Thecate heterotrophic dinoflagellates: feeding behavior and mechanism. Journal of Phycology **22**:249-258.
Jacobson, D. M., and D. M. Anderson. 1996. Widespread phagocytosis of ciliates and other protists by marine mixotrophic and heterotrophic thecate dinoflagellates. Journal of Phycology **32**:279-285.
Jeong, H. J. 1999. The Ecological Roles of Heterotrophic Dinoflagellates in Marine Planktonic Community1. Journal of Eurkaryotic Microbiology **46**:390-396.

Jeong, H. J., Y. D. Yoo, J. Y. Park, J. Y. Song, S. T. Kim, S. H. Lee, K. Y. Kim, and W. H. Yih. 2005. Feeding by phototrophic red-tide dinoflagellates: five species newly revealed and six species previously known to be mixotrophic. Aquatic Microbial Ecology **40**:133-150.

Kates, M. 1977. The phytanyl ether-linked polar lipids and isoprenoid neutral lipids of extremely halophilic bacteria. Progress in the Chemistry of Fats and other Lipids **15**:301-342.

Katz, M. E., D. K. Pak, G. R. Dickens, and K. G. Miller. 1999. The source and fate of massive carbon input during the latest Paleocene thermal maximum. Science **286**:1531-1533.

Kelly, D. C., T. J. Bralower, J. C. Zachos, I. Premoli Silva, and E. Thomas. 1996. Rapid diversification of planktonic foraminifera in the tropical Pacific (ODP Site 865) during the late Paleocene thermal maximum. Geology **24**.

Kelly, D. C., J. C. Zachos, T. J. Bralower, and S. A. Schellenberg. 2005. Enhanced terrestrial weathering/runoff and surface ocean carbonate production during the recovery stages of the Paleocene-Eocene thermal maximum. Paleoceanography **20**:doi:10.1029/2005PA001163.

Kennett, J. P., and L. D. Stott. 1991. Abrupt deep-sea warming, palaeoceanographic changes and benthic extinctions at the end of the Palaeocene. Nature **353**:225-229.

Kim, J.-H., S. Schouten, E. C. Hopmans, B. Donner, and J. S. Sinninghe Damste. 2008. Global sediment core-top calibration of the TEX86 paleothermometer in the ocean. Geochimica et Cosmochimica Acta **72**:1154-1173.

Koch, P. L., J. C. Zachos, and P. D. Gingerich. 1992. Correlation between isotope records in marine and continental carbon reservoirs near the Palaeocene/Eocene boundary. Nature **358**:319-322.

Lessard, E. J., and E. Swift. 1985. Species-specfic grazing rates of heterotrophic dinoflagellates in oceanic water. Marine Biology **87**:289-296.

Liu, Z., M. Pagani, D. Zinniker, R. DeConto, M. Huber, H. Brinkhuis, S. R. Shah, R. M. Leckie, and A. Pearson. 2009. Global Cooling During the Eocene-Oligocene Climate Transition. Science **323**:1187-1190.

Loeblich, A. R. J. 1984. Dinoflagellate physiology and biochemistry. Academic Press, New York.

Lourens, L. J., A. Sluijs, D. Kroon, J. C. Zachos, E. Thomas, U. Röhl, J. Bowles, and I. Raffi. 2005. Astronomical pacing of late Palaeocene to early Eocene global warming events. Nature **435**:1083-1087.

MacRae, R. A., R. A. Fensome, and G. L. Williams. 1996. Fossil dinoflagellate diversity, originations, and extinctions and their significance. Canadian Journal of Botany **74**:1687-1694.

Mancini, E. A. 1981. Lithostratigraphy and biostratigraphy of Paleocene subsurface strata in southwest Alabama. Gulf Coast Assoc. Geol. Soc. Trans. **31**:359-367.

Matthiessen, J., K. A. F. Zonneveld, A. DeVernal, M. J. Head, and R. Harland. 2005. Recent and Quaternary organic-walled dinoflagellate cysts in arctic marine environments and their paleoenvironmental significance. Paläontologische Zeitschrift **79**:3-51.

Mertens, K. N., S. Ribeiro, I. Bouimetarhan, H. Caner, N. Combourieu Nebout, B. Dale, A. De Vernal, M. Ellegaard, M. Filipova, A. Godhe, E. Goubert, K. Grøsfjeld, U. Holzwarth, U. Kotthoff, S. A. G. Leroy, L. Londeix, F. Marret, K. Matsuoka, P. J. Mudie, L. Naudts, J. L. Peña-Manjarrez, A. Persson, S.-M. Popescu, V. Pospelova, F. Sangiorgi, M. T. J. van der Meer, A. Vink, K. A. F. Zonneveld, D. Vercauteren, J. Vlassenbroeck, and S. Louwye. 2009. Process length variation in cysts of a dinoflagellate, Lingulodinium machaerophorum, in surface sediments: Investigating its potential as salinity proxy. Marine Micropaleontology **70**:54-69.

Moldowan, J. M., and N. M. Talyzina. 1998. Biogeochemical evidence for dinoflagellate ancestors in the Early Cambrian. Science **281**:1168-1170.
Pagani, M., K. Caldeira, D. Archer, and J. C. Zachos. 2006a. An Ancient Carbon Mystery. Science **314**:1556-1557.
Pagani, M., N. Pedentchouk, M. Huber, A. Sluijs, S. Schouten, H. Brinkhuis, J. S. Sinninghe Damsté, G. R. Dickens, and T. Expedition 302 Scientists. 2006b. Arctic hydrology during global warming at the Palaeocene-Eocene thermal maximum. Nature **442**:671-675.
Pearson, P. N., B. E. van Dongen, C. J. Nicholas, R. D. Pancost, S. Schouten, J. M. Singano, and B. S. Wade. 2007. Stable warm tropical climate through the Eocene Epoch. Geology **35**:211-214.
Peterse, F., S. Schouten, J. van der Meer, M. T. J. van der Meer, and J. S. Sinninghe Damsté. 2009. Distribution of branched tetraether lipids in geothermally heated soils: Implications for the MBT/CBT temperature proxy. Organic Geochemistry **40**:201-205.
Powell, A. J. 1988. A modified dinoflagellate cyst biozonation for latest Palaeocene and earliest Eocene sediments from the central North Sea. Review of Palaeobotany and Palynology **56**:327-344.
Powell, A. J., H. Brinkhuis, and J. P. Bujak. 1996. Upper Paleocene - Lower Eocene dinoflagellate cyst sequence biostratigraphy of southeast England. Pages 145-183 *in* R. W. O. B. Knox, R. M. Corfield, and R. S. Dunay, editors. Correlation of the Early Paleogene in Northwest Europe, Geological Society Special Publication, 101.
Pross, J., and H. Brinkhuis. 2005. Organic-walled dinoflagellate cysts as paleoenvironmental indicators in the Paleogene; a synopsis of concepts. Paläontologische Zeitschrift **79**:53-59.
Reichart, G.-J., H. Brinkhuis, F. Huiskamp, and W. J. Zachariasse. 2004. Hyper-stratification following glacial overturning events in the northern Arabian Sea. Paleoceanography **19**:PA2013. 2010.1029/2003PA000900.
Robert, C., and J. P. Kennett. 1994. Antarctic subtropical humid episode at the Paleocene-Eocene boundary: clay mineral evidence. Geology **22**:211-214.
Röhl, U., H. Brinkhuis, A. Sluijs, and M. Fuller. 2004a. On the search for the Paleocene/Eocene Boundary in the Southern Ocean: Exploring ODP Leg 189 Holes 1171D and 1172D, Tasman Sea. Pages 113-125 *in* N. F. Exon, M. Malone, and J. P. Kennett, editors. The Cenozoic Southern Ocean: Tectonics, Sesimentation, and Climate Change Between Australia and Antarctica. Geophysical Monograph Series 151.
Röhl, U., H. Brinkhuis, C. E. Stickley, M. Fuller, S. A. Schellenberg, G. Wefer, and G. L. Williams. 2004b. Sea level and astronomically induced environmental changes in Middle and Late Eocene sediments from the East Tasman Plateau. Pages 127-151 *in* N. F. Exon, M. Malone, and J. P. Kennett, editors. The Cenozoic Southern Ocean: Tectonics, Sedimentation, and Climate Change Between Australia and Antarctica. American Geophysical Union Geophysical Monograph Series, 151.
Röhl, U., T. Westerhold, T. J. Bralower, and J. C. Zachos. 2007. On the duration of the Paleocene – Eocene thermal maximum (PETM). Geochemistry, Geophysics, Geosystems **8**:doi:10.1029/2007GC001784.
Röhl, U., T. Westerhold, S. Monechi, E. Thomas, J. C. Zachos, and B. Donner. 2005. The third and final early Eocene thermal maximum: characteristics, timing, and mechanisms of the "X" event. *in* Geological Society of America Annual Meeting. Abstr. 37 (7), p. 264.
Schellenberg, S. A., H. Brinkhuis, C. E. Stickley, M. Fuller, F. T. Kyte, and G. L. Williams. 2004. The Cretaceous/Paleogene transition on East Tasman Plateau, southwestern Pacific. *in* N. F. Exon, M. Malone, and J. P. Kennett, editors. The Cenozoic Southern Ocean: Tectonics, Sedimentation, and Climate Change

Between Australia and Antarctica. American Geophysical Union Geophysical Monograph Series, 151.
Schmitz, B., F. Asaro, E. Molina, S. Monechi, K. von Salis, and R. P. Speijer. 1997. High-resolution iridium, $\delta^{13}C$, $\delta^{18}O$, foraminifera and nannofossil profiles across the latest Paleocene benthic extinction event at Zumaya Spain. Palaeogeography, Palaeoclimatology, Palaeoecology **133**:49-68.
Schmitz, B., and V. Pujalte. 2003. Sea-level, humidity, and land-erosion records across the initial Eocene thermal maximum from a continental-marine transect in northern Spain. Geology **31**:689-692.
Schnepf, E., and M. Elbrachter. 1992. Nutritional strategies in dinoflagellates. A review with emphasis on cell biological aspects. European journal of protistology **28**:3-24.
Schouten, S., E. C. Hopmans, R. D. Pancost, and J. S. S. DamstÃ©. 2000. Widespread occurrence of structurally diverse tetraether membrane lipids: Evidence for the ubiquitous presence of low-temperature relatives of hyperthermophiles. Proceedings of the National Academy of Sciences of the United States of America **97**:14421-14426.
Schouten, S., E. C. Hopmans, E. Schefuß, and J. S. Sinninghe Damsté. 2002. Distributional variations in marine crenarchaeotal membrane lipids: a new tool for reconstructing ancient sea water temperatures? Earth and Planetary Science Letters **204**:265-274.
Shellito, C. J., L. C. Sloan, and M. Huber. 2003. Climate model sensitivity to atmospheric CO_2 levels in the Early-Middle Paleogene. Palaeogeography, Palaeoclimatology, Palaeoecology **193**:113-123.
Sluijs, A., G. J. Bowen, H. Brinkhuis, L. J. Lourens, and E. Thomas. 2007a. The Palaeocene-Eocene thermal maximum super greenhouse: biotic and geochemical signatures, age models and mechanisms of global change. Pages 323-347 *in* M. Williams, A. M. Haywood, F. J. Gregory, and D. N. Schmidt, editors. Deep time perspectives on Climate Change: Marrying the Signal from Computer Models and Biological Proxies. The Micropalaeontological Society, Special Publications. The Geological Society, London, London.
Sluijs, A., and H. Brinkhuis. 2009. A dynamic climate and ecosystem state during the Paleocene-Eocene Thermal Maximum--inferences from dinoflagellate cyst assemblages at the New Jersey Shelf. Biogeosciences Discussions **6**:5163-5215.
Sluijs, A., H. Brinkhuis, E. M. Crouch, C. d. M. John, L. Handley, D. Munsterman, S. M. Bohaty, J. C. Zachos, G.-J. Reichart, S. Schouten, R. D. Pancost, J. S. S. DamstÃ©, N. L. D. Welters, A. F. Lotter, and G. R. Dickens. 2008a. Eustatic variations during the Paleocene-Eocene greenhouse world. Paleoceanography **23**.
Sluijs, A., H. Brinkhuis, S. Schouten, S. M. Bohaty, C. M. John, J. C. Zachos, J. S. Sinninghe Damsté, E. M. Crouch, and G. R. Dickens. 2007b. Environmental precursors to light carbon input at the Paleocene/Eocene boundary. Nature **450**:1218-1221.
Sluijs, A., H. Brinkhuis, C. E. Stickley, J. Warnaar, G. L. Williams, and M. Fuller. 2003. Dinoflagellate cysts from the Eocene/Oligocene transition in the Southern Ocean; results from ODP Leg 189. Pages 1-42 *in* N. F. Exon, J. P. Kennett, and M. J. Malone, editors. Proceedings Ocean Drilling Program, Scientific Results 189.
Sluijs, A., J. Pross, and H. Brinkhuis. 2005. From greenhouse to icehouse; organic-walled dinoflagellate cysts as paleoenvironmental indicators in the Paleogene. Earth-Science Reviews **68**:281-315.
Sluijs, A., U. Röhl, S. Schouten, H.-J. Brumsack, F. Sangiorgi, J. S. Sinninghe Damsté, and H. Brinkhuis. 2008b. Arctic late Paleocene–early Eocene paleoenvironments with special emphasis on the Paleocene-Eocene thermal

maximum (Lomonosov Ridge, Integrated Ocean Drilling Program Expedition 302). Paleoceanography **23**:PA1S11, doi:10.1029/2007PA001495.
Sluijs, A., S. Schouten, M. Pagani, M. Woltering, H. Brinkhuis, J. S. Sinninghe Damsté, G. R. Dickens, M. Huber, G.-J. Reichart, R. Stein, J. Matthiessen, L. J. Lourens, N. Pedentchouk, J. Backman, K. Moran, and T. Expedition 302 Scientists. 2006. Subtropical Arctic Ocean temperatures during the Palaeocene/Eocene thermal maximum. Nature **441**:610-613.
Smayda, T. J. 1997. Harmful Algal Blooms: Their Ecophysiology and General Relevance to Phytoplankton Blooms in the Sea. Limnology and Oceanography **42**:1137-1153.
Smith, T., K. Rose, D., and P. Gingerich, D. 2006. Rapid Asia–Europe–North America geographic dispersal of earliest Eocene primate *Teilhardina* during the Paleocene–Eocene Thermal Maximum Proceedings of the National Academy of Sciences of the United States of America **103**:11223-11227.
Stickley, C. E., H. Brinkhuis, S. A. Schellenberg, A. Sluijs, U. Röhl, M. Fuller, M. Grauert, M. Huber, J. Warnaar, and G. L. Williams. 2004. Timing and nature of the deepening of the Tasmanian Gateway. Paleoceanography **19**:doi:10.1029/2004PA001022.
Stoecker, D. K. 1999. Mixotrophy among Dinoflagellates1. Journal of Eurkaryotic Microbiology **46**:397-401.
Taylor, F. J. R., editor. 1987. The biology of dinoflagellates. Blackwell Scientific Publications, London.
Thomas, D. J., J. C. Zachos, T. J. Bralower, E. Thomas, and S. Bohaty. 2002. Warming the fuel for the fire: Evidence for the thermal dissociation of methane hydrate during the Paleocene-Eocene thermal maximum. Geology **30**:1067-1070.
Thomas, E., and N. J. Shackleton. 1996. The Palaeocene-Eocene benthic foraminiferal extinction and stable isotope anomalies. Pages 401-441 *in* R. W. O. B. Knox, R. M. Corfield, and R. E. Dunay, editors. Correlation of the Early Paleogene in Northwestern Europe, Geological Society London Special Publication, 101. Geological Society of London, London, United Kingdom.
Toulmin, L. D. 1977. Stratigraphic distribution of Paleocene and Eocene fossils in the eastern Gulf Coast region. Alabama Geol. Survey Monogr. **13**:602.
Tripati, A., and H. Elderfield. 2005. Deep-Sea Temperature and Circulation Changes at the Paleocene-Eocene Thermal Maximum. Science **308**:1894-1898.
Uda, I., A. Sugai, Y. Itoh, and T. Itoh. 2001. Variation in molecular species of polar lipids from Thermoplasma acidophilum depends on growth temperature. Lipids **36**:103-105.
van Simaeys, S., H. Brinkhuis, J. Pross, G. L. Williams, and J. C. Zachos. 2005. Arctic dinoflagellate migrations mark the stongest Oligocene glaciations. Geology **33**:709-712.
Wall, D., B. Dale, G. P. Lohmann, and W. K. Smith. 1977. The environmental and climatic distribution of dinoflagellate cysts in modern marine sediments from regions in the North and South Atlantic Oceans and adjacent seas. Marine Micropaleontology **2**:121-200.
Weijers, J. W. H., S. Schouten, E. C. Hopmans, J. A. J. Geenevasen, O. R. P. David, J. M. Coleman, R. Pancost, and J. S. Sinninghe Damsté. 2006a. Membrane lipids of mesophilic anaerobic bacteria thriving in peats have typical archaeal traits. Environmental Microbiology **8**:648-657.
Weijers, J. W. H., S. Schouten, A. Sluijs, H. Brinkhuis, and J. S. Sinninghe Damste. 2007a. Warm arctic continents during the Palaeocene-Eocene thermal maximum. Earth and Planetary Science Letters **261**:230-238.
Weijers, J. W. H., S. Schouten, O. C. Spaargaren, and J. S. Sinninghe Damsté. 2006b. Occurrence and distribution of tetraether membrane lipids in soils:

Implications for the use of the TEX86 proxy and the BIT index. Organic Geochemistry **37**:1680-1693.
Weijers, J. W. H., S. Schouten, J. C. van den Donker, E. C. Hopmans, and J. S. Sinninghe Damste. 2007b. Environmental controls on bacterial tetraether membrane lipid distribution in soils. Geochimica et Cosmochimica Acta **71**:703-713.
Westerhold, T., U. Röhl, J. Laskar, I. Raffi, J. Bowles, L. J. Lourens, and J. C. Zachos. 2007. On the duration of Magnetochrons C24r and C25n, and the timing of early Eocene global warming events: Implications from the ODP Leg 208 Walvis Ridge depth transect. Paleoceanography **22**:doi:10.1029/2006PA001322.
Williams, G. L., H. Brinkhuis, M. A. Pearce, R. A. Fensome, and J. W. Weegink. 2004. Southern Ocean and global dinoflagellate cyst events compared; index events for the Late Cretaceous-Neogene. Pages 1-98 *in* N. F. Exon, J. P. Kennett, and M. J. Malone, editors. Proceedings Ocean Drilling Program, Scientific Results.
Wolfe, A., and D. L. Dilcher. 2000. Late Paleocene through middle Eocene climates in lowland North America. GFF **122**:184-185.
Zachos, J., M. Pagani, L. Sloan, E. Thomas, and K. Billups. 2001. Trends, rhythms, and aberrations in global climate 65 Ma to present. Science **292**:686-693.
Zachos, J. C., G. R. Dickens, and R. E. Zeebe. 2008. An early Cenozoic perspective on greenhouse warming and carbon-cycle dynamics. Nature **451**:279-283.
Zachos, J. C., U. Röhl, S. A. Schellenberg, A. Sluijs, D. A. Hodell, D. C. Kelly, E. Thomas, M. Nicolo, I. Raffi, L. J. Lourens, H. McCarren, and D. Kroon. 2005. Rapid Acidification of the Ocean during the Paleocene-Eocene Thermal Maximum. Science **308**:1611-1615.
Zachos, J. C., S. Schouten, S. Bohaty, T. Quattlebaum, A. Sluijs, H. Brinkhuis, S. Gibbs, and T. J. Bralower. 2006. Extreme warming of mid-latitude coastal ocean during the Paleocene-Eocene Thermal Maximum: Inferences from TEX_{86} and Isotope Data. Geology **34**:737-740.
Zachos, J. C., M. W. Wara, S. Bohaty, M. L. Delaney, M. R. Petrizzo, A. Brill, T. J. Bralower, and I. Premoli Silva. 2003. A transient rise in tropical sea surface temperature during the Paleocene-Eocene thermal maximum. Science **302**:1551-1554.

Appendices

Appendix I. Compilation of the carbon isotope record

Figure I shows the $\delta^{13}C$ record of the low resolution study on the Harrell core (run 1 and 2; grey closed circles) together with 32 of the finely spaced samples (run 3; black closed circles) as well as 10 additional samples (run 4; black open circles) that were selected from intervals that gained most interest. The 32 samples show a pattern that is roughly in agreement with the low resolution study. They confirm the occurrence of two phases of more depleted $\delta^{13}C$ interrupted by one sample with an extremely heavy signal at 120.5 mbs. Also the additional 10 finely spaced samples fit the pattern and the additional samples confirm that the extremely high and low values are representing true fluctuations rather than a measuring error. The finely spaced samples, however, are slightly less depleted in heavy carbon during the pre-CIE interval. Drift during mass spectrometry has been corrected whenever required and should therefore not be the cause of the offset.

In order to study the offset between the high and low resolution records in the pre-CIE interval of the record, several samples of both the low and high resolution series have been measured multiple times (run 4 and 5; grey and black triangles). Of the low resolution series, 2 samples have been re-measured using 2 and 10% of the previously used amount of sediment (run 5). At 123.9 mbs, the sample of 2% sediment is by 0.2‰ more enriched, while the sample of 10% sediment is 0.5‰ more enriched in ^{13}C. The sample at 122.8 mbs shows a $\delta^{13}C$ of -25.71‰ and -25.76‰ using 10% and 2% sediment in run 5 which is very similar to the -25.79‰ measured in the first low resolution run. One low resolution sample at 122.2 mbs, however, is almost 1.3‰ more enriched in ^{13}C in a second analysis (run 4). The oldest high resolution sample is duplicated once in run 4 and shows a similar value. A sample at 122.8 mbs contained too much carbon for a reliable detection of the isotope ratio and was re-measured using 50% and 10% of the previously analyzed amount of sediment in run 5. Same was applied for a sample at 122.1 mbs. All four samples that were measured using different amounts of sediment show 0.05 to 0.55‰ more depleted values for the measurements using less sediment. This is unlikely to be an analytical error, since the $\delta^{13}C$ values have been corrected whenever a correlation between sample size and $\delta^{13}C$ was detected.

The five different runs described here have been corrected for drift and/or sample size using the international standard GQ that was measured in all runs. Run 1 contains 14 useful GQs that show a drift of 0.0065‰ per sample. Also, all values of this run are shifted -0.9959‰ as the GQ values deviate this much from their actual values of -26.68‰. All 7 reliable GQs of run 2 show no drift. There is, however, a sample size effect of 0.0241‰ per total area of the peaks in the mass spectrometry output. In addition, values are shifted +0.4892‰. Run 3 is corrected for drift by 0.0016 and shifted -0.3648‰. Run 4 is corrected for drift by 0.0109 and shifted -0.3780‰. Run 5 lacks a significant drift. The sample size effect in this run is corrected by 0.0053 and all values are shifted -0.1130‰. In this way, all corrected values of all runs should be comparable.

The apparent offset between the low resolution samples (run 1 and 2) and the high resolution samples (run 3 and 4) now seems insignificant as duplicates of both series show values that range between them. This also suggests there is no difference in chemical composition of the finely spaced samples in comparison to the much earlier sampled and stored coarsely spaced samples. Heterogeneity of the sediment could explain deviating values for one sample in different runs, but would

not explain consistently more depleted values in the pre-CIE interval for the low resolution series.

Conclusively, all data obtained from the five runs will be further used in this study. Duplicate samples show that there is some inconsistency within the lowest part of the record, especially at 122.2 mbs.

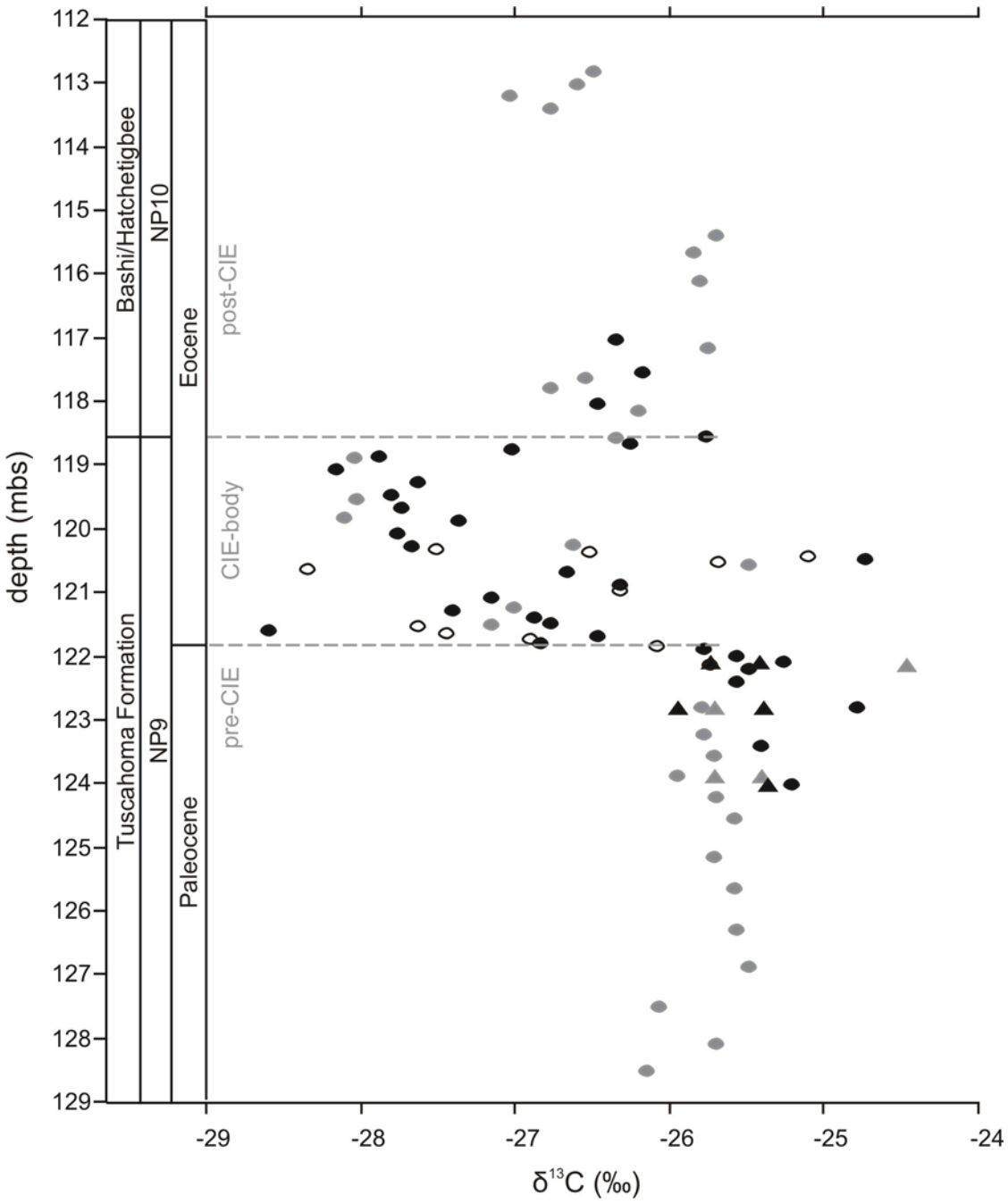

Figure I. Stable carbon isotopes. Pilot study (grey closed circles) and duplicates (grey triangles) plotted together with high resolution samples (black closed circles), extra high resolution samples (black open circles) and high resolution duplicates (black triangles).

Appendix II. TEX_{86}

Figure II shows the raw TEX_{86} data based on isoprenoid GDGTs. Between 124.1 and 121.9 mbs TEX_{86} shows values of 0.70 and 0.71 with peaks that increase in intensity (0.73 to 0.80) and abundance towards the top of this interval. An increase occurs between 121.9 and 121.8 mbs from 0.71 to 0.89. Values keep increasing slightly to a maximum of 0.91 at 120.7 mbs and gradually decrease back to 0.87 in the top of the Tuscahoma Formation. This decrease continues within the Bashi-Hatchetigbee Formation to 0.71 at 117.0 mbs.

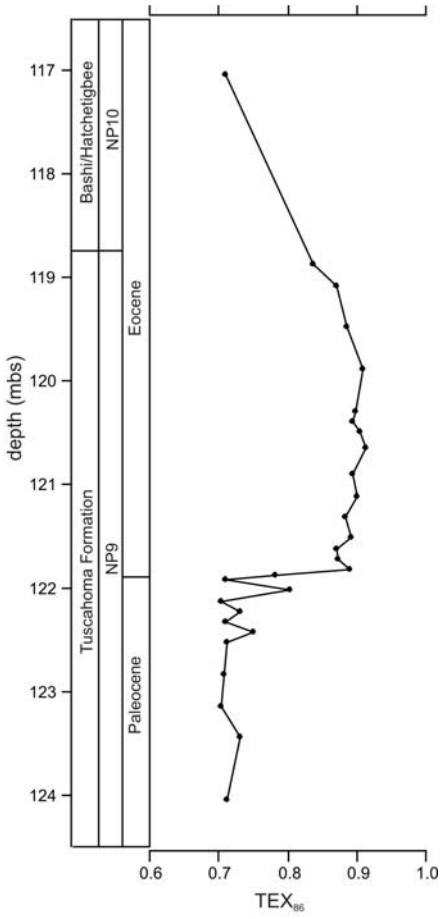

Figure II. TEX_{86} of the Harrell core.

List of dinocyst species

Species found in the studied palynological residues of the Harrell core are listed below. Taxonomy follows Fensome and Williams (2004) unless indicated otherwise. Plate references are added to species that are discussed or belong to a complex that is discussed in chapters 5 and 6. Plates 1-3 with photographs are enclosed after this list.

Achomosphaera spp.
Adnatosphaeridium multispinosum
Adnatosphaeridium robustum
Apectodinium homomorphum
Apectodinium hyperacantum
Apectodinium quinquelatum
Apectodinium parvum
Apectodinium homomorphum 'astra', fraction of *Apectodinium homomorphum* that has furcations at the tips of the processes (see chapter 4.5)
Apectodinium hyperacantum 'astra', fraction of *Apectodinium hyperacantum* that has furcations at the tips of the processes (see chapter 4.5)
Apectodinium quinquelatum 'astra', fraction of *Apectodinium quinquelatum* that has furcations at the tips of the processes (see chapter 4.5)
Apectodinium parvum 'astra', fraction of *Apectodinium parvum* that has furcations at the tips of the processes (see chapter 4.5)
Areoligera coronata
Areoligera spp. (pars)
Areoligera complex: consists of *Adnatosphaeridium, Areoligera* and *Glaphyrocysta.*
Cerebrocysta spp.
Cordosphaeridium fibrospinosum
Cordosphaeridium fibrospinosum complex: consists of *Cordosphaeridium fibrospinosum, Fibrocysta* spp., *Kenleyia spp., Lanternosphaeridium lanosum* and *Muratodinium fimbriatum*.
Deflandrea?
Dinogymnium spp., reworked
Diphyes colligerum, variation with smaller cyst size
Fibrocysta spp.
Florentinia reichartii, described by Sluijs and Brinkhuis (2009)
Glaphyrocysta ordinata
Glaphyrocysta pastielsii
Glaphyrocysta spp. (pars)
Hystrichosphaeridium spp.
Hystrichokolpoma spp.
Kenleyia spp.
Lanternosphaeridium lanosum
Leptodinium spp.
Membranosphaera spp.
Muratodinium fimbriatum
Operculodinium israelianum
Operculodinium severinii
Operculodinium spp. (pars)
Phthanoperidinium spp.
Senegalinium spp.
Senegalinium complex: consists of *Deflandrea?, Phthanoperidinium* and *Senegalinium.*

Spinidinium densispinatum
Spiniferites spp.
Spiniferites complex: consists of *Achomosphaera* and *Spiniferites.*

Plate 1

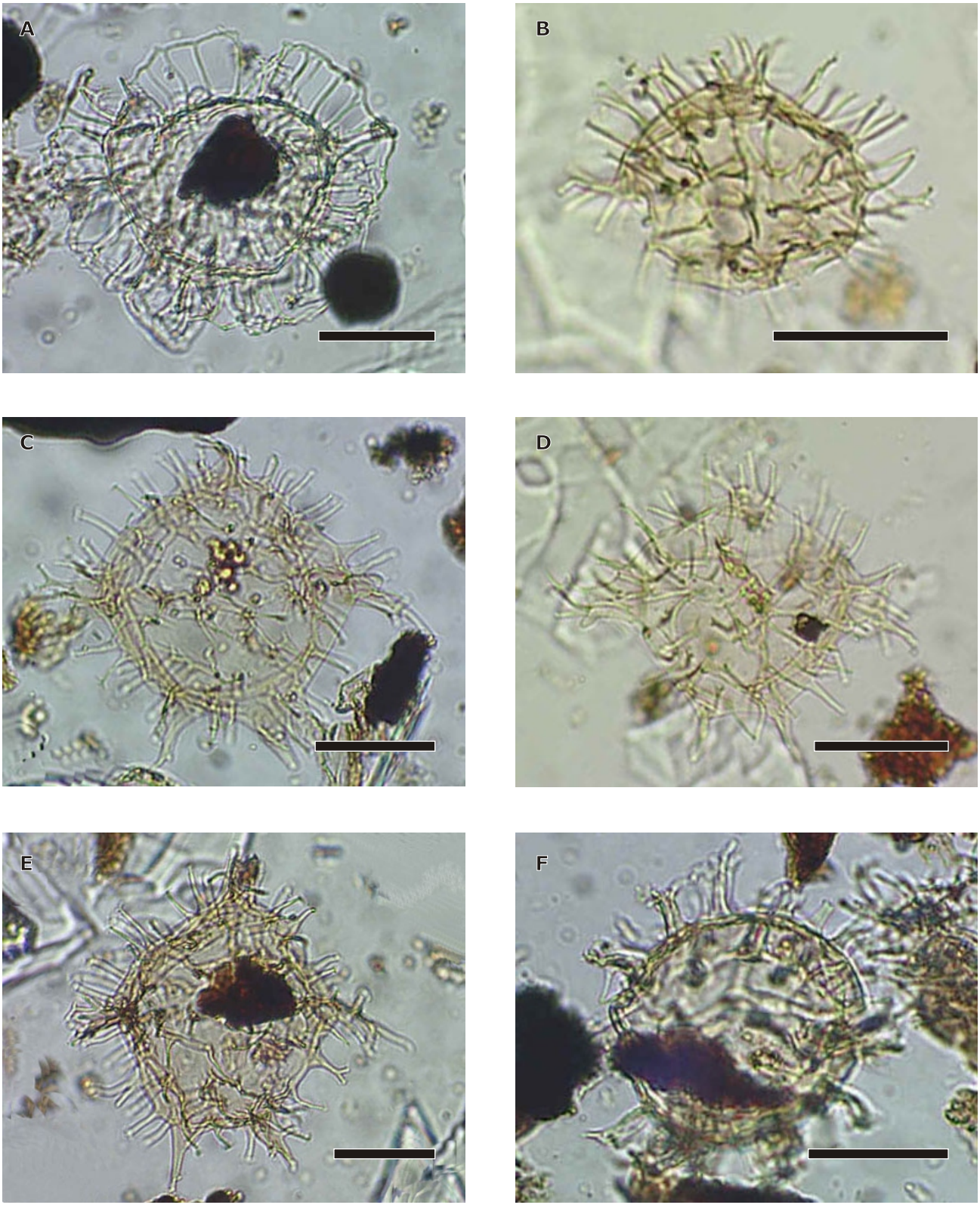

Plate 1. (A) *Adnatosphaeridium* sp. (120.09 mbs, H56-3), (B) *Apectodinium homomorphum* (120.90 mbs, T54-3), (C) *Apectodinium homomorphum* 'astra' (120.09 mbs, J58-2), (D) *Apectodinium quinquelatum* (120.90 mbs, W54-3), (E) *Apectodinium quinquelatum* 'astra' (120.09 mbs, J58-3), (F) *Cordosphaeridium fibrospinosum* (117.55 mbs, H47-2). All specimens are from slide #1 of samples indicated by depth, coordinates following England Finder. Scale bar represents 20 μm.

Plate 2

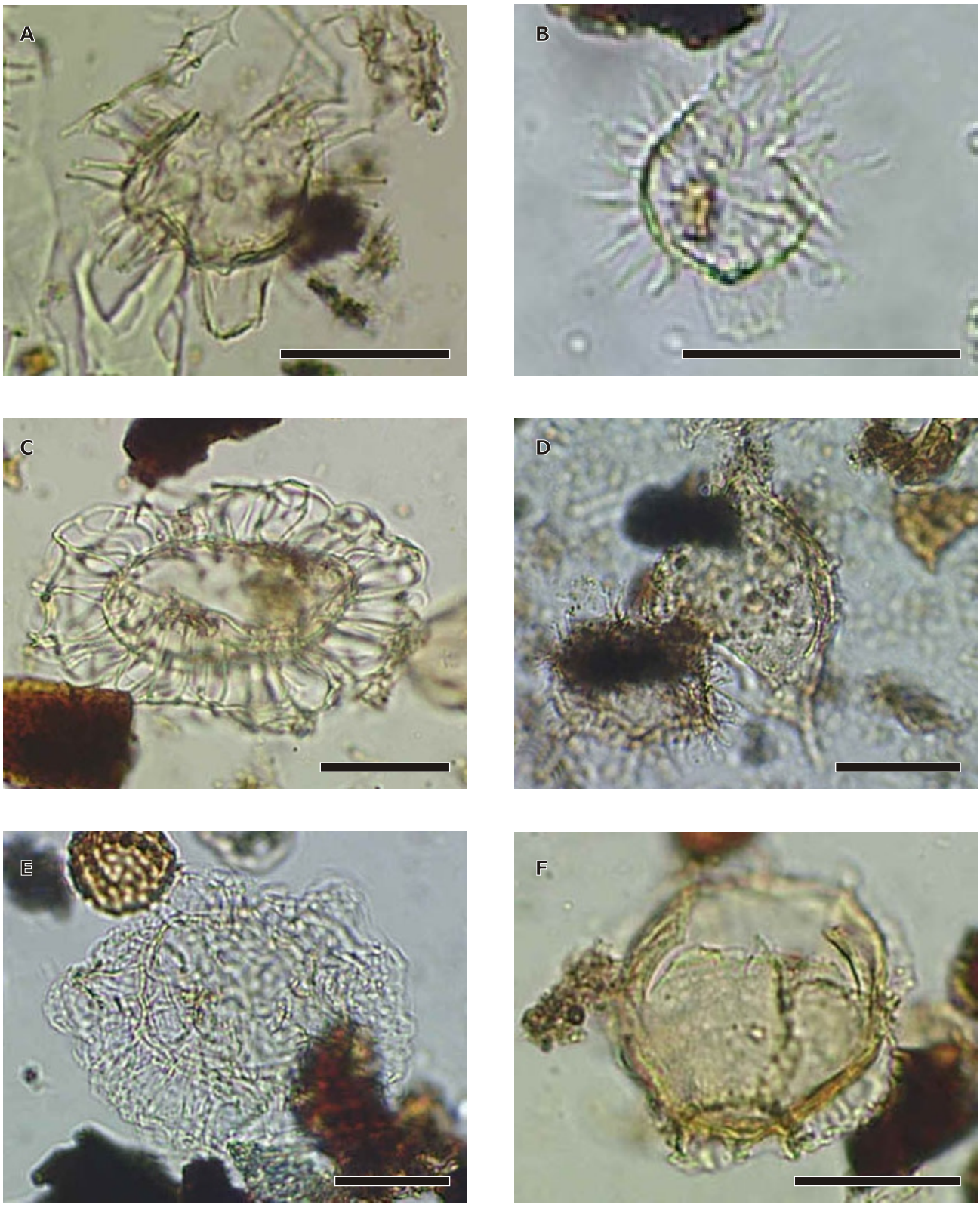

Plate 2. (A) *Diphyes colligerum* (120.90 mbs, Q57-2), (B) *Florentinia reichartii* (120.09 mbs, F47-1), (C) *Glaphyrocysta* sp. (117.55 mbs, F52-3), (D) *Kenleyia* sp. (119.48 mbs, F43-3), (E) *Lanternosphaeridium lanosum* (112.81 mbs, G41-2), (F) *Muratodinium fimbriatum* (117.55 mbs, E46-2). All specimens are from slide #1 of samples indicated by depth, coordinates following England Finder. Scale bar represents 20 μm.

Plate 3

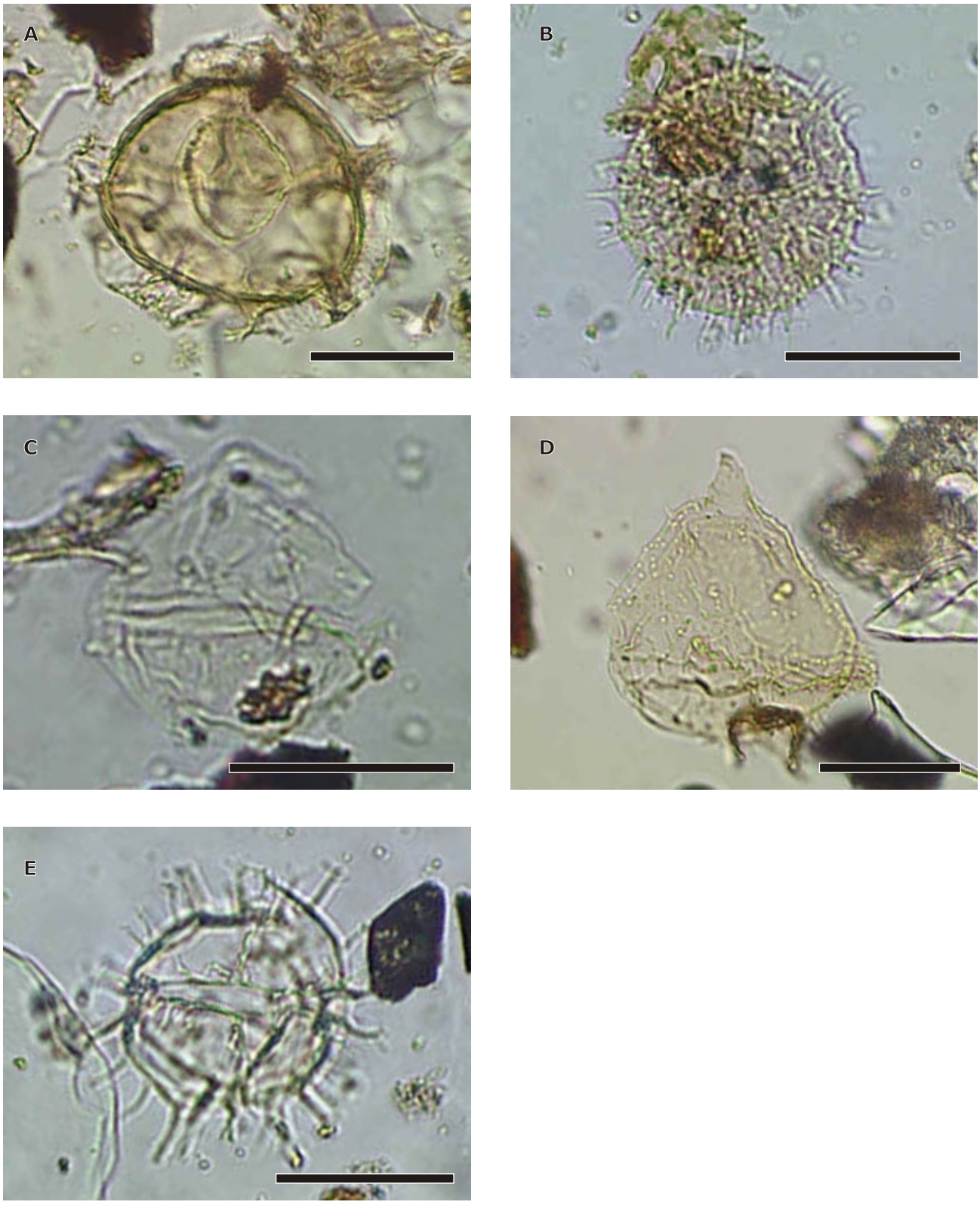

Plate 3. (A) *Muratodinium fimbriatum* (117.55 mbs, F43-2), (B) *Operculodinium severinii* (117.55 mbs, E60-2), (C) *Senegalinium* sp. (G45-1), (D) *Spinidinium densispinosum* (112.81 mbs), (E) *Spiniferites* sp. (120.09 mbs, H48-2). All specimens are from slide #1 of samples indicated by depth, coordinates following England Finder. Scale bar represents 20 μm.

Carbon isotopic fractionation in marine and terrestrial palynomorphs in North America during the Paleocene – Eocene Thermal Maximum

Linda van Roij

Supervision by

Dr. Appy Sluijs
Prof. Dr. Henk Brinkhuis

Palaeoecology, Institute of Environmental Biology,
Laboratory of Palynology and Palaeobotany,
Department of Biology, Faculty of Sciences, Utrecht University

and

Dr. Gert-Jan Reichart

Geochemistry,
Department of Earth Sciences, Faculty of Geosciences, Utrecht University

Outline

1. Introduction

The Paleocene – Eocene Thermal Maximum (PETM) represents a period of extreme warming, circa 55.5 Ma ago, superimposed on the greenhouse conditions of the early Paleogene (Kennett and Stott 1991, Zachos et al. 2001, Röhl et al. 2007). The onset of the PETM is marked by an abrupt negative carbon isotope excursion (CIE) due to the release of ^{13}C-depleted carbon (Dickens et al. 1995). A possible explanation for the CIE considers destabilization of methane hydrates which potentially have a δ^{13}C value of ~-60‰ (Dickens et al. 1995, Dickens et al. 1997). The released methane caused, due to a reaction with oxygen, a rapid increase of carbon dioxide in the atmosphere that would have had a large impact on global air and sea water temperature as well as on ocean acidification.

The shape of the CIE and its recovery is different for every site and measured substrate. A general picture has been sketched, however, so various records can be compared (Bowen et al. 2006, Sluijs et al. 2007a)(Figure 1). The onset of the CIE is characterized by a sharp drop in δ^{13}C that established in only a few thousands of years (Röhl et al. 2000). This CIE has a magnitude up to -3.5‰ in marine carbonates (Thomas and Shackleton 1996) and even up to -8‰ in plant organic matter and soil carbonates (Koch et al. 1992, Bains et al. 2003, Pagani et al. 2006, Schouten et al. 2007). In between the onset and the recovery, low δ^{13}C values maintain during a phase termed the CIE-body. This phase may represent a fundamentally different climate state compared to the latest Paleocene due to increased humidity and changes in carbon cycling (Bowen et al. 2004). Since δ^{13}C remains low, this suggests that ^{13}C depleted carbon remained in the ocean and atmosphere reservoirs before it was buried (Bowen et al. 2006). Subsequently, the δ^{13}C curves gradually return towards higher values comparable to the latest Paleocene during the recovery phase.

Usually bulk carbonate (BC) or total organic matter (TOC) is analyzed to identify the PETM (e.g. Sluijs et al. 2007b, Van Roij 2009). When studying the magnitude of the CIE, however, the bulk signal will be affected by changes in the relative input of multiple carbon sources. This is due to differences in carbon fractionation between various calcifying and non-calcifying organisms providing this carbon. These organisms not only show different δ^{13}C values. They also show different magnitudes of the CIE as their fractionation may be affected by variables such as temperature and growth rate (see Background information). As a result, the magnitude of the CIE can be determined for single taxa or specific compounds.

Marine carbonate shells of planktonic and benthic foraminifera from globally dispersed sites have been measured for their δ^{13}C values across the PETM (Kennett and Stott 1991, Thomas and Shackleton 1996, Thomas et al. 2002, Zachos et al. 2006, John et al. 2008). Benthic foraminifera generally show a CIE of ~-2‰ (Kennett and Stott 1991, Thomas and Shackleton 1996, Thomas et al. 2002), whereas planktonic foraminifera shift by ~-4‰ in δ^{13}C (Thomas and Shackleton 1996, Zachos et al. 2007, John et al. 2008). Also δ^{13}C measurements on single shells of two species of planktonic foraminifera generate a ~-3to -4.5 ‰ CIE (Zachos et al. 2007, John et al. 2008). The magnitude of the CIE in benthic foraminifera is considered to decline with water depth due to carbonate dissolution (McCarren et al. 2008). The ~-3.5‰ CIE derived from benthic foraminifera of the shallowest site of this depth dependency study is considered to be the least truncated (McCarren et al. 2008). Stable carbon isotope measurements on the organic cysts of dinoflagellates (dinocyst) assemblages strongly dominated by *Apectodinium* show a CIE of -4 to -4.5‰ (Sluijs et al. 2007b).

The CIE measured on terrestrial substrates is generally larger compared to marine carbonates (Koch et al. 1995, Bowen et al. 2001, Thomas et al. 2002,

Schmitz and Pujalte 2003, Zachos et al. 2003, Bowen et al. 2006, Smith et al. 2007). For example, soil carbonates show a CIE of ~-6‰ (Koch et al. 1992, Bowen et al. 2002). Furthermore, compound specific $\delta^{13}C$ for n-C_{27} and n-C_{29} alkanes assigned to leaf waxes of higher plants show a CIE of ~-4.5‰ (Pagani et al. 2006). The difference between the marine and terrestrial CIE can be explained by either a too small CIE recorded in marine carbonates or an amplified CIE signal in terrestrial substrates. Firstly, increased ocean acidification during the PETM would increase the concentration of carbonate ions in the ocean water, thereby decreasing the magnitude of the CIE in marine carbonates (Bowen et al. 2004). This is because carbonate ions are less depleted in ^{13}C compared to dissolved carbon dioxide (CO_2). Secondly, increased soil productivity and turnover rates cause a decrease in $\delta^{13}C$ of soil carbonates (Bowen et al. 2004). More importantly, terrestrial plants appear to have increased their fractionation due to increased humidity during the PETM (Bowen et al. 2004). When testing this hypothesis using an Arctic site, an arid pre-PETM climate state is required which is unlikely for the Arctic region during the latest Paleocene (Pagani et al. 2006). Furthermore, climate models are inconsistent in predicting regional precipitation patterns (Huber and Sloan 1999, Shellito et al. 2003).

Another explanation for the larger terrestrial CIE is an increase in the more ^{13}C-depleted angiosperms relatively to gymnosperms requiring a global, synchronous change (Pagani et al. 2006) (Schouten et al. 2007, Smith et al. 2007). The average ~-4.5‰ CIE of n-alkanes measured by Pagani et al. (2006) is in fact a mixture of both angiosperm and gymnosperm compounds (Schouten et al. 2007, Smith et al. 2007). Compared to gymnosperms, angiosperms fractionate more efficiently resulting in a lower $\delta^{13}C$ of their n-alkanes by approximately 3‰ (Chikaraishi and Naraoka 2003). As a result, the larger -6‰ CIE measured by Pagani et al. (2006) may be associated with a shift towards an angiosperm dominating flora during the PETM. This is consistent with observations for an Arctic site. Here, angiosperm pollen have been observed to dominate gymnosperm pollen during the PETM (Sluijs et al. 2006). For the same site, a biomarker derived from angiosperms shows a -6‰ CIE, whereas biomarkers associated with conifers, an important group of gymnosperms in temperate environments, shift only by -3‰ (Schouten et al. 2007). The globally variable magnitude of the CIE in n-alkanes can be explained by locally different floral compositions (Smith et al. 2007).

Resulting from the discussion above, the true atmospheric CIE may be in the order of –3 to –4‰ $\delta^{13}C$ based on the CIE recorded in gymnosperm biomarkers and planktonic foraminifera. Apart from the measurements on single shells of planktonic foraminifera (Zachos et al. 2007, John et al. 2008), no true species specific CIE has been measured. Sluijs et al. (2007b) use *Apectodinium* dominated assemblages, but the effect of other components should not be overlooked. Therefore, a single dinocyst taxon should be isolated so that the magnitude of the CIE can be determined purely for this taxon. The CIE in dinocysts could be compared to the planktonic foraminifer species to study differences in fractionation in the sea surface. Phytoplankton is useful as they live in the mixed ocean surface and may be close to representing the atmospheric CIE. Furthermore, pollen grains of a single species should be isolated to determine the magnitude of the CIE in specific terrestrial plants.

In this study, two North American shallow marine sediment cores from Bass River, New Jersey and Meridian, Mississippi which include an extensive interval of the PETM are used to isolate specimens of individual species of marine dinoflagellate cysts (dinocysts) and terrestrial pollen grains for stable carbon isotope analysis. Taxon specific $\delta^{13}C$ of dinocyst *Apectodinium* and pollen *Thomsonipollis magnificus*

and *Nudopollis terminalis* will show a CIE that is no longer biased by a variable assemblage composition and can be compared to earlier derived records from these sites based on bulk carbonate and foraminifer species. Also, comparisons between the CIE expressed in dinoflagellate cysts and pollen grains will indicate differences in fractionation between the terrestrial and marine realm. Species specific $\delta^{13}C$ records may help estimating the magnitude of the true atmospheric CIE.

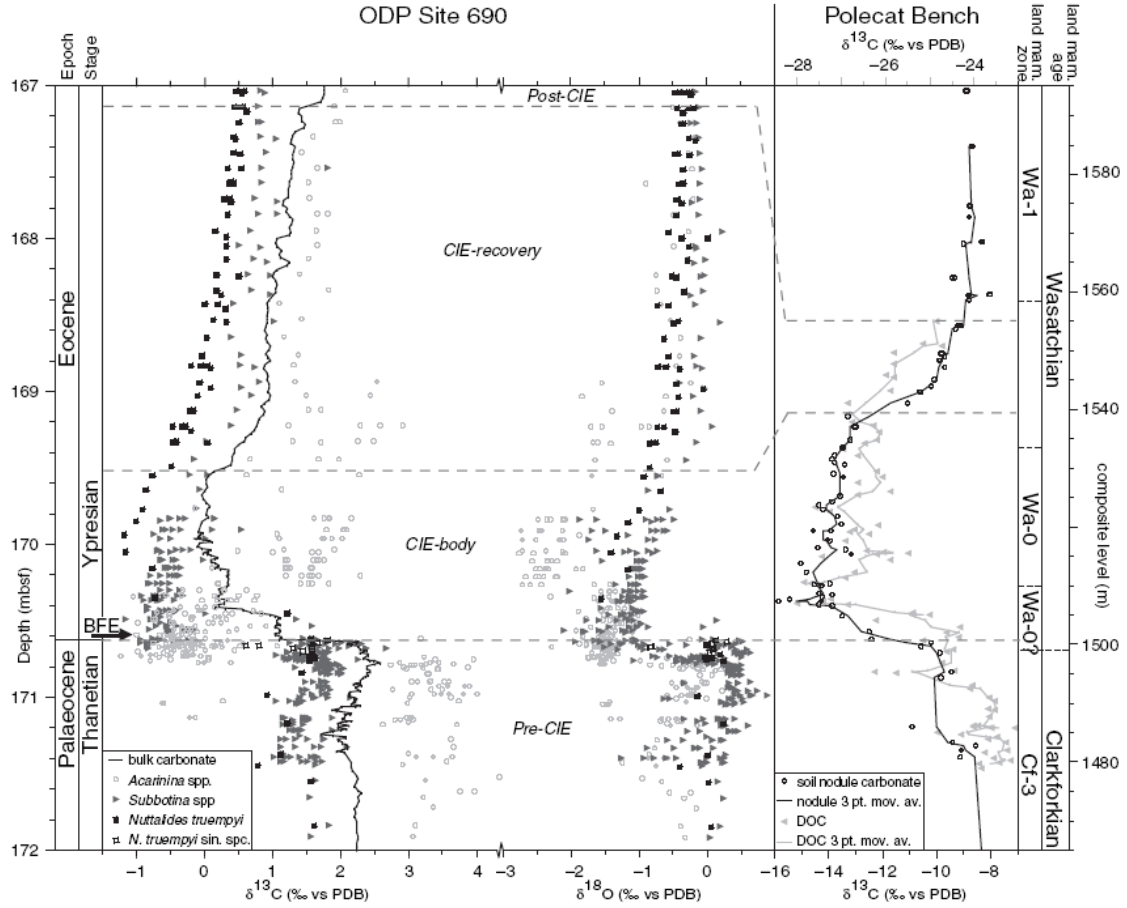

Figure 1. Compilation of $\delta^{13}C$ and $\delta^{18}O$ records. Values derived from planktonic foraminifera (surface-dweller *Acarinina* and thermocline-dweller *Subbotina* spp.; mostly single specimen), benthic foraminifera (*Nuttallides truempyi*) and bulk carbonate from ODP Site 690 in the Weddell Sea (data from (Kennett & Stott 1991; Bains et al. 1999; Thomas et al. 2002; Kelly et al. 2005), soil carbonate nodule (Bowen et al. 2001) and dispersed organic carbon (DOC) (Magioncalda et al. 2004) d13C records from the Polecat Bench section in the Bighorn Basin, Wyoming, USA. BFE refers to the main phase of benthic foraminifer extinction according to Thomas (2003). Mbsf, meters below sea-floor. From Sluijs et al., 2007a.

2. Background information

2.1. Carbon isotopic fractionation

The carbon isotopic composition of Standard Mean Ocean Water (SMOW) is by definition 0‰. Dissolved inorganic carbon is by 1‰ enriched in ^{13}C. Present day photoautotrophic plankton fractionates this carbon to $\delta^{13}C$ of -22‰. Higher plants take up atmospheric carbon of -7‰ and fractionate to an average value of -25‰ (Ruddiman 2001).

Marine algae and C_3 plants contain the 1,5-bisphosphate carboxylase oxygenase enzyme (rubisco). This enzyme is associated with the Calvin cycle where it catalyzes

the first step in carbon fixation (Campbell and Reece 2002). Rubisco has a low affinity for its substrate carbon dioxide (CO_2) and a low turnover rate (Rost et al. 2006). Moreover, it is also susceptible for a reaction with oxygen (O_2). This reaction results into photorespiration which suppresses the rate of carbon fixation (Rost et al. 2006). Due to the catalytic inefficiency of rubisco, carbon assimilation of photoautotrophs is limited (Rost et al. 2006).

The fractionation in marine phototrophic eukaryotic algae is variable between species as they respond differently to changes in atmospheric pCO_2, temperature and growth rate (Hinga et al. 1994, Bidigare et al. 1997, Popp et al. 1998, Rost et al. 2006). Culture studies on various phototrophic marine eukaryotic algae show that growth rate and the concentration of dissolved carbon dioxide are significantly correlated with carbon isotopic fractionation (Popp et al. 1998). Atmospheric CO_2 dissolved in the ocean almost completely reacts with water to form carbonic acid. HCO_3^- (bicarbonate) and CO_3^{2-} (carbonate) are formed when carbonic acid speciates. Phytoplankton uses CO_2 concentrating mechanisms (CCMs) to prevent carbon limitation in photosynthesis under conditions of low CO_2 concentration (Rost et al. 2006). CCMs enhance the concentration of CO_2 within the cell by active uptake of CO_2 and/or HCO_3^- (bicarbonate). Furthermore, the enzyme carbonic anhydrase (CA) catalyzes the conversion between HCO_3^- and CO_2. Also the loss in intracellular CO_2 has to be limited for efficient carbon fixation. Phytoplankton species differ in catalytic efficiency of rubisco (Badger et al. 1998, Tortell 2000) and in the functioning of their CCMs (Burkhardt et al. 2001, Beardall and Giordano 2002, Rost et al. 2003), resulting in variable sensitivity to CO_2 concentrations. Several dinoflagellate species have shown that with increased pH the enzyme CA becomes more active, suggesting increased intracellular CO_2 availability (Rost et al. 2006). Increased temperature causing increased fractionation in diatom *Skeletonema costaturn* is shown in a culture experiment (Hinga et al. 1994). Higher temperatures may stimulate growth rates which would cause a decline in fractionation. On the other hand, higher molecular diffusion rates as a result of higher temperatures may explain the increased fractionation (Hinga et al. 1994). As temperature affects many cellular processes as well as the concentration of dissolved CO_2 in the oceans, the actual temperature effect on the fractionation of algae is difficult to quantify.

The isotopic signature of heterotrophs is different from autotrophs in two ways. Firstly, respiration leads to the favorable release of ^{12}C and thus decreased fractionation. Secondly, the carbon source of heterotrophs as well as the isotopic composition of this source may change through time. So far, both factors are unknown.

During the PETM, atmospheric and dissolved CO_2 increases and pH decreases. As a result, activity of CA may be reduced in phytoplankton so that less HCO_3^- is used. Also, the access to CO_2 increases which is more energy efficient to use directly than when converted from HCO_3^-. Since carbon in dissolved CO_2 has a lower $\delta^{13}C$ value than the carbon derived from HCO_3^-, increased uptake of CO_2 relatively to HCO_3^- would result in a larger CIE compared to the atmospheric CIE. Effects of increasing temperature during the PETM are more difficult to determine. *Apectodinium* is possibly a heterotrophic genus as it may be related to present day heterotrophs (Bujak and Brinkhuis 1998). It increases globally in abundance during the PETM (Crouch et al. 2001, Sluijs et al. 2006, van Roij in prep.). Sluijs et al. (2007b) measured $\delta^{13}C$ on *Apectodinium* dominated dinocyst assemblages from two sites on the New Jersey shelf, namely Bass River and Wilson Lake. The -4‰ CIE is in the order of the CIE in planktonic foraminifera (Thomas and Shackleton 1996, Zachos et al. 2007, John et al. 2008). Potential amplification of the CIE in *Apectodinium* can be explained by increased fractionation in the photoautotrophs they feed on as

previously explained by decreased CA activity and increased CO_2 uptake. Suppression of the atmospheric CIE could be due to respiration or a change in carbon source.

Carbon fixation in higher terrestrial plants is affected by temperature as well as water use efficiency (Jahren 2004, Schouten et al. 2007). Schouten et al. (2007) suggested that the -6‰ CIE observed for angiosperm biomarkers is due to increased fractionation on top of a smaller actual CIE. The authors state that if WUE is kept more or less constant, fractionation would increase with increasing atmospheric pCO_2. On the other hand, if fractionation did not increase, WUE must have been increased with increasing atmospheric pCO_2 (Schouten et al. 2007). Since all plants have a different WUE, their isotopic fractionation is expected to vary as well. A positive temperature effect on pollen $\delta^{13}C$ has been observed for *Pinus sylvestris* (Loader and Hemming 2001). Data from other species, however, show both positive and negative correlations between temperature and pollen $\delta^{13}C$ depending on the plant species (Jahren 2004). Pollen grains are likely to show an offset with $\delta^{13}C$ of n-alkanes, as they also show offsets with both leaf tissue and stem $\delta^{13}C$ (Jahren 2004).

During the PETM, atmospheric pCO_2 and temperatures increased. Fractionation by angiosperms was more efficiently compared to gymnosperms, suggesting that angiosperms may have kept their WUE constant (Schouten et al. 2007). When assuming that gymnosperms kept their ^{13}C-fractionation relatively constant by improving their WUE, their -3‰ CIE may approach the actual atmospheric CIE. If the positive temperature effect on $\delta^{13}C$ of *Pinus sylvestris* pollen is applicable to other widespread conifers, this may also explain the smaller CIE observed for gymnosperms relatively to angiosperms.

2.2. Marine and terrestrial palynomorphs in North America

Organic remains of Early Paleogene organisms found in shallow marine sediments are mainly terrestrial pollen and spores as well as marine foraminiferal linings, acritarchs and dinocysts (Sluijs et al. 2006, van Roij in prep.). Typical shelf taxa of dinocysts across the Paleocene – Eocene boundary comprise *Areoligera*, *Glaphyrocysta*, *Spiniferites* and *Operculodinium* (Zachos et al. 2006, Sluijs and Brinkhuis 2009, van Roij in prep.). Although the PETM is correlated to major extinctions of benthic foraminifera in the marine realm (Thomas and Shackleton 1996), dinocyst evolutionary radiation and extinction appear to be unaffected by this event. However, the expansion of dinocyst *Apectodinium* from tropical regions as far as the polar regions is characteristic for the PETM (Sluijs et al. 2006). Moreover, extinctions and migrations have been observed for vertebrate fauna, while terrestrial plants show no massive extinctions (Harrington 2001). North American pollen records contain present day tropical and subtropical families such as Anacardiaceae, Annonaceae, Apocynaceae, Bombaceae, Burseraceae, Loranthaceae, Nyssaceae, Sterculiaceae and Symplocaceae (Harrington 2001, Harrington 2003, 2008). Wind-pollinating trees of Juglandaceae, Myricaceae-Betulaceae, Taxodiaceae and Ulmaceae are also present as well as swamp taxa (Harrington 2008). Rather than a latitudinal vegetation pattern, the North American pollen record distinguishes the interior continent from the marginal areas (Harrington 2003). First occurrences in the Eocene include *Brosipollis*, *Dicolpopollis*, *Intratriporopollenites instructus*, *Nuxpollenites psilatus* and *Platycarya platycaryoides*, although they originate after the PETM (Wing et al. 2005, Harrington 2008). Furthermore, none of these immigrants occur throughout entire North America and their relative abundances are generally insignificant (Harrington 2003).

3. Material and methods

3.1. Material

Bass River is an Ocean Drilling Program (ODP) site located at the New Jersey shelf, currently at ~40°N (Zachos et al. 2006). Its shallow marine sediments include a stratigraphically expanded interval of the Paleocene – Eocene transition. This interval contains abundant *Apectodinium* at least shortly prior to and during the PETM (Sluijs et al. 2007b). Stable carbon isotopes have been measured on bulk carbonate, single planktonic foraminifera and the 40 to 125 µm size fraction of the palynological residues which almost exclusively exists of dinocysts (DC)(Sluijs et al. 2007b, Zachos et al. 2007). The palynological residue of one pre-CIE sample at 357.58 meters below surface (mbs) and two CIE-onset samples at 357.21 and 357.12 mbs are used for the isolation of specimens of *Apectodinium* (Figure 2). Also, the entire palynological residue with a size fraction of 15 to 125 µm is measured for its isotopic composition.

Lower Paleogene sediments are also found along the Gulf Coast of Mississippi, currently at ~32°N (Gibson and Bybell 1994, Harrington and Kemp 2001, Harrington 2003). The Harrell core was drilled near Meridian and contains latest Paleocene and earliest Eocene sediments. It contains *Apectodinium* throughout the entire studied interval and is especially abundant during the PETM (van Roij in prep.). Both *Thomsonipollis magnificus* and *Nudopollis terminalis* are fairly common among other pollen taxa within the pre-CIE interval. For this core, stable carbon isotopes have been measured on TOC (van Roij in prep.). This record shows a CIE-onset that is comprised of two steps and a CIE-body that contains large fluctuations in $\delta^{13}C$. One sample used for isolation of *Apectodinium* at 121.87 mbs coincides with the onset of the first step of the CIE based on TOC (Figure 3). A sample at 121.62 mbs corresponds to the earliest CIE-body and is therefore assumed to represent the full initial CIE, whereas a sample at 120.09 mbs is further up in the CIE-body. All three samples are also measured for the $\delta^{13}C$ of the total palynological residue. Since the pre-CIE interval of the Harrell core does not contain abundant *Apectodinium*, a sample is used from an outcrop in Bell's Landing, Alabama. The marl bed named after this locality is a shelly glauconitic bed within the Tuscahoma Formation and is slightly older than the studied interval of the Tuscahoma Formation obtained at Meridian, Mississippi. It contains abundant dinocysts including *Apectodinium*. The pre-CIE interval of the Harrell core does contain abundant pollen and therefore a sample at 124.05 mbs is used for the isolation of *Thomsonipollis magnificus* and *Nudopollis terminalis*.

3.2. Methods

In earlier studies, the palynological residue was obtained by crushing freeze dried sediments, removing carbonates and siliciclastic material using 30% HF and 30% HCl and sieving through a 15 and 125 µm sieve (Sluijs et al. 2007b, van Roij in prep.). Additional samples such as Bells Landing Marl and the initial CIE sample of the Harrell core are processed in the exact same way at the Laboratory of Palaeobotany and Palynology at Utrecht University and stored in water. Residues stored in glycerin water are sieved with warm water through a 15 µm sieve to remove the glycerin and are stored in water.

A few drops of the residue are transferred to a glass petri-dish and further diluted using demineralized water if required. The flame heated tip of a glass pipette is extended to narrow its diameter. This micropipette is connected to a tube and is used to isolate specimens of dinocysts or pollen from the assemblage. This is assemblage is placed on an inverted microscope at the Ocean Sciences department of the University of California in Santa Cruz (UCSC). Specimens are pushed back out of the pipette tip onto a second glass petri-dish. After the isolation of sufficient

specimens, the process of isolation is repeated from the second petri-dish to a third. This is done in order to eliminate the organic particles or undesired species that may have entered the pipette by accident. The third petri-dish can be studied under the inverted microscope, so the last few unwanted particles can be removed. The remaining sample containing nothing other than the desired taxon is transferred to a 0.6 ml Eppendorf tube. A test sample showed that 250 specimens of *Apectodinium* generate a voltage in the isotope ratio mass spectrometer (IRMS) which is sufficiently high for a reliable determination of the isotope ratio. Assuming equal density and equal carbon content of the organic matter as well as a diameter half the size of an *Apectodinium* cyst, approximately 1000 pollen grains are required to obtain enough mass of carbon.

The cups, samples and standards are prepared and analyzed at the stable isotope laboratory (Silab) of Earth and Planetary Sciences at UCSC. Silver cups used for the elemental analyzer are first cleaned by heating them for 8 hours at 450°C. Three batches are made in this way, all generating a low blank signal. The samples in the Eppendorf tubes are dried under a nitrogen flow. Subsequently, the cysts are dissolved in 10 µl of demineralized water and transferred to silver cups. After, the last bit of water is also evaporated under a nitrogen flow, the cups are closed. Used standards during each analysis are the in-house international standard Pugel, a gelatin from Princeton University ($\delta^{13}C$ = -12.60‰ ± 0.1), and the international standard Acetanilide from Schimmelmann, Indiana University ($\delta^{13}C$ = -29.34‰ ± 0.01). In addition to these standards, a new standard is created using sucrose solutions. Pure sucrose from the stock of the Silab at UCSC (Mallinckrodt Inc., batch 643464102) is used to make solutions containing 0.01 to 1 µg of carbon per µl. A detailed protocol for making these solutions and actual carbon content of processed batches are attached in Appendix I. Of each solution 10 µl is transferred to a silver cup. The first batch is dried under a fume hood, whereas the second and third batch are dried under a nitrogen flow. Analyses are done in three runs using a Carlo Erba Instruments CHNS-0 EA-1108 Elemental Analyzer connected via a Finnigan Conflo III to a Finnigan Delta Plus XP. Each run is only corrected for the offset with the Pugel standard. Stable carbon isotope ratios are expressed following $\delta^{13}C = (({}^{13}C/{}^{12}C)_{sample} / ({}^{13}C/{}^{12}C)_{standard} - 1) * 1000$. The standard is Vienna PeeDee Belemnite (VPDB).

4. Results

Sluijs et al. (2007b) measured stable carbon isotopes on the 40 to 125 µm size fraction of the palynological residue of sediments from Bass River ($\delta^{13}C_{40\text{-}125}$) (Figure 2). This size fraction represents *Apectodinium* dominated dinocyst assemblages. This record shows an initial CIE of ~-1‰. Above an interval of relatively stable $\delta^{13}C$, a larger negative excursion results into the full CIE magnitude of ~4.5‰. The total palynological residue with a size range of 15 to 125 µm shows an initial CIE of ~-2.5‰ $\delta^{13}C_{15\text{-}125}$ (Figure 2). Values are slightly higher for the 15 to 125 µm compared to the 40 to 125 µm fraction. Stable carbon isotope values of *Apectodinium* cysts ($\delta^{13}C_{Apecto}$) are ~2.5‰ higher than for the 15 to 125 µm size fraction. The initial CIE is 1.3 and 2.0‰ for the first and second run, respectively. At 357.12 mbs, $\delta^{13}C_{Apecto}$ is similar to the pre-CIE sample at 357.58 mbs. Measurements on single shells of planktonic foraminifer of the *Acarinina* and *Morozovella* genera have been done by John et al. (2008) (Figure 2). Both genera show a ~-4‰ CIE. *Acarinina* is by ~1‰ more depleted in ^{13}C compared to *Morozovella*.

Total organic carbon (TOC) was measured across the PETM in the Harrell core (van Roij in prep.) (Figure 3). The $\delta^{13}C_{TOC}$ record shows an initial CIE of ~-1.5‰ at 121.9 mbs. After a slight recovery, the full CIE is recorded at 121.6 mbs with a

magnitude of ~-3‰. The total palynological residue shows a ~-2.8‰ CIE between the pre-CIE and the CIE-body. The sample at 121.87 mbs represents the initiation of the CIE by a ~-1‰ shift in $\delta^{13}C_{15\text{-}125}$. The sample at 121.62 mbs corresponds to the full ~-3‰ CIE in the $\delta^{13}C_{TOC}$ record, but shows only a ~-1.8‰ CIE in $\delta^{13}C_{15\text{-}125}$. The first series of $\delta^{13}C$ of *Apectodinium* ($\delta^{13}C_{Apecto}$) shows a ~-1.2‰ CIE between the pre-CIE and the sample at 121.87 mbs. At 121.62 mbs, two duplicates go back to pre-CIE $\delta^{13}C_{Apecto}$ values. In the second run, one duplicate shows a $\delta^{13}C_{Apecto}$ only slightly lower than the pre-CIE value at 121.72 mbs. The other duplicate suggests a ~-2.2‰ CIE. The sample at 120.09 mbs in the CIE-body shows a ~1.8‰ lower $\delta^{13}C_{Apecto}$ compared to the pre-CIE value.

Unfortunately, none of the samples contain sufficient *Thomsonipollis magnificus* or *Nudopollis terminalis* to collect enough carbon for reliable analysis. Therefore, the course and extent of the CIE in pollen grains cannot be determined and no comparison between fractionation by these higher plant species and marine dinocyst *Apectodinium* can be made.

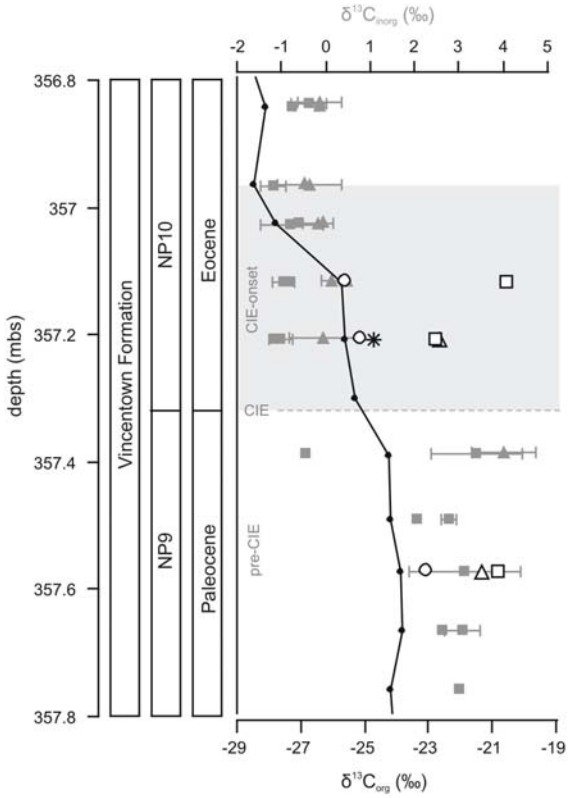

Figure 2. Stable carbon isotope record of organic and inorganic carbon substrates from Bass River. Dinocyst (40-125 µm) fraction (line, closed circles) from Sluijs et al. (2007b). Single shells of planktonic foraminifer *Acarinina* (grey, closed square) and *Morozovella* (grey, closed triangle) from John et al. (2008). Total palynological residue (15-125 µm; open circles), *Apectodinium* test sample (asterisk), 1st run *Apectodinium* (open triangles), and 2nd run *Apectodinium* (open squares). Dashed line indicates the initial CIE. Shaded area indicates the CIE-onset.

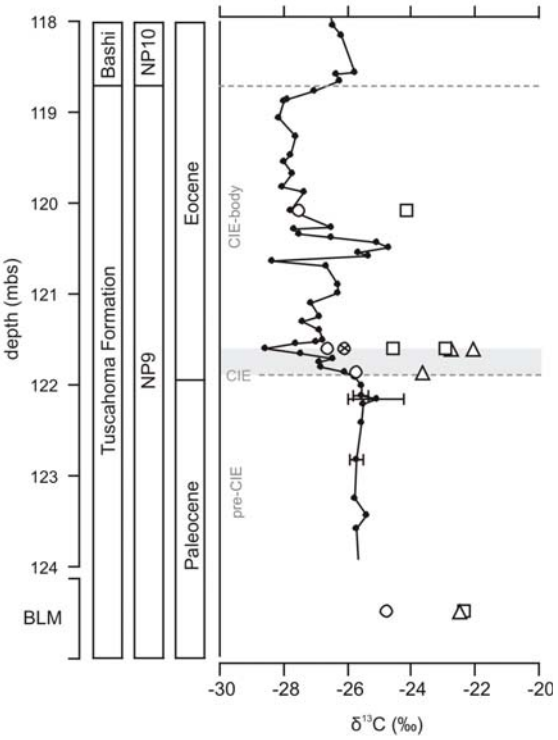

Figure 3. Stable carbon isotopes of organic carbon substrates of the Harrell core. Total organic carbon (line, closed circles) from van Roij (in prep.). Total palynological residue (15-125 µm; open circles, circle with cross for the residue without dinocysts), 1st run *Apectodinium* (open triangles) and 2nd run *Apectodinium* (open squares). Dashed lines indicate the initial CIE and its termination. Shaded area indicates the CIE-onset. Depth of Bells Landing Marl (BLM) is not to scale.

5. Discussion

5.1. Technical and analytical issues

Various complications occurred during the generation of the analyses. These complications will first be discussed before the data is further used for interpretations.

Firstly, the palynological residues of Bass River have been stored in glycerin water for several years, whereas most Harrell samples have been stored for approximately four months. A few residues were isolated only shortly before the stable isotope analyses. Furthermore, the stored residues were sieved to remove the glycerin water and stored in regular tap water. Tap water contains extremely small amounts of total (dissolved and particulate) organic carbon (TOC) with a total of less than 2 mg/L. Total alkalinity is dominated by dissolved inorganic carbon (DIC) as bicarbonate and carbonate ions and has a concentration of ~200 mg/L. TOC and DIC are considered to be removed during the isolation of *Apectodinium* cysts using dematerialized water. However, the full palynological residue may have contained some modern TOC and DIC. The present day atmospheric $\delta^{13}C$ is higher compared to the Early Paleogene, thereby biasing $\delta^{13}C_{15\text{-}125}$ of the samples towards higher values.

During the isolation of *Apectodinium* several samples have been dried out on the petri-dish or in an Eppendorf tube. If degradation occurred, this may have affected the isotopic composition of the cysts. All samples of the first run have dried out. Of the second run, the duplicate with the higher $\delta^{13}C_{Apecto}$ value at 121.62 mbs of the Harrell core also dried out. Interestingly, at all sample levels the dried and non-dried samples show very similar values with the exception of the sample at 121.62 mbs of the Harrell core. Here, the only non-dried sample shows ~-1.5 to -2.5‰ lower values than the three dried samples. However, since this offset is not observed at other sample levels, this deviation is most probably not due to this drying.

The extremely small amounts of carbon measured led to more complications. The measuring cups of the EA had to be cleaned using different techniques until a way was found that no longer caused contamination of the blank signal. The test run showed that 0.5 µg of carbon is sufficient for generating a reliable $\delta^{13}C$ based on the sucrose solutions (Appendix II). However, the first and second run both indicate that at least 0.8 µg of sucrose derived carbon is required. The analyzed carbon is oxidized to form CO_2 which is variable in weight due to its isotopic composition. The mass spectrometer generates a voltage during the time that CO_2 molecules of a certain mass are detected. The more molecules are detected, the higher the voltage. In this way, a peak is formed with its shape defined by the amount and time interval of molecules passing the detector. The area below such a peak is expressed in volts times seconds (V*s). As the lighter molecules are detected earlier than the heavier molecules, each peak can be assigned to a CO_2 molecule with a certain weight. The area below the peak corresponding to CO_2 with a mass of 44 g/mole (Area 44) is used for calculating the $\delta^{13}C$ values. For sucrose samples containing 0.5 µg of carbon, this Area 44 is 1 V*s. However, samples with 0.8 µg of carbon generate a larger Area 44 of 1.5 V*s. All *Apectodinium* samples easily exceed the lower Area 44 limit, but both CIE-onset samples of Bass River on *Apectodinium* are not sufficiently large when regarding the higher Area 44 limit in the second run. Samples that are too small would generate a signal that tends towards the lower blank signal. However, the $\delta^{13}C_{Apecto}$ at 357.21 mbs of Bass River is very similar to the first run value. Furthermore, since the value at 357.12 mbs is higher than expected from the measurements on the dinocysts assemblages (Sluijs et al. 2007b), $\delta^{13}C_{Apecto}$ is unlikely to be too low.

Corrections for the raw $\delta^{13}C$ data were simplified by only shifting all values, so that the average Pugel value would fit its true standard value. However, the acetanilide standard varies enormously by -3, +2.6 and +2‰ between the test run, first run and second run, respectively. Although the standard value of sucrose is yet unknown, their average varies by 1.5‰ between runs. None of the runs show a significant drift in the EA ($R^2<0.08$), so no correction is made for that. There is no correlation between Area 44 of Pugel, sucrose or the samples and their raw $\delta^{13}C$ values in the test run and first run ($R^2<0.13$). In the second run, however, there is a correlation between Area 44 of sucrose and its $\delta^{13}C$ ($R^2=0.52$) and between Area 44 of the *Apectodinium* samples and their $\delta^{13}C$ ($R^2=0.55$). When performing this sample size correction, the trends in $\delta^{13}C_{15\text{-}125}$ and $\delta^{13}C_{Apecto}$ are more or less flattened out and the offset between the two $\delta^{13}C_{Apecto}$ records of the Harrell core increases. This correction is used since the correlations were not found in the other runs and the alternative trends are very different from the trends observed in both the raw data and the earlier obtained $\delta^{13}C_{TOC}$ and $\delta^{13}C_{40\text{-}125}$.

5.2. Comparison of stable carbon isotope records

At Bass River, the $\delta^{13}C_{40\text{-}125}$ record of Sluijs et al. (2007b) is only slightly more depleted in ^{13}C than the $\delta^{13}C_{15\text{-}125}$ values (Figure 2). Since the palynological residues almost completely exist of dinocysts, there is no large offset between these two records. However, the small difference suggests that the 15 to 40 µm size fraction of the total residue has a relatively high $\delta^{13}C$. This is hard to explain since the dinocyst fraction is almost entirely of marine origin and a possible presence of some terrestrial compounds in the palynological residue would result into lower $\delta^{13}C_{15\text{-}125}$ values. Alternatively, the $\delta^{13}C$15-125 could in fact be more depleted considering $\delta^{13}C_{15\text{-}125}$ and $\delta^{13}C_{40\text{-}125}$ have been analyzed in different studies. Furthermore, the 15 to 40 µm size fraction contains marine derived structures with high $\delta^{13}C$ values. The $\delta^{13}C_{Apecto}$ values are by >2‰ higher than $\delta^{13}C_{15\text{-}125}$. If this offset would be due to the presence of more ^{13}C-depleted terrestrial components in the palynological residue, $\delta^{13}C_{40\text{-}125}$ should have values more similar to $\delta^{13}C_{Apecto}$. As a result, the offset of $\delta^{13}C_{Apecto}$ with the $\delta^{13}C_{15\text{-}125}$ and $\delta^{13}C_{40\text{-}125}$ records seems to be due to genus specific fractionation. The $\delta^{13}C_{40\text{-}125}$ record thus implies that the dinocyst taxa other than *Apectodinium* within the 40 to 125 µm fraction have to show an extremely low $\delta^{13}C$ signal. As *Apectodinium* was possibly a heterotrophic genus (Bujak and Brinkhuis 1998), higher $\delta^{13}C$ values relatively to photoautotrophic dinocysts can be explained by respiration or a change in diet. The carbonate shells of *Acarinina* show lower $\delta^{13}C$ values compared to *Morozovella*. Temperature reconstructions based on $\delta^{18}O$ suggest *Morozovella* may have been living at shallower depths. Therefore, the difference in $\delta^{13}C$ may be a result of differences in ocean water chemistry in terms of pH and DIC content.

The Harrell core has values similar for $\delta^{13}C_{TOC}$ compared to $\delta^{13}C_{15\text{-}125}$ at 121.87 and 120.09 mbs (Figure 3). The sample at 121.62 mbs shows a higher $\delta^{13}C_{15\text{-}125}$ value than the $\delta^{13}C_{TOC}$ record. Although there is no $\delta^{13}C_{TOC}$ value of the Bell's Landing Marl sample which is used for the pre-CIE $\delta^{13}C_{15\text{-}125}$, the relative stable $\delta^{13}C_{15\text{-}125}$ of the pre-CIE interval of the Harrell core suggests that the pre-CIE $\delta^{13}C_{15\text{-}125}$ is higher than $\delta^{13}C_{TOC}$. Differences between the measured substrates are the absence of organic matter smaller than 15 µm and larger than 125 µm in the palynological residue compared to the TOC. The two deviating samples may contain more of these smallest or largest particles which seem to be more depleted in ^{13}C and are possibly derived from higher plants. However, the loss of the 15 to 40 µm size fraction in the $\delta^{13}C_{40\text{-}125}$ record of Bass River shows the opposite effect. Future research should focus on differences in composition and isotopic signature of the substrates in the

smaller than 15 µm, larger than 125 µm and 15 to 40 µm size fractions of TOC. This may reveal the source of the carbon with the higher or lower $\delta^{13}C$ values. At 121.62 mbs, the palynological residue of which the dinocysts have been removed shows a higher $\delta^{13}C$ than the total residue. This suggests that the removed dinocysts have a lower $\delta^{13}C$ value than the total residue. Also at the Harrell core, however, $\delta^{13}C_{Apecto}$ values are by >2‰ higher than $\delta^{13}C_{15\text{-}125}$. Autotrophic dinoflagellates with a high sensitivity to increased CO_2 could be responsible for the lower $\delta^{13}C$ values. These autotrophs would fractionate more in ^{13}C as dissolved CO_2 increases during the PETM and thus explain the larger CIE in $\delta^{13}C_{40\text{-}125}$ compared to $\delta^{13}C_{Apecto}$. Since *Apectodinium* makes up the largest part of the dinocyst assemblage, it seems unlikely that other dinocyst species would be responsible for the low $\delta^{13}C_{15\text{-}125}$ signal. Other dinoflagellate species should be measured for their isotopic composition to test this hypothesis. Especially photoautotrophs are of interest as they directly interact with carbon from the atmosphere and ocean reservoir and may be susceptible to dissolved CO_2 increase (Rost et al. 2006). Alternatively, the 0.5‰ offset between the total residue and the residue with dinocysts may also be considered to be the result of heterogeneity within the palynological residue or an analytical error. The latter is supported by large variability in $\delta^{13}C_{Apecto}$ of the four duplicates at 121.62 mbs.

The $\delta^{13}C_{15\text{-}125}$ and $\delta^{13}C_{Apecto}$ records of Bass River are approximately 2‰ higher compared to the same records of the Harrell core (Figures 2 and 3). As $\delta^{13}C$ of marine organisms generally reflects the $\delta^{13}C$ of DIC, the differences between the cores may be due to the relative concentrations of dissolved CO_2, HCO_3^- and CO_3^{2-}. Furthermore, temperature reconstructions show that the sea surface was equally warm at both localities (van Roij in prep.), suggesting the that the offset is not due to effects of temperature.

5.3. Shape and magnitude of the CIE

At Bass River, the studied interval only includes part of the CIE-onset (Sluijs et al. 2007b) (Figure 2). This first step has a CIE of ~0.5‰ larger for $\delta^{13}C_{15\text{-}125}$ compared to $\delta^{13}C_{40\text{-}125}$. Although the palynological residues of this core hardly contain any terrestrial material, these compounds may explain the larger CIE compared to fully marine material. Besides the larger fractionation by terrestrial organisms, also the increase in abundance of the more ^{13}C depleted compounds may explain the larger CIE in the total residue. However, the relative increase of terrestrially derived compounds is in contradiction with the sea level rise observed for this site (Sluijs et al. 2008). The CIE in $\delta^{13}C_{Apecto}$ between the pre-CIE and the duplicates of the sample at 357.21 mbs is comparable to the CIE in $\delta^{13}C_{40\text{-}125}$ for the same interval. However, the *Apectodinium* sample at 357.12 mbs has a $\delta^{13}C_{Apecto}$ value comparable to the pre-CIE values. This could suggest an instant recovery in $\delta^{13}C$ by *Apectodinium* and raises the question whether a further decrease could be observed in the CIE-body. The CIE in the $\delta^{13}C$ records of *Acarinina* and *Morozovella* are ~-4‰. Neither records show intermediate values, but an abrupt shift.

The $\delta^{13}C_{TOC}$ record of the Harrell core shows a CIE-onset comprised of two steps of decrease in $\delta^{13}C$ (van Roij in prep.) (Figure 3). The full CIE has a magnitude of ~-3‰ at 121.62 mbs, whereas the first CIE step is ~-1.3‰. Although this record has large unexplained fluctuations in $\delta^{13}C_{TOC}$, the average value for the CIE-body is by ~-1.5‰ more depleted than the pre-CIE interval (van Roij in prep.). The CIE in $\delta^{13}C_{15\text{-}125}$ is similar to the magnitude in $\delta^{13}C_{TOC}$. The offset between $\delta^{13}C_{TOC}$ and $\delta^{13}C_{15\text{-}125}$ at 121.62 mbs is much larger than the offsets for the other samples. For this sample, the smaller than 15 µm and larger than 150 µm size fractions of the TOC may not just represent lower $\delta^{13}C$ values, but could also have increased in abundance. A temporary increase in more ^{13}C depleted carbon could be a result of enhanced river

inflow supplying larger amounts of terrestrial compounds and/or increased angiosperm abundance. The first measurements on *Apectodinium* cysts show a CIE of ~-1.2‰ between the pre-CIE and 121.87 mbs. Interestingly, both duplicates at 121.62 mbs are more comparable to the pre-CIE sample rather than showing a further depletion. This consistent with the pattern observed for Bass River. In the second run, however, another two duplicates at 121.61 mbs show $\delta^{13}C_{Apecto}$ suggesting a ~-0.6 and a ~-2.2‰ CIE. This suggests there may be either no CIE, a small CIE or a moderate CIE at this sample level. The sample at 120.09 mbs shows a ~-1.8‰ CIE, suggesting that a complete $\delta^{13}C_{Apecto}$ record would show a CIE-body similar to the $\delta^{13}C_{TOC}$ record. However, the largest magnitude of the CIE in $\delta^{13}C_{Apecto}$ is smaller than observed in the $\delta^{13}C_{TOC}$ and $\delta^{13}C_{15\text{-}125}$ records.

The ~2‰ offset between the records of Bass River and the Harrell core is more or less constant throughout the studied interval (Figures 2 and 3). Since the CIE in the $\delta^{13}C_{Apecto}$ and $\delta^{13}C_{15\text{-}125}$ records of Bass River only comprise part of the CIE-onset, a comparison between the full CIE magnitudes with of the Harrell core is not possible. However, the CIE in $\delta^{13}C_{15\text{-}125}$ at Bass River seems to be larger than for the Harrell core when assuming the $\delta^{13}C_{15\text{-}125}$ at Bass River continues to decrease similar to the $\delta^{13}C_{40\text{-}125}$ record. This is likely since the 40 to 125 µm size fraction makes up the largest part of the 15 to 125 15 µm size fraction. This would also be consistent with the ~-4.5‰ CIE in the $\delta^{13}C_{40\text{-}125}$ record. Also the CIE in $\delta^{13}C_{Apecto}$ could become larger at Bass River. A further decrease in $\delta^{13}C_{Apecto}$ within the CIE-body is suggested by the *Apectodinium* sample at 120.09 mbs in the Harrell core. Furthermore, the 40 to 125 µm size fraction consists mainly of *Apectodinium* and shows a ~-4.5‰ CIE. If both suggestions above are valid, the CIE in the various substrates are ~-3‰ for the Harrell core and ~-4‰ at Bass River. The larger CIE at Bass River suggests that at this site changes in DIC composition must have been more significant. However, if the $\delta^{13}C_{Apecto}$ does not show further decrease at Bass River, the CIE in $\delta^{13}C_{Apecto}$ is smaller than in $\delta^{13}C_{15\text{-}125}$. This would be consistent with the smaller CIE in $\delta^{13}C_{Apecto}$ compared to the CIE in $\delta^{13}C_{TOC}$ and $\delta^{13}C_{15\text{-}125}$ in the Harrell core. Also the ~2‰ offset between the $\delta^{13}C_{40\text{-}125}$ and the $\delta^{13}C_{Apecto}$ record indicates that these substrates are very different in isotopic composition and may therefore also show different CIE magnitudes. Apparently, *Apectodinium* shows both less fractionation in ^{13}C and less increase in fractionation during the PETM compared to the TOC, the dinocyst fraction and the full palynological residue. A smaller CIE in $\delta^{13}C_{Apecto}$ could be explained by increased respiration by *Apectodinium* during the PETM. Moreover, the species specific positive CO_2 effect on fractionation as described by Popp et al. (1998) may be insignificant for *Apectodinium*. Also, an increased growth rate larger than the increase in the diffusion rate of molecules into and out of the cells may also explain a decrease in fractionation (Hinga et al. 1994). Furthermore, the unknown effects of temperature on other cellular processes (Hinga et al. 1994) and the unknown food source of *Apectodinium* and the isotopic composition of this source may contribute to a smaller CIE.

6. Conclusions

Despite possible analytical issues and the lack of data in the CIE-body at Bass River, several observations can be pointed out. Firstly, the $\delta^{13}C_{15\text{-}125}$ and $\delta^{13}C_{Apecto}$ records of Bass River are approximately 2‰ higher compared to the same records of the Harrell core (Figures 2 and 3). This difference may be due to the ratio of DIC and thus its isotopic composition. Secondly, $\delta^{13}C_{Apecto}$ values are consistently higher than $\delta^{13}C_{TOC}$, $\delta^{13}C_{DC}$ and $\delta^{13}C_{15\text{-}125}$. Unfortunately, no clear CIE could be detected for *Apectodinium* so comparison with other substrates is difficult. Apparently,

Apectodinium fractionates less efficiently compared to the average of other dinocysts and terrestrial organisms. The $\delta^{13}C_{Apecto}$ record of the Harrell core suggests that the increase in fractionation during the PETM is smaller than observed in TOC and the palynological residue. This could be due to increased respiration.

Major complications during the interpretation of the data are the lack of knowledge on carbon isotopic fractionation in phytoplankton. Many variables affect this fractionation in opposed directions and the sensitivity of each species to these variables appears to be different. Furthermore, differences between the measured substrates are mostly due to the removal of a size fraction. The palynological residue is the TOC without the smaller than 15 and larger than 125 µm size fraction and the dinocyst fraction is the palynological residue without the 15 to 40 µm size fraction. The content of the removed size fractions is unclear. The smaller than 15 µm and larger than 150 µm size fractions of the TOC seems to contain structures with a low $\delta^{13}C$ signature. These structures are derived from organisms that increased their fractionation during the PETM more than the organisms that produced the structures in the 15 to 125 µm size fraction. The 15 to 40 µm size fraction of the palynological residue has a relatively high $\delta^{13}C$ which is hard to explain. Therefore, the smaller than 15 µm, 15 to 40 µm and larger than 150 µm size fractions should be studied for their actual content and isotopic composition. The difference between the dinocyst fraction and *Apectodinium* is the presence of other dinocyst taxa. These taxa seem to fractionate a lot more efficiently. Especially photoautotrophs should be studied for their isotopic signature as they directly interact with carbon from the atmosphere and ocean reservoir. Also the fractionation of terrestrial plants along the Gulf Coast and changes in fractionation during the PETM remain unknown due to a lack of significant pollen abundances.

More samples should reveal the full CIE in $\delta^{13}C_{15\text{-}125}$ and $\delta^{13}C_{Apecto}$ records at Bass River. A more complete $\delta^{13}C_{Apecto}$ may indicate whether the $\delta^{13}C_{Apecto}$ shows further decreases with the CIE-body. Furthermore, it should clarify whether *Apectodinium* indeed shows less increase in fractionation during the PETM compared to the TOC and the full palynological residue.

Acknowledgements

Quite a few people were involved with this study and owe my humble regard. First of all, the crazy idea of isolating dinocysts one by one came from Gert-Jan. Many thanks for that! Henk always kept an eye on my progress and introduced me to Jim Zachos who welcomed me to his lab. My trip to UCSC was mainly funded by the LPP, Dr. Christine Buisman Fund and the Trajectum scholarship. Jocelyn Sessa provided me with information on the Harrell core. Guy Harrington kindly introduced me to the field of Early Paleogene pollen in North America and suggested species for species specific isotope analysis. For the isolation of specimens I was allowed to use the equipment in the lab of Raphael Kudela and assisted by Kendra Hayashi. Dyke Andreasen and Pratigya Polissar were very helpful during isotope analyses and involved in dealing with practical issues. Jan van Tongeren processed an additional sample for obtaining its palynological residue. Appy was closely involved with this project from the birth of the idea until the final version of this report.

References

Badger, M. R., T. J. Andrews, S. M. Whitney, M. Ludwig, D. C. Yellowlees, W. Leggat, and G. D. Price. 1998. The diversity and coevolution of Rubisco, plastids, pyrenoids, and chloroplast-based CO2-concentrating mechanisms in algae. Canadian Journal of Botany **76**:1052-1071.

Bains, S., R. D. Norris, R. M. Corfield, G. J. Bowen, P. D. Gingerich, and P. L. Koch. 2003. Marine-terrestrial linkages at the Paleocene-Eocene boundary. Pages 1-9 *in* S. L. Wing, P. D. Gingerich, B. Schmitz, and E. Thomas, editors. Causes and Consequences of Globally Warm Climates in the Early Paleogene. Geological Society of America Special Paper 369. Geological Society of America, Boulder, Colorado, USA.

Beardall, J., and M. Giordano. 2002. Ecological implications of microalgal and cyanobacterial CO₂ concentrating mechanisms, and their regulation. Functional Plant Biology **29**:335-347.

Bidigare, R. R., A. Fluegge, K. H. Freeman, K. L. Hanson, J. M. Hayes, D. Hollander, J. P. Jasper, L. L. King, E. A. Laws, J. Milder, F. J. Millero, R. Pancost, B. N. Popp, P. A. Steinberg, and S. G. Wakeham. 1997. Consistent fractionation of ^{13}C in nature and in the laboratory: Growth-rate effects in some haptophyte algae. Global Biogeochemical Cycles **11**:279-292.

Bowen, G. J., D. J. Beerling, P. L. Koch, J. C. Zachos, and T. Quattlebaum. 2004. A humid climate state during the Palaeocene/Eocene thermal maximum. Nature **432**:495-499.

Bowen, G. J., T. J. Bralower, M. L. Delaney, G. R. Dickens, D. C. Kelly, P. L. Koch, L. R. Kump, J. Meng, L. C. Sloan, E. Thomas, S. L. Wing, and J. C. Zachos. 2006. Eocene Hyperthermal Event Offers Insight Into Greenhouse Warming. EOS, Transactions, American Geophysical Union **87**:165, 169.

Bowen, G. J., W. C. Clyde, P. L. Koch, S. Y. Ting, J. Alroy, T. Tsubamoto, Y. Q. Wang, and Y. Wang. 2002. Mammalian dispersal at the Paleocene/Eocene boundary. Science **295**:2062-2065.

Bowen, G. J., P. L. Koch, P. D. Gingerich, R. D. Norris, S. Bains, and R. M. Corfield. 2001. Refined isotope stratigraphy across the continental Paleocene-Eocene boundary on Polecat Bench in the Northern Bighorn Basin. Pages 73-88 *in* P. D. Gingerich, editor. Paleocene-Eocene Stratigraphy and Biotic Change in the Bighorn and Clarks Fork Basins, Wyoming. University of Michigan Papers on Paleontology 33.

Bujak, J. P., and H. Brinkhuis. 1998. Global warming and dinocyst changes across the Paleocene/Eocene Epoch boundary. Pages 277-295 *in* M.-P. Aubry, S. G. Lucas, and W. A. Berggren, editors. Late Paleocene - early Eocene climatic and biotic events in the marine and terrestrial records. Columbia University Press, New York.

Burkhardt, S., G. Amoroso, U. Riebesell, and D. Sultemeyer. 2001. CO2 and HCO3- uptake in marine diatoms acclimated to different CO2 concentrations. Limnology and Oceanography **46**:1378-1391.

Campbell, N. A., and J. B. Reece. 2002. Biology, 6th edition. Benjamin Cummings, San Francisco.

Chikaraishi, Y., and H. Naraoka. 2003. Compound-specific $\delta^{13}C$ analyses of n-alkanes extracted from terrestrial and aquatic plants. Phytochemistry **63**:361-371.

Crouch, E. M., C. Heilmann-Clausen, H. Brinkhuis, H. E. G. Morgans, K. M. Rogers, H. Egger, and B. Schmitz. 2001. Global dinoflagellate event associated with the late Paleocene thermal maximum. Geology **29**:315-318.

Dickens, G. R., M. M. Castillo, and J. C. G. Walker. 1997. A blast of gas in the latest Paleocene: Simulating first-order effects of massive dissociation of oceanic methane hydrate. Geology **25**:259-262.
Dickens, G. R., J. R. O'Neil, D. K. Rea, and R. M. Owen. 1995. Dissociation of oceanic methane hydrate as a cause of the carbon isotope excursion at the end of the Paleocene. Paleoceanography **10**:965-971.
Gibson, T. G., and L. M. Bybell. 1994. Sedimentary Patterns across the Paleocene-Eocene boundary in the Atlantic and Gulf coastal plains of the United States. Bulletin de la Société Belge de Géologie **103**:237-265.
Harrington, G. J. 2001. Impact of Paleocene/Eocene Greenhouse Warming on North American Paratropical Forests. Palaios **16**:266-278.
Harrington, G. J. 2003. Geographic patterns in the floral response to Paleocene-Eocene warming. Pages 381-393 *in* S. L. Wing, P. D. Gingerich, B. Schmitz, and E. Thomas, editors. Causes and Consequences of Globally Warm Climates in the Early Paleogene. Geological Society of America Special Paper 369, Boulder, Colorado.
Harrington, G. J. 2008. Comparisons between Palaeocene - Eocene paratropical swamp and marginal marine pollen flores from Alabama and Mississippi, USA. Palaeontology **51**:611-622.
Harrington, G. J., and S. J. Kemp. 2001. US Gulf Coast vegetation dynamics during the latest Palaeocene. Palaeogeography Palaeoclimatology Palaeoecology **167**:1-21.
Hinga, K. R., M. A. Arthur, M. E. Q. Pilson, and D. Whitaker. 1994. Carbon Isotope Fractionation by Marine Phytoplankton in Culture: The Effects of CO2 Concentration, pH, Temperature, and Species. Global Biogeochemical Cycles **8**:91-102.
Huber, M., and L. C. Sloan. 1999. Warm climate transitions: A general circulation modeling study of the Late Paleocene Thermal Maximum (~56 Ma). Journal of Geophysical Research **104**:16,663-616,655.
Jahren, A. H. 2004. The carbon stable isotope composition of pollen. Review of Palaeobotany and Palynology **132**:291-313.
John, C. M., S. M. Bohaty, J. C. Zachos, A. Sluijs, S. J. Gibbs, H. Brinkhuis, and T. J. Bralower. 2008. North American continental margin records of the Paleocene-Eocene thermal maximum: Implications for global carbon and hydrological cycling. Paleoceanography **23**:PA2217, doi:2210.1029/2007PA001465.
Kennett, J. P., and L. D. Stott. 1991. Abrupt deep-sea warming, palaeoceanographic changes and benthic extinctions at the end of the Palaeocene. Nature **353**:225-229.
Koch, P. L., J. C. Zachos, and D. L. Dettman. 1995. Stable isotope stratigraphy and paleoclimatology of the Paleogene Bighorn Basin (Wyoming, USA). Palaeogeography, Palaeoclimatology, Palaeoecology **115**:61-89.
Koch, P. L., J. C. Zachos, and P. D. Gingerich. 1992. Correlation between isotope records in marine and continental carbon reservoirs near the Palaeocene/Eocene boundary. Nature **358**:319-322.
Loader, N. J., and D. L. Hemming. 2001. Spatial variation in pollen δ13C correlates with temperature and seasonal development timing. Holocene **11**:587-592.
McCarren, H., E. Thomas, T. Hasegawa, U. Röhl, and C. Zachos James. 2008. Depth dependency of the Paleocene-Eocene carbon isotope excursion: Paired benthic and terrestrial biomarker records (Ocean Drilling Program Leg 208, Walvis Ridge). Geochemistry Geophysics Geosystems **9**.
Pagani, M., N. Pedentchouk, M. Huber, A. Sluijs, S. Schouten, H. Brinkhuis, J. S. Sinninghe Damsté, G. R. Dickens, and T. Expedition 302 Scientists. 2006. Arctic

hydrology during global warming at the Palaeocene-Eocene thermal maximum. Nature **442**:671-675.
Popp, B. N., E. A. Laws, R. R. Bidigare, J. E. Dore, K. L. Hanson, and S. G. Wakeham. 1998. Effect of Phytoplankton Cell Geometry on Carbon Isotopic Fractionation. Geochimica et Cosmochimica Acta **62**:69-77.
Röhl, U., T. J. Bralower, G. Norris, and G. Wefer. 2000. A new chronology for the late Paleocene thermal maximum and its environmental implications. Geology **28**:927-930.
Röhl, U., T. Westerhold, T. J. Bralower, and J. C. Zachos. 2007. On the duration of the Paleocene – Eocene thermal maximum (PETM). Geochemistry, Geophysics, Geosystems **8**:doi:10.1029/2007GC001784.
Rost, B., K.-U. Richter, U. Riebesell, and P. J. Hansen. 2006. Inorganic carbon acquisition in red tide dinoflagellates. Plant, Cell and Environment **29**:810-822.
Rost, B., U. Riebesell, and D. Sultemeyer. 2003. Carbon acquisition of bloom-forming marine phytoplankton. Limnology and Oceanography **48**:55-67.
Ruddiman, W. F. 2001. Earth's climate: Past and Future. WH Freeman, New York.
Schmitz, B., and V. Pujalte. 2003. Sea-level, humidity, and land-erosion records across the initial Eocene thermal maximum from a continental-marine transect in northern Spain. Geology **31**:689-692.
Schouten, S., M. Woltering, W. I. C. Rijpstra, A. Sluijs, H. Brinkhuis, and J. S. Sinninghe Damsté. 2007. The Paleocene-Eocene carbon isotope excursion in higher plant organic matter: Differential fractionation of angiosperms and conifers in the Arctic. Earth and Planetary Science Letters **258**:581-592.
Shellito, C. J., L. C. Sloan, and M. Huber. 2003. Climate model sensitivity to atmospheric CO_2 levels in the Early-Middle Paleogene. Palaeogeography, Palaeoclimatology, Palaeoecology **193**:113-123.
Sluijs, A., G. J. Bowen, H. Brinkhuis, L. J. Lourens, and E. Thomas. 2007a. The Palaeocene-Eocene thermal maximum super greenhouse: biotic and geochemical signatures, age models and mechanisms of global change. Pages 323-347 *in* M. Williams, A. M. Haywood, F. J. Gregory, and D. N. Schmidt, editors. Deep time perspectives on Climate Change: Marrying the Signal from Computer Models and Biological Proxies. The Micropalaeontological Society, Special Publications. The Geological Society, London, London.
Sluijs, A., and H. Brinkhuis. 2009. A dynamic climate and ecosystem state during the Paleocene-Eocene Thermal Maximum--inferences from dinoflagellate cyst assemblages at the New Jersey Shelf. Biogeosciences Discussions **6**:5163-5215.
Sluijs, A., H. Brinkhuis, E. M. Crouch, C. d. M. John, L. Handley, D. Munsterman, S. M. Bohaty, J. C. Zachos, G.-J. Reichart, S. Schouten, R. D. Pancost, J. S. S. DamstÃ©, N. L. D. Welters, A. F. Lotter, and G. R. Dickens. 2008. Eustatic variations during the Paleocene-Eocene greenhouse world. Paleoceanography **23**.
Sluijs, A., H. Brinkhuis, S. Schouten, S. M. Bohaty, C. M. John, J. C. Zachos, J. S. Sinninghe Damsté, E. M. Crouch, and G. R. Dickens. 2007b. Environmental precursors to light carbon input at the Paleocene/Eocene boundary. Nature **450**:1218-1221.
Sluijs, A., S. Schouten, M. Pagani, M. Woltering, H. Brinkhuis, J. S. Sinninghe Damsté, G. R. Dickens, M. Huber, G.-J. Reichart, R. Stein, J. Matthiessen, L. J. Lourens, N. Pedentchouk, J. Backman, K. Moran, and T. Expedition 302 Scientists. 2006. Subtropical Arctic Ocean temperatures during the Palaeocene/Eocene thermal maximum. Nature **441**:610-613.
Smith, F. A., S. L. Wing, and K. H. Freeman. 2007. Magnitude of the carbon isotope excursion at the Paleocene-Eocene thermal maximum: The role of plant community change. Earth and Planetary Science Letters **262**:50-65.

Thomas, D. J., J. C. Zachos, T. J. Bralower, E. Thomas, and S. Bohaty. 2002. Warming the fuel for the fire: Evidence for the thermal dissociation of methane hydrate during the Paleocene-Eocene thermal maximum. Geology **30**:1067-1070.

Thomas, E., and N. J. Shackleton. 1996. The Palaeocene-Eocene benthic foraminiferal extinction and stable isotope anomalies. Pages 401-441 *in* R. W. O. B. Knox, R. M. Corfield, and R. E. Dunay, editors. Correlation of the Early Paleogene in Northwestern Europe, Geological Society London Special Publication, 101. Geological Society of London, London, United Kingdom.

Tortell, P. D. 2000. Evolutionary and ecological perspectives on carbon acquisition in phytoplankton. Limnology and Oceanography **45**:744-750.

van Roij, L. in prep. The Paleocene - Eocene Thermal Maximum in the Gulf of Mexico. Master thesis. Universiteit Utrecht, Utrecht.

Wing, S. L., G. J. Harrington, F. A. Smith, J. I. Bloch, D. M. Boyer, and K. H. Freeman. 2005. Transient Floral Change and Rapid Global Warming at the Paleocene-Eocene Boundary. Science **310**:993-996.

Zachos, J., M. Pagani, L. Sloan, E. Thomas, and K. Billups. 2001. Trends, rhythms, and aberrations in global climate 65 Ma to present. Science **292**:686-693.

Zachos, J. C., S. M. Bohaty, C. M. John, H. McCarren, D. C. Kelly, and T. Nielsen. 2007. The Palaeocene-Eocene carbon isotope excursion: constraints from individual shell planktonic foraminifer records. Philosophical Transactions of the Royal Society A **365**:1829-1842.

Zachos, J. C., S. Schouten, S. Bohaty, T. Quattlebaum, A. Sluijs, H. Brinkhuis, S. Gibbs, and T. J. Bralower. 2006. Extreme warming of mid-latitude coastal ocean during the Paleocene-Eocene Thermal Maximum: Inferences from TEX_{86} and Isotope Data. Geology **34**:737-740.

Zachos, J. C., M. W. Wara, S. Bohaty, M. L. Delaney, M. R. Petrizzo, A. Brill, T. J. Bralower, and I. Premoli Silva. 2003. A transient rise in tropical sea surface temperature during the Paleocene-Eocene thermal maximum. Science **302**:1551-1554.

Appendix I. Sucrose solutions for EA

Protocol set up for UCSC Stable Isotope Lab, May 2009

1. Use of sucrose solutions

Sucrose solutions can be used when running the EA for samples containing very small amounts of carbon. In this way, effects of contaminated boats and the machine's capacity are tested. Especially when measuring samples smaller than 10 microgram these effects are increasingly significant.

2. Sucrose stock solution

The sucrose solution with the highest concentration of carbon is the stock solution. Solutions with lower concentrations can be made from this stock.

An amount of 10 µl is relatively easy to insert in the boats. For a stock solution containing 10 µg of carbon in 10 µl of solution, dissolve 47.5 mg of sucrose in 20 g of demineralized and degassed water. Sucrose ($C_{12}H_{22}O_{11}$) has a total weight of 342 g/mole of which 144 g/mole is carbon, so 47.5 mg of sucrose contains 20 mg of carbon. As a result, the stock solution will contain 1 µg of carbon per 1 µl of solution. For an overview, see Table 1.

Table 1. Sucrose stock solution. Water, sucrose and carbon content.

Water (µl)	Sucrose (µg)	C (µg)	Concentration (µg C/µl)	µg C in 10 µl
20000	47500	20000	1	10

3. Sucrose solutions

When making solutions containing less than 1 µg of carbon per µl of solution, the stock solution can be diluted by adding degassed water. For example, a solution containing 0.8 µg/µl requires a dilution factor of 1.25 (1/0.8). A solution of 200 µl would then consist of 160 µl (200/1.25) stock solution and 40 µl (200-160) water.

For concentrations smaller than 0.1 µg/µl, however, such small amounts of stock solution are needed that they are no longer possible to be injected by a pipette. Instead, solutions with 0.1 to 0.8 µg/µl can be further diluted. Most easily is to dilute by a factor of 10. For example, use a 0.3 µg/µl solution to make a 0.03 µg/µl solution using 20 µl of the 0.3 µg/µl solution and 180 µl of water.

For an overview of stock and water ratios for solutions 0.01 to 1 µg/µl, see Table 2.

Table 2. Sucrose solutions. Concentration, number of dilutions and composition of the solutions regarding stock solution, water and/or solutions.

Concentration (µg C/µl)	µg C in 10 µl	**Dilutions**	**Stock** (µl)	**Solution** (µl; concentration)	**Water** (µl)	**Total volume** (µl)
1	10	1	200		0	200
0.8	8	1.25	160		40	200
0.5	5	2	100		100	200
0.3	3	3.33	60		140	200
0.1	1	10	20		180	200
0.08	0.8	12.5	16	20 µl of 0.8	180	200
0.05	0.5	20	10	20 µl of 0.5	180	200
0.03	0.3	33.33	6	20 µl of 0.3	180	200
0.01	0.1	100	2	20 µl of 0.1	180	200

4. Processed batches of sucrose solutions

So far, several series of sucrose solutions have been made. As evaporation may change the concentration of the solutions over time, it is recommended to make a new series for each run on the EA.

Earlier processed batches and the exact composition of the stock solutions are shown in Table 3a. The exact concentrations for each solution of these batches are listed in Table 3b.

Table 3a. Batches of sucrose solutions. Date of processing and composition of stock solutions.

Batch	**Date**	**Water** (mg)	**Sucrose** (mg)	**Carbon** (mg)	**Concentration** (µg/µl)
Batch 1	25/3/2009	20.93	49.09	20.67	0.99
Batch 2	28/4/2009	20.49	47.74	20.10	0.98
Batch 3	6/5/2009	21.08	47.74	20.10	0.95

Table 3b. Theoretical and actual concentrations. Actual concentration of carbon in each sucrose solution of all batches listed next to the aimed concentration.

Theoretical concentration (µg/µl)	**Actual concentration** (µg/µl) **Batch 1**	**Batch 2**	**Batch 3**
1	0.987263	0.981162	0.95351
0.8	0.789811	1.226452	0.762808
0.5	0.493632	1.962324	0.476755
0.3	0.296179	3.27054	0.286053
0.1	0.098726	9.81162	0.095351
0.08	0.078981	12.26452	0.076281
0.05	0.049363	19.62324	0.047676
0.03	0.029618	32.7054	0.028605
0.01	0.009873	98.1162	0.009535

Appendix II. EA outputs

The table below (Table 4) lists the corrected $\delta^{13}C$ data of the test run, first and second run and includes the sample codes used in the EA output. Tables 5, 6 and 7 contain the raw EA output data as well as the $\delta^{13}C$ corrected for the offset between the average Pugel $\delta^{13}C$ and its standard value. The data obtained for the Bass River and Harrell core sample in the test run and first run are on *Apectodinium*. The second run includes data of *Apectodinium* samples as well as the total palynological residue. Furthermore, the lower CIE-sample of the Harrell core (HC 034) is also measured for the palynological residue of which the dinocysts have been removed.

Table 4. Corrected $\delta^{13}C$ data and sample codes. Test run, first run and second run are measurements on *Apectodinium*. Second run also includes $\delta^{13}C$ of the total palynological residue. Sample HC 034 was measured twice on *Apectodinium* in the first and second run (sample and dup1, dup2 and dup3). Dup stands for duplicate. The duplicate sample for HC 034 on the palynological residue is without dinocysts.

Site	Interval	Code	Depth (mbs)	Test run	First run, Apecto	Second run, Apecto	Second run, paly.
Bass River	CIE-onset, upper	BR 74	357,12			-20,56	-25,63
Bass River	CIE-onset, lower	BR 75/76	357,21	-24,71	-22,65	-22,75	-25,16
Bass River	pre-CIE	BR 80	357,58		-21,34	-20,79	-23,09
Harrell core	CIE-body, upper	HC 064	120,09			-24,11	-27,52
Harrell core	CIE-body, lower	HC 034	121,62		-22,77	-22,90	-26,61
Harrell core	CIE-body, lower	HC 034, dup	121,62		-22,07	-24,57	-26,10
Harrell core	CIE-onset	HC 029	121,87		-23,64		-25,72
Harrell core	pre-CIE	BLM	130,00		-22,48	-22,34	-24,76

Table 5. EA output of the test run. Identifier 1 lists the carbon substrate measured, whereas identifier 2 shows the batch of cups and sucrose used. Area 44 is the area below the peak generated by the samples that corresponds to CO_2 with a mass of 44 g/mole. $\delta^{13}C$ is the raw data corrected based on Pugel.

Identifier 1	Identifier 2	Amount	Area 44	1/Area 44	Raw $\delta^{13}C$	$\delta^{13}C$
Sucrose	Cup 2, Sucrose 2	10	19,23	0,05	-11,48	-11,39
Sucrose	Cup 2, Sucrose 2	8	13,93	0,07	-11,60	-11,51
Sucrose	Cup 2, Sucrose 2	5	9,54	0,10	-11,47	-11,39
Sucrose	Cup 2, Sucrose 2	3	4,81	0,21	-11,72	-11,63
Sucrose	Cup 2, Sucrose 2	1	1,91	0,52	-11,24	-11,16
Sucrose	Cup 2, Sucrose 2	0,8	1,21	0,83	-11,79	-11,71
Sucrose	Cup 2, Sucrose 2	0,5	0,75	1,34	-11,69	-11,60
Sucrose	Cup 2, Sucrose 2	0,3	0,38	2,65	-12,82	-12,74
Pugel	Cup 2	4	4,24	0,24	-12,81	-12,73
Pugel	Cup 2	13	11,21	0,09	-12,77	-12,69
Pugel	Cup 2	5	5,65	0,18	-12,71	-12,62
Pugel	Cup 2	8	7,91	0,13	-12,73	-12,65
Pugel	Cup 2	10	9,28	0,11	-12,39	-12,31
Pugel	Cup 2	7	9,59	0,10	-17,69	-17,61
Acetanilide	Cup 2	3	44,99	0,02	-32,38	-32,29
Blank	True, no cup	0	45,82	0,02	-33,01	-32,93
Pugel	Cup 1	4	3,85	0,26	-12,86	-12,78
Pugel	Cup 1	11	11,60	0,09	-12,66	-12,58
Pugel	Cup 1	8	6,86	0,15	-12,54	-12,45
Blank	Cup 1	0	45,74	0,02	-33,01	-32,93
BR 75/76	Cup 1		4,23	0,24	-24,80	-24,71
Sucrose	Cup 1, Sucrose 2	10	15,28	0,07	-12,16	-12,08
Sucrose	Cup 1, Sucrose 2	5	9,16	0,11	-10,83	-10,74
Sucrose	Cup 1, Sucrose 2	1	1,69	0,59	-11,59	-11,51
Sucrose	Cup 1, Sucrose 2	0,8	0,93	1,08	-15,66	-15,57
Sucrose	Cup 1, Sucrose 1	10	18,65	0,05	-10,53	-10,45
Sucrose	Cup 1, Sucrose 1	8	14,93	0,07	-10,70	-10,62
Sucrose	Cup 1, Sucrose 1	5	4,18	0,24	-10,61	-10,52
Sucrose	Cup 1, Sucrose 1	3	5,48	0,18	-10,59	-10,51
Sucrose	Cup 1, Sucrose 1	1	1,64	0,61	-11,57	-11,49
Sucrose	Cup 1, Sucrose 1	0,8	1,09	0,92	-13,28	-13,19
Sucrose	Cup 1, Sucrose 1	0,5	0,66	1,51	-13,97	-13,88
Sucrose	Cup 1, Sucrose 1	0,3	0,37	2,68	-11,23	-11,15

Table 6. EA output of the first run. Identifier 1 lists the carbon substrate measured, whereas identifier 2 shows the batch of cups and sucrose used. Area 44 is the area below the peak generated by the samples that corresponds to CO_2 with a mass of 44 g/mole. $\delta^{13}C$ is the raw data corrected based on Pugel. HC 034 dup1 is the first duplicate of this *Apectodinium* sample.

Identifier 1	Identifier 2	Amount	Area 44	1/Area 44	Raw $\delta^{13}C$	$\delta^{13}C$
Acetanilide	Cup 3	4	5,29	0,19	-30,00	-26,73
Pugel	Cup 3	0	3,64	0,28	-14,12	-10,85
Pugel	Cup 3	5	10,24	0,10	-14,26	-10,99
Pugel	Cup 3	12	1,10	0,91	-16,24	-12,96
Pugel	Cup 3	3	3,45	0,29	-14,34	-11,06
Pugel	Cup 3	4	1,53	0,65	-15,78	-12,50
Pugel	Cup 3	3	63,62	0,02	-31,36	-28,09
HC 034 dup1	Cup 3		10,07	0,10	-25,35	-22,07
BR 80	Cup 3		3,91	0,26	-24,62	-21,34
BR 75/76	Cup 3		3,88	0,26	-25,92	-22,65
BLM	Cup 3		7,05	0,14	-25,75	-22,48
HC 029	Cup 3		4,08	0,25	-26,92	-23,64
HC 034	Cup 3		7,75	0,13	-26,05	-22,77
Sucrose	Cup 3, Sucrose 3	0,1	62,86	0,02	-31,86	-28,59
Sucrose	Cup 3, Sucrose 3	0,3	62,70	0,02	-31,60	-28,32
Sucrose	Cup 3, Sucrose 3	0,5	0,72	1,40	-13,28	-10,00
Sucrose	Cup 3, Sucrose 3	0,8	1,49	0,67	-15,94	-12,66
Sucrose	Cup 3, Sucrose 3	1	1,80	0,56	-17,86	-14,58
Sucrose	Cup 3, Sucrose 3	3	6,53	0,15	-15,34	-12,06
Sucrose	Cup 3, Sucrose 3	5	10,90	0,09	-15,39	-12,11
Sucrose	Cup 3, Sucrose 3	8	17,67	0,06	-15,21	-11,93
Sucrose	Cup 3, Sucrose 3	10	21,67	0,05	-15,20	-11,92
Blank	Cup 3	0	61,84	0,02	-33,01	-29,74
Blank	Cup 3	0	61,77	0,02	-33,01	-29,74
Pugel	Cup 3	8	6,84	0,15	-18,78	-15,50
Pugel	Cup 3	2	1,03	0,97	-17,61	-14,34

Table 7. EA output of the second run. Identifier 1 lists the carbon substrate measured, whereas identifier 2 shows the batch of cups and sucrose used. Area 44 is the area below the peak generated by the samples that corresponds to CO_2 with a mass of 44 g/mole. $\delta^{13}C$ is the raw data corrected based on Pugel. HC 034 dup2 and dup3 are the second and third duplicates of this *Apectodinium* sample. Paly stands for palynological residue.

Identifier 1	Identifier 2	Amount	Area 44	1/Area 44	Raw $\delta^{13}C$	$\delta^{13}C$
Acetanilide	Cup 3	4	3,75	0,27	-26,82	-27,29
Pugel	Cup 3	17	15,75	0,06	-11,72	-12,19
Pugel	Cup 3	50	64,25	0,02	-12,12	-12,60
Pugel	Cup 3	32	36,91	0,03	-12,14	-12,61
Pugel	Cup 3	22	14,46	0,07	-11,91	-12,38
BR 80 paly	Cup 3		6,58	0,15	-22,62	-23,09
BR 75/75 paly	Cup 3		7,88	0,13	-24,69	-25,16
BR 74 paly	Cup 3		9,96	0,10	-25,16	-25,63
BLM paly	Cup 3		49,76	0,02	-24,29	-24,76
HC 029 paly	Cup 3		36,97	0,03	-25,25	-25,72
HC 064 paly	Cup 3		29,44	0,03	-27,05	-27,52
HC 034 paly, no cysts	Cup 3		6,46	0,15	-25,63	-26,10
HC 034 paly	Cup 3		8,92	0,11	-26,14	-26,61
Pugel	Cup 3	8	7,56	0,13	-13,20	-13,67
Pugel	Cup 3	2	1,88	0,53	-12,99	-13,46
Pugel	Cup 3	3	2,23	0,45	-12,32	-12,80
Pugel	Cup 3	4	3,02	0,33	-11,91	-12,38
Pugel	Cup 3	3	2,46	0,41	-11,17	-11,64
BR 80 dup1	Cup 3		1,82	0,55	-20,31	-20,79
BR 75/76 dup1	Cup 3		1,29	0,78	-22,28	-22,75
BR 74	Cup 3		1,22	0,82	-20,09	-20,56
BLM dup1	Cup 3		3,30	0,30	-21,87	-22,34
HC 064	Cup 3		2,88	0,35	-23,64	-24,11
HC 034 dup3	Cup 3		3,16	0,32	-24,09	-24,57
HC 034 dup2	Cup 3		15,70	0,06	-22,43	-22,90
Pugel	Cup 3	1	11,79	0,08	-11,82	-12,29
Blank	Cup 3, not crushed	0	56,08	0,02	-32,82	-33,29
Blank	Cup 3	0	56,11	0,02	-32,82	-33,29
Sucrose	Cup 3, Sucrose 3	0,1	56,16	0,02	-32,85	-33,32
Sucrose	Cup 3, Sucrose 3	0,3	0,78	1,28	-14,44	-14,91
Sucrose	Cup 3, Sucrose 3	0,5	0,91	1,10	-11,85	-12,32
Sucrose	Cup 3, Sucrose 3	0,8	1,38	0,73	-8,98	-9,45
Sucrose	Cup 3, Sucrose 3	1	1,90	0,53	-9,32	-9,79
Sucrose	Cup 3, Sucrose 3	3	6,70	0,15	-9,61	-10,08
Sucrose	Cup 3, Sucrose 3	5	12,17	0,08	-9,94	-10,41
Sucrose	Cup 3, Sucrose 3	8	19,24	0,05	-9,99	-10,46
Sucrose	Cup 3, Sucrose 3	10	22,88	0,04	-9,97	-10,44
Blank	Cup 3	0	56,38	0,02	-32,86	-33,33
Pugel	Cup 3	7	3,08	0,32	-12,67	-13,14
Pugel	Cup 3	38	42,99	0,02	-11,56	-12,03